Transient Hydraulic Transport in Pipelines

On flow assurance influenced by slurry dynamics

de Hoog, E.

DOI
10.4233/uuid:63109a8b-fec3-48f3-85b4-10923801f093

Publication date
2024

Document Version
Final published version

Citation (APA)
de Hoog, E. (2024). *Transient Hydraulic Transport in Pipelines: On flow assurance influenced by slurry dynamics*. [Dissertation (TU Delft), Delft University of Technology]. https://doi.org/10.4233/uuid:63109a8b-fec3-48f3-85b4-10923801f093

Important note
To cite this publication, please use the final published version (if applicable).
Please check the document version above.

Transient Hydraulic Transport in Pipelines

On flow assurance influenced by slurry dynamics

Edwin de Hoog

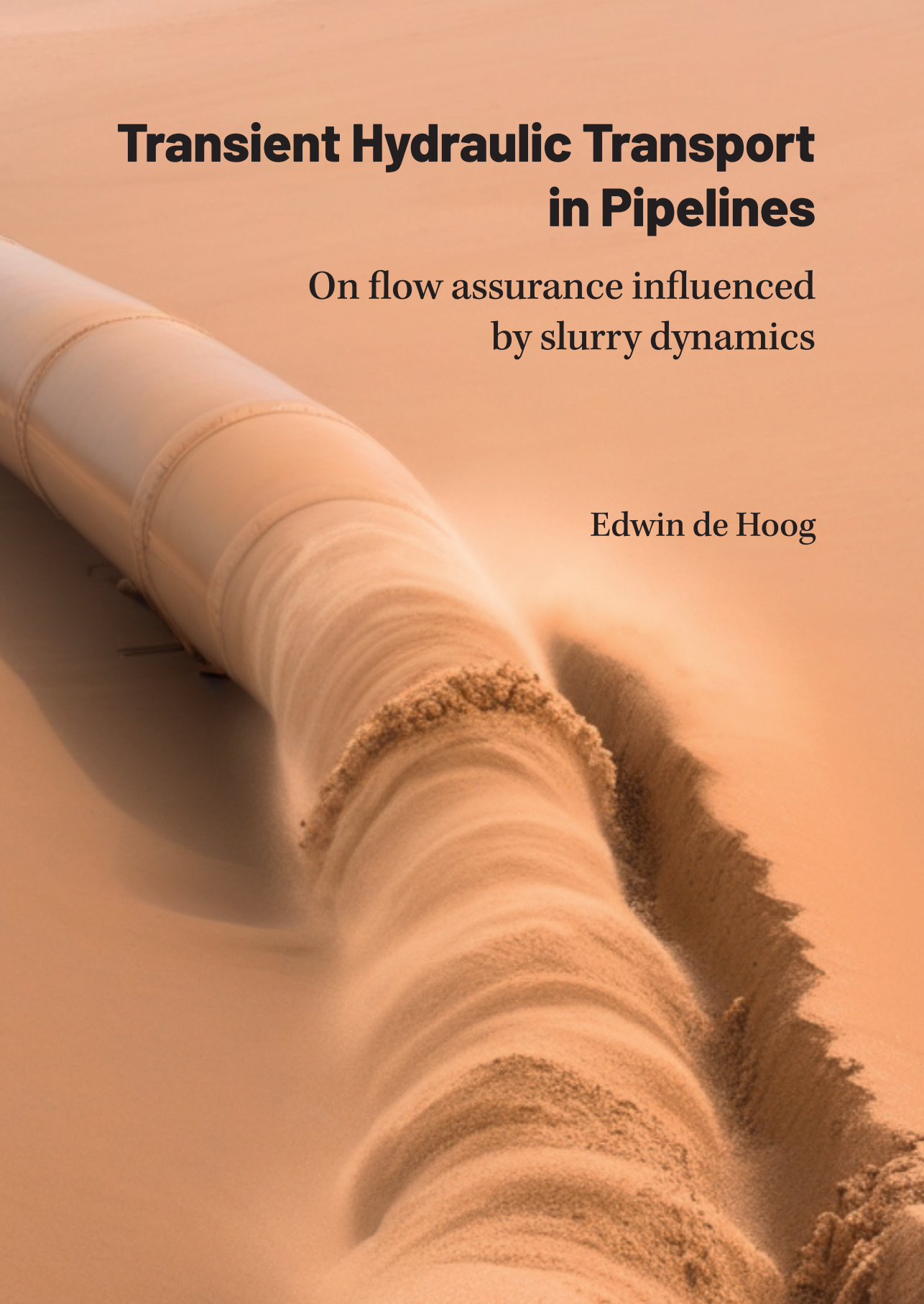

TRANSIENT HYDRAULIC TRANSPORT IN PIPELINES

ON FLOW ASSURANCE INFLUENCED BY SLURRY DYNAMICS

TRANSIENT HYDRAULIC TRANSPORT IN PIPELINES

ON FLOW ASSURANCE INFLUENCED BY SLURRY DYNAMICS

Proefschrift

ter verkrijging van de graad van doctor
aan de Technische Universiteit Delft,
op gezag van de Rector Magnificus prof. dr. ir. T.H.J.J. van der Hagen,
voorzitter van het College voor Promoties,
in het openbaar te verdedigen op dinsdag 9 Juli 2024 om 12:30 uur

door

Edwin DE HOOG

Master of Science in Offshore and Dredging Engineering,
Technische Universiteit Delft, Nederland,
geboren te Zoetermeer, Nederland.

Dit proefschrift is goedgekeurd door de promotoren.

Samenstelling promotiecommissie bestaat uit:

Rector Magnificus,	voorzitter
Dr. ir. R.L.J. Helmons	Technische Universiteit Delft, promotor
Dr. ir. A.M. Talmon	Technische Universiteit Delft, copromotor
Onafhankelijke leden:	
em. Prof. dr. ir. A. Bezuijen	Universiteit Gent, België
Prof. dr. ir. R.A.W.M. Henkes	Technische Universiteit Delft
Prof. dr. ing. V. Matoušek	Technische Universiteit Tsjechië, Tsjechië
Prof. dr. ir. D.L. Schott	Technische Universiteit Delft
Dr. G.V. Messa	Polytechnische Universiteit Milaan, Italië

Prof. dr. ir. C. van Rhee† heeft in zeer belangrijke mate aan de totstandkoming van het proefschrift bijgedragen.

Keywords: Hydraulic transport, transients, slurry dynamics, denisty waves, flow assurance, 1D-CFD, Driftflux, mixture modelling

Printed by: Ridderprint, Alblasserdam

Front & Back: This is what you get if you ask AI to generate an image of: "A sand wave inside a pipeline" (www.midjourneyai.ai).

ISBN 978-94-6506-147-4

An electronic version of this dissertation is available at
http://repository.tudelft.nl/.

To my family and friends

SUMMARY

Hydraulic transport is a core transportation technology in many industries, such as dredging, (wet) mining and in the near future deep-seabed mining. Simply explained, hydraulic transport entails mixing solids (i.e. sand, gravel and ores) with water and pumping them through a pipeline, by using for instance a centrifugal pump. Up to this date, these pipelines are mainly designed using steady-state principles and models. Pipeline design parameters such as the mixture velocity and solids concentration are assumed to be constant in time and space, and are evaluated to represent a maximum loading case of the pump-pipeline system.

However, local variations of the solids concentration can affect the entire pipeline. For instance a large density wave of solids that flows through the centrifugal pump, triggers a mixture velocity change across the entire length of the pipeline, due to the incompressibility of water. This pump-pipeline coupling effect is well known. However, often ignored is the fact that these transients can cause a pipeline system to become unstable, which increases the risk of blockages and pump-drive failures.

Experiments in a vertical experimental flow loop, conducted in the summer of 2017 in Halsbrücke (Freiberg), Germany, demonstrated how particles can redistribute into large density waves while flowing through the pipeline. The concentration peaks of these undesirable density waves strained the pump-drive beyond its designed power, which was determined with the best available steady-state design models. This case showed how slurry dynamics and local pipeline transients can lead to an unstable pipeline. Furthermore, these density waves were not predicted during the steady-state design phase of the pipeline, due to the limitations of the steady-state design method.

Self-amplifying density waves have also been encountered in long pipelines in the dredging industry, although these cases are not frequently reported publicly. Only one such case is reported in literature, which is the density wave case of the 1981 Prins Clausplein pipeline. Solids entered the 10 kilometer pipeline at a relatively constant concentration, but exited the pipeline as strong density waves. These waves strained the pump drives and impeded the safety of the pipeline system.

In this research, three mechanisms responsible for self-amplifying density waves have been identified. Two mechanisms are specific to horizontally oriented pipes, where density waves amplify from a stationary particle bed layer if the mixture flow rate in the pipeline is too low. These two density waves have been characterized as "erosion driven" and "sliding bed driven" density waves. The third mechanism occurs when there is a large difference in local particle velocity between two pipeline segments, for instance a vertical and a horizontal pipe. These waves are referred to as "transient accumulation" density waves, and do not require a bed layer to occur.

The recent Freiberg case showed that there is a need for transient modelling of a pipeline system, to take into account time domain effects, as part of flow assurance studies. As such, a large portion of this dissertation is devoted to developing a 1D-Driftflux

model that incorporates all important transient effects of a pump-pipeline system, and can predict the occurrence of density waves. The main features incorporated into the the developed 1D-Driftflux model are: particle slip (as a function of pipe orientation, particle size and concentration), a lower layer to model a stationary particle bed, and a centrifugal pump model. In the current state of development, the 1D-Driftflux model predicts transient accumulation density waves and erosion driven density waves. Furthermore, the 1D-Driftflux model was successfully applied to compare the effectiveness of several measures to mitigate the impact of density waves, such as reducing the pipe diameter in certain sections of a pipeline and the application of flow feedback control.

The main conclusion of this dissertation is that instabilities in hydraulic transport pipelines are triggered by local pipeline effects, which have system-wide consequences. The most impactful instabilities are the three density wave amplification mechanisms. Each of the three density wave types has it own set of conditions to trigger. As such, designers of pump-pipelines systems must understand which type of density wave could form for specific slurry parameters or pipeline configurations. Mitigation measures and alternative design approaches have been analyzed to assure that pipelines can be designed with the lowest possible risk on flow assurance due to instabilities. As recommendation for future research, this dissertation addresses the lack of particle slip models and experimental data for larger pipeline diameters and coarse particles. In general, better slip models are useful for pipeline designers to estimate the pipeline production as part of steady-state design. Furthermore, improved slip models are also very valuable to make the 1D-Driftflux model applicable for larger pipe diameters. It is also recommended to expand the 1D-Driftflux model to incorporate sliding bed driven density waves. By doing this, the interaction between booster pumps and sliding bed driven density waves can be studied, for long horizontal pipelines. Understanding this interaction, combined with implementation of better feedback-controllers aimed at providing transient stability, enables more efficient long distance pipeline transport by facilitating higher concentrations and/or lower transport velocities.

SAMENVATTING

Hydraulisch transport is een veel toegepaste kerntechnologie in de bagger-, (natte) mijnbouw- en de toekomstige diepzeemijnbouwindustrie. Hydraulisch transport kan men simpelweg uitleggen als het proces waarbij een vaste stof, zoals zand, grind of erts, met water wordt vermengd en verpompt in een pijpleiding. Een veelgebruikte type pomp voor deze toepassing is de zogenaamde centrifugaalpomp, die het mogelijk maakt grote korrels te verpompen. Tot vandaag de dag worden deze pomp-pijpleiding systemen ontworpen met modellen en methodes die zijn gebaseerd op steady-state principes, waarbij geacht wordt dat de hoeveelheid deeltjes en de snelheid waarmee ze getransporteerd worden, constant zijn in de tijd en de plaats in de pijpleiding. Zo kunnen ontwerpers een maximaal belastingscenario van het systeem evalueren.

Echter lokale verschillen in deeltjes- concentratie, snelheid of slip kunnen invloed hebben op de gehele pijpleiding. Een voorbeeld is wanneer een dichtheidsgolf door de centrifugaalpomp stroomt. Omdat water incompressibel is, leidt deze lokale dichtheidsgolf tot een verandering in mengselsnelheid in de gehele pijpleiding. Dit effect is zeer bekend. Echter wat vaak onderschat wordt, is dat dergelijke effecten kunnen leiden tot een instabiele pijpleiding en daarmee een hoog risco op verstoppingen of het falen van pompaandrijvingen.

In de zomer van 2017 vond er een meetcampagne plaats in Halsbrücke (Freiberg), Duitsland. De meetopstelling betrof een circulaire pijpleiding met lange verticale secties. Tijdens het proevenprogramma herverdeelden de deeltjes zich tot dichtheidsgolven terwijl de deeltjes door de pijpleiding stroomden. Deze zelfversterkende dichtheidsgolven waren ongewenst, verhoogden de belasting op de pompaandrijving en deze instabiele pijpleiding kon gemiddeld niet langer dan een uur veilig draaien. Deze pijpleiding was ontworpen met de best beschikbare steady-state ontwerpmodellen, desondanks vormden er dichtheidsgolven en was de pijpleiding instabiel.

Zelfversterkende dichtheidsgolven zijn vaker opgemerkt in de baggerindustrie, echter blijft publieke literatuur over dit onderwerp schaars. Het enige publiekelijk bekend voorbeeld is de 10 kilometer lange pijpleiding die gebruikt werd tijdens de uitbreiding van het Prins Clausplein in 1981. Deze pijpleiding had zeer veel last van zelfversterkende dichtheidsgolven. Zand werd in de pijpleiding geïnjecteerd met een relatief constant debiet, maar verliet de pijpleiding in de vorm van sterke dichtheidsgolven. De golven verhoogden de belasting op de pompaandrijving en brachten de veiligheid en stroomzekerheid van de pijpleiding in gevaar.

Tijdens het onderzoek voor deze dissertatie zijn drie typen zelfversterkende dichtheidsgolven geïdentificeerd. Twee mechanismen komen voor in horizontale pijpleidingen. Deze beschrijven we als erosie-gedreven en glijdend bed gedreven dichtheidsgolven. Deze golven versterken zich uit deeltjesdepots die ontstaan in de pijpleiding als de mengselsnelheid te laag is. Het derde type dichtheidsgolf kan ontstaan in een leidingsysteem met horizontale en verticale secties, waarbij een significant verschil in deel-

tjessnelheid tussen de secties aanwezig is. Deze zelfversterkende dichtheidsgolf wordt beschreven als een transiënte accumulatie golf, en heeft geen depot nodig om uit te onstaan.

De recente Freiberg casus legt de behoefte bloot om tijdsdomein effecten te kunnen overwegen in de ontwerpfase van een leidingsysteem, er is immers een risico op een instabiel systeem. Daarom is een groot deel van dit onderzoek gewijd aan het ontwikkelen van een 1D-Driftflux model. Het 1D-Driftflux model is in staat om het gehele leidingsysteem met mengsel en centrifugaalpomp(en) te simuleren in de tijd. Het model bevat elementen zoals deeltjessnelheidsverschillen als functie van concentratie en pijp oriëntatie, depotvorming en een centrifugaalpompmodel. Daarmee is het model in staat om zelfversterkende dichtheidsgolven te simuleren en te voorspellen. In zijn huidige staat kan het 1D-Driftflux model transiënt accumulatie golven en erosie-gedreven dichtheidsgolven voorspellen. Het model is succesvol toegepast om diverse dichtheidsgolfmitigatietechnieken te onderzoeken en te valideren, zoals het reduceren van de leidingdiameter in specifieke delen van de pijpleiding, en het toepassen van een constantestromingsregelaar.

De hoofdconclusie van deze dissertatie is dat instabiliteiten in een pijpleiding veroorzaakt worden door lokale effecten, die de gehele pijpleiding beïnvloeden. De instabiliteiten met de meeste impact zijn de drie typen dichtheidsgolven. Het is zeer belangrijk dat ontwerpers begrijpen wanneer welk type dichtheidsgolf kan plaatsvinden, gezien dit afhankelijk is van zowel de mengseleigenschappen als de pijpleidingconfiguratie. In de conclusies vindt men ook nieuwe ontwerpmethoden om het risico op instabiliteiten in een transportleiding zo ver mogelijk te verlagen. Een belangrijk punt voor vervolgonderzoek is het gebrek aan experimentele data en modellen om goed de slip van deeltjes in een pijpleiding te kunnen schatten. Specifiek is er een tekort voor grotere pijpleidingdiameters en grovere korrels. In het algemeen zijn betere slipmodellen nuttig om de productie van een pijpleiding in te schatten. In het bijzonder zijn verbeterde slipmodellen zeer nuttig om het 1D-Driftflux model breder toepasbaar te maken voor een groter bereik aan pijpleidingdiameters. Ook wordt aanbevolen om het 1D-Driftflux model uit te breiden om glijdend bed aangedreven dichtheidsgolven te simuleren. Hiermee kan de interactie tussen pomp boosterstations en dichtheidsgolven in lange transportpijpleidingen beter worden bestudeerd. Nieuwe inzichten omtrent deze interactie, in combinatie met verbeterde pijpleidingregelaars, maakt het mogelijk om efficiëntere langeafstandspijpleidingen te ontwerpen, die met een hogere transportconcentratie en/of lagere mengselsnelheid sediment kunnen transporteren.

CONTENTS

List of Symbols

Latin symbols

A	Pipe cross-sectional discharge area	m^2
c	Volumetric particle concentration	–
$c^{'}$	Wave amplitude	–
C_D	Drag coefficient	–
c_k	Phase concentration	–
c_b	Bed concentration	–
c_{loop}	Mean flow loop volumetric concentration	–
c_{max}	Maximum concentration	–
c_{mean}	Mean pipe concentration with density waves	–
c_{nb}	Near bed concentration	–
c_{vd}	Volumetric delivered concentration	–
$c_{w,mean}$	Mean wave concentration	–
$c_{w,min}$	Wave minimum concentration	–
$c_{w,peak}$	Wave peak concentration	–
$c_{w,ptp}$	Peak to peak wave concentration	–
D	Pipe diameter	m
d	Particle diameter	m
D_h	Hydraulic diameter of the discharge area above a bed layer	m
d_{50}	Mass median particle diameter	m
$d_{\#}$	Weight fraction (# %) smaller particle diameter	m
d_m	Mass mean particle diameter	m
E	Erosion flux	$kg/m^2/s$
E_h	Hindered erosion flux	$kg/m^2/s$

e_t	Controller error at time step t	m/s
e_{NRMS}	Normalized root mean square error	–
F	Flux	m/s
f	Darcy-Weisbach friction factor	–
f_e	van Wijk (2016) axial dispersion factor	–
f_c	Stepanoff (1965) pump deration factor	–
f_i	Internal forces per unit area	Pa
f_k	Phase volumetric source term	$1/s$
f_t	Sobota and Kril (1992) particle velocity factor	–
F_b	Frictional force on top of the bed layer	N
$F_{e,k}$	Phase external force term	N
F_e	Mixture external force term	N
F_m	Mixture frictional forces	N
F_s	Hydrostatic force on the mixture	N
F_s	Pump pressure force on the mixture	N
g	Gravitational constant	m/s^2
h	Height of a vertical concentration profile	m
h_s	Height of a shear layer	m
K	Appendage friction factor	–
K_D	Controller differential gain	–
K_I	Controller integral gain	–
K_P	Controller proportional gain	–
k_s	Pipe wall roughness	m
k_{max}	Maximum bed permeability	m/s
L	Pipeline length	m
L_w	Wave length	m
$L_w^{'}$	Wave length adjusted for the area above the bed	m
m	Hindered erosion exponent	–

N	Amount	–
n	Richardson and Zaki (1954) exponent	–
n_0	Bed layer porosity	–
N_a	Number of appendages	–
N_c	Number of numerical cells	–
n_{cr}	Pump revolutions of a constant revolutions drive	$1/s$
n_{max}	Maximum porosity	–
n_{min}	Minimum porosity	–
n_{pump}	Pump revolutions	$1/s$
O	Surface area of the wetted pipe wall	m^2
p	Pressure	Pa
p_m	Pressure on the mixture	Pa
p_p	Pressure of a pump	Pa
$p_{man,0}$	Pump manometric pressure at revolutions of $n_{pump,0}$	Pa
$p_{man,n}$	Pump manometric pressure at revolutions of n_{pump}	Pa
p_{man}	Manometric pump pressure	Pa
$P_{max,cr}$	Maximum pump power at constant revolutions	W
P_{max}	Maximum pump power	W
q	Generic numerical source term	
Q_0	Pump flow rate at reference revolutions of $n_{pump,0}$	m^3/s
Q_f	Fluid flow rate	m^3/s
Q_n	Pump flow rate at revolutions of n_{pump}	m^3/s
Q_s	Solids flow rate	m^3/s
R	Bend radius	m
R_s	Slip ratio	–
Re_p	Particle Reynolds number	–
S	Sedimentation flux	$kg/m^2/s$
S_h	Hindered sedimentation flux	$kg/m^2/s$

S_p	Pump pressure source term	Pa
St	Stokes number	–
T	Period of a pipeline	s
t	Time	s
t_f	Fluid reaction time	s
t_p	Particle reaction time	s
T_w	Period of a density wave	s
U	Generic scalar quantity	
u^*	Shear velocity	m/s
u_f	Fluid velocity	m/s
u_k	Phase velocity	m/s
u_m	Volumetric mixture velocity	m/s
u_r	Particle velocity relative to the fluid	m/s
u_s	Solids velocity	m/s
u_{crit}	Critical velocity	m/s
u_{dl}	Deposit limit velocity	m/s
$u_{k/m}$	Phase velocity relative to the mixture velocity	m/s
$u_{m,0}$	Initial mixture velocity	m/s
$u_{m,set}$	Controller set-point	m/s
$u_{m,t}$	Mixture velocity at time step t	m/s
$u_{m,w}$	Mean mixture velocity during a density wave	m/s
$u_{s/m}$	Particle velocity relative to the mixture velocity	m/s
u_{th}	Threshold velocity for transient accumulation density waves	m/s
u_w	Wave celerity	m/s
$u_w^{'}$	Wave celerity adjusted for the area above the bed	m/s
V	Numerical cell volume of the flowing mixture	m^3
V_b	Numerical cell volume of the bed layer	m^3
v_{hs}	Hindered settling velocity	m/s

v_{sed}	Sedimentation velocity of a bed layer	m/s
v_{ts}	Terminal settling velocity	m/s
W	Surface area of the bed layer top	m^2
x	Axial coordinate of a pipe	m
y_b	Bed layer height	m
$\hat{u}_m$	Mass mixture velocity	m/s

Greek symbols

α	Constant in Eq. 2.7	–
β	Constant in Eq. 2.7	–
ϵ	Axial dispersion coefficient	–
ϵ_{Taylor}	Taylor diffusion coefficient	–
η	Pump efficiency	–
Γ_m	Mass source term	kg/s
Γ_v	Volumetric source term	$1/s$
λ_b	Bisschop (2018) turbulent bursts coefficient	–
μ_f	Fluid dynamic viscosity	$Pa\,s$
μ_{sf}	Coulombic sliding friction factor of a bed layer	–
ν_f	Fluid kinematic viscosity	m^2/s
ω	Pipe inclination angle	–
ϕ	Internal friction angle	–
ρ_f	Fluid density	kg/m^3
ρ_k	Phase density	kg/m^3
ρ_m	Mixture density	kg/m^3
ρ_s	Solids density	kg/m^3
τ_f	Fluid shear stress	Pa
τ_m	Mixture shear stress	Pa
τ_s	Solids shear stress	Pa
τ_{ml}	Minor losses shear stress	Pa

Abbreviations

1D	1 Dimensional
1D-2L-HT	1 Dimensional Two Layer Hydraulic Transport (model)
1DHT	1 Dimensional Hydraulic Transport (model)
1DVHT	1 Dimensional Vertical Hydraulic Transport (model)
2D	2 Dimensional
3D	3 Dimensional
CCM	Conductance Concentration Meter
CFD	Computational Fluid Dynamics
EMF	Electro Magnetic Flow meter
ERT	Electrical Resistance Tomograph
FVM	Finite Volume Method
PSD	Particle Size Distribution
PTP	Peak to Peak (value)

1

INTRODUCTION

The oldest known hydraulic transport concept "is an old one and the earliest known use was by Hercules, who removed a decade's accumulation of animal droppings from King Augeas' stable by diverting two rivers to form an open-channel slurry transport system."

K.C. Wilson, G.R. Addie, A. Sellgren and R. Clift

Since Hercules, hydraulic transport has come a long way. By mixing solid particles with water, vast amounts of material can be pumped and transported efficiently through pipelines many kilometers long. Hydraulic transport has developed to become the back-bone technology in the dredging-, (wet) mining- and the upcoming deep sea mining industry. For decades designing pipelines was based on steady-state empirical principles and models. However, in recent years these have shown to fall short on occasions. This led to the need to study the unstable transients associated with hydraulic transport, the topic of this thesis, and to study their role in destabilizing pipeline flows.

This chapter introduces hydraulic transport to the reader, and explains the traditional steady-state methodology for designing pipelines. The shortcomings in the steady-state assumptions are addressed, which lead to the main motivations, objectives and research questions of this dissertation.

This dissertation is in fact a collection of four peer reviewed journal articles and one conference article, each its own chapter. Therefore, the introduction chapter also addresses the outline of the thesis, which acts as a reading guide to explain the chosen order of the chapters.

1

1.1. Background

1.1.1. The relevance of hydraulic transport in Dredging, Mining and Deep Sea Mining

During hydraulic transport solid granular material is mixed with water and pumped as a mixture, also called a slurry, through a pipeline system. In dredging, centrifugal pumps are the preferred choice to power the pipeline, since these can cope with large particles, up-to boulder sized for the largest available dredge pumps (see Figure 1.1). Hydraulic transport is the backbone technology in the dredging industry for transporting sediments like sand, clay, rock and gravel and is chosen in many deep sea mining concepts as the main technology for hoisting deep sea ore deposits to the sea surface. Hydraulic transport allows for more energy efficient and economical transportation of vast volume rates of sediments compared to mechanical conveying methods, like using trucks, bucket conveyors or conveyor belts (Visintainer et al., 2023).

Figure 1.1: An 8500 kW dredge pump with a 1050 mm diameter suction pipe and a 2520 mm diameter impeller (source: Royal IHC).

Because of the efficient nature of hydraulic transport, this method grew to become vital to sustain our global welfare and state of technology. For instance many mining pipelines are used over the world to transport ore concentrates, coal, oil and gas, supplying the minerals and fuel of our modern economy. These pipelines can be over hundred kilometers long. To illustrate the large and efficient transport capacity of such a pipeline, consider this example of the Samarco pipeline in Brazil. This is a 560/610 mm diameter pipeline, transporting iron ore at a mixture velocity of $\sim 1.5 m/s$ and a solids concentration of ~ 0.33 by volume. This pipeline can transport close to 1400 m^3 per hour of ore. This is equivalent to 114 trucks per hour, one every 31 seconds (van den Berg, 2013).

Dredging is vital to maintain and protect our coast lines worldwide, which are under increasing threat due to sea level rise and alluvial flooding. This is especially important, since as of the year 2023 an estimated 2.15 billion people live in near-coastal areas, specifically within 100 km of the coast and below an elevation of 100 m (Reimann et al.,

2023).

Dredging also plays an important role in advancing the world wide economy, through increasing global trade and expanding maritime infrastructure. This is achieved by land reclamation, for instance to construct new harbor terminals or airports. Another example is by maintenance or the construction of new harbor fairways and shipping lanes. To name a few recent notable examples: the Rotterdam Harbor expansion finished in 2013 (Maasvlakte II), the expansion and deepening of the Suez canal in 2016, the reclamation of 1700 hectors of land for the Manilla Airport in 2022 and the Abu Qir Port in Egypt reclaiming 1000 hectors of land 2023. These example projects used long land based pipelines to transport sand from the dredge vessels to the construction sites.

A new emerging industry where hydraulic transportation plays an important role is deep sea mining, which entails the gathering of minerals from the ocean floor. The emergence of deep sea mining is driven by the depletion of terrestrial minerals deposits, changes of the geopolitical landscape which reduces the availability of rare earth metals, and the increase in demand of metals like copper, nickle and cobalt to enable the energy transition. Copper, nickle and cobalt are key materials for the production of lithium-ion batteries, while rare-earth metals are important to produce permanent magnets used for the construction of wind turbines and electric motors. Transitioning to a fully sustainable society will require vast amount of the aforementioned materials, and deep sea mining can play an important role in providing these.

1.1.2. Hydraulic transport within Dredging, Mining and Deep Sea Mining

The solid particles in dredging mixtures are typically coarser than mixtures pumped through mining pipelines. In mining, the solids are often ground into a powder form, with particle size smaller than 100 μm. This significantly simplifies the transportation process, because these small particles experience limited settling out of the water, and therefore form little risk of creating a blockage. In dredging, particles are coarser, for example sand ranging from 100 μm to 2 mm in diameter. Also gravel, rocks and even boulders are pumped through the pipeline, up-to tens of centimeters in size. The requirement to pump these large particles drove the design of specialized dredge pumps.

In a trailing suction hopper dredger, clay, sand or gravel is excavated from the sea floor and thereafter transported hydraulically to the hopper of the dredge vessel. The hopper dredger can thereafter transport the sediment by sailing to the required destination. Depending on the type of dredging work, the soil can either be pumped onshore to reach land based civil construction sites several kilometers from the coast, or discharged on the sea floor through bottom doors or by means of rain-bowing (see Figure 1.2a). A cutter suction dredger excavates rock, clay or sand using a cutter head, and is usually constantly coupled to a partially floating pipeline, pumping the material to another location (see Figure 1.2b). These pipelines can reach over 10 kilometers.

(a) Rain-bowing by a Trailing Suction Hopper Dredger (source: Royal IHC).

(b) A Cutter Suction Dredger discharging on a floating pipeline (source: Royal IHC).

Figure 1.2: The two main hydraulic transport based dredging vessels.

Deep sea mining aims at three different mineral deposits, each requiring a specific collection technique (see Figure 1.3 and 1.4):

1. Cobalt crusts, which formed on top of a substrate rock layer over a period of millions of years. These are attractive for their high content of cobalt and can be found in relatively shallow depths, from a few hundreds of meters up-to 2.5 km. A disadvantage of cobalt crusts is that the crusts are physically attached to a substrate rock and therefore require some form of mechanical excavation with a cutting device.

2. Seafloor Massive Sulfides are old marine volcanic ore deposits, which are found close to marine hydro-thermal vents. These ancient dormant or active hydro-thermal vents are found at various depths, up-to 4 km. The downside of these sites is that they are relatively small in area and require excavation with a cutting tool.

3. Poly-metallic nodules are found on the abyssal ocean planes at depths from 4-6 km. Poly-metallic nodules are spherical shaped nodules ranging in size from a few centimeters up-to tens of centimeters. Despite the vast depth at which they are found, poly-metallic nodules lie loosely on the sea floor and are therefore relatively easy to collect. A simple suction device is sufficient to dislodge them from the sea floor.

Regardless of the deep sea minerals deposit, each deposit requires a similar method to transport the ore to the mining support vessel at the sea surface. A typical production requirement for a deep sea mining transport system is 300-500 dry tons of ore per hour (van Wijk, 2018). Again due to the efficiency of the hydraulic transport method, transport by pipeline is often the preferred choice in most deep sea mining concepts. However, it is still a challenge to transport the ore to the sea surface from depths up-to 6 kilometers by means of a vertical pipeline system. These vertical hydraulic pipeline systems tend to be complex in terms of the amount of pipe sections with different orientations. Pipe

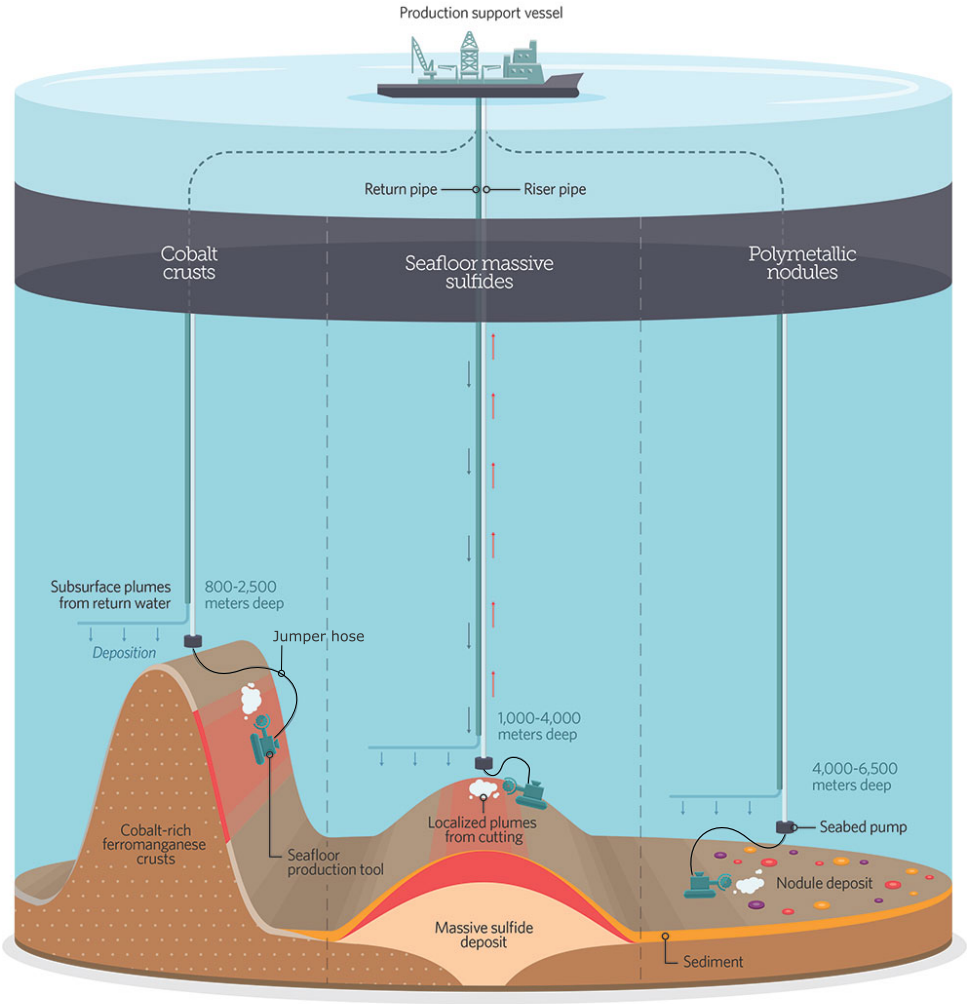

Figure 1.3: The main deep sea mining concepts. From left to right: Cobalt crusts, Seafloor Massive Sulfides and Poly-metallic nodules (Modified, source: New Zealand Environment Guide)

(a) Cobalt rich ferro-manganese crusts (Source: JAMSTEC).

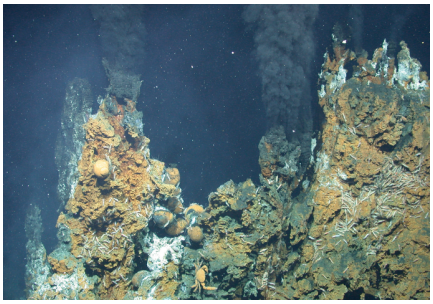

(b) Seafloor Massive Sulfides deposits (Source: MARUM – Center for Marine and Environmental Sciences, University of Bremen).

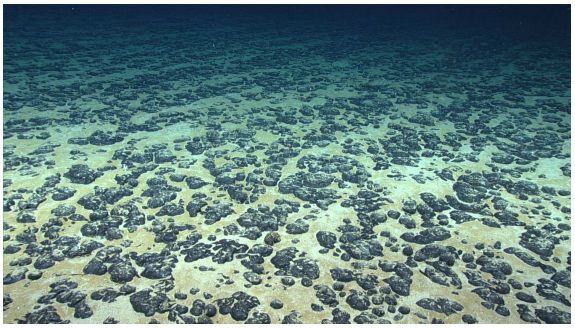

(c) Poly-metallic nodules in the form of manganese nodules on the sea floor of the Pacific Ocean (Source: NOAA).

Figure 1.4: Three photographs of mineral deposits which Deep Sea Mining aims for.

sections can be orientated either vertically, horizontally, contain flexible wavy shaped jumper hoses or inclined pipes with constantly varying inclination angle. There are two concepts for vertical hydraulic transport systems which at the most mature level out of other concepts. The first is a system driven by centrifugal pumps mounted along the riser pipeline, similar pumps used in dredging. The alternative is an airlift. An airlift is driven by compressed air, injected half way into the vertical riser pipeline. This creates buoyancy in the upper half of the pipeline, which drives the system. The advantage of airlift is the low complexity of the riser, while the main advantage of centrifugal pumps is a higher ore throughput and better energy efficiency. Which vertical transport system will prove to be the best, will become apparent in the coming years.

1.2. Traditional steady-state pipeline design

1.2.1. The history of empirical hydraulic transport research

In the 1950's and 60's groundbreaking contributions by Durand and Condolios (1952), Durand and Condolios (1956), Worster and Denny (1955) and Gibert (1960) laid the foundation of hydraulic transport research and design philosophies. Large data sets

with a wide variety in particle sizes and pipe diameters were used to develop empirical relationships to predict frictional energy losses of the mixture in the pipeline and adequate transportation velocities. These empirical relationships came in the form of easy to use mathematical formulae and are great for designing slurry transport systems from a steady-state perspective.

A great improvement in the estimation of frictional energy losses came in the 1970's when a new physics-based approach was applied in predictive modelling, by modelling the slurry transport process with two layers. In these layered models a fluid layer, with or without suspended particles, is considered separately above a sliding bed layer of particles. A set of volume and force balances over the two layers forms the foundation of the model. These steady-state layered models enable the estimation of frictional losses and the transport rate of solids (the average velocity difference between the phases). These layered models are more difficult to use, but incorporate more physics and therefore perform better, especially when scaling outside of the empirical calibration range. The layered modelling started with the Wilson-type two-layer model. Details on the model can be found in many literature sources with one of the first being Wilson (1976) and some later sources are Gillies et al. (1991), Wilson (1997) and Wilson et al. (2006). A three-layer model was proposed by Doron et al. (1987) and Doron et al. (1997) to facilitate a larger range of flow regimes. Later a Wilson two-layer model version was used by Matoušek (1997) and since then heavily researched and improve in layered model variations by Matoušek and Krupička (2010), Matoušek (2011) and Matoušek et al. (2018), to incorporate inclined pipes and bed-load transport.

Independent of the model type, a model always requires experimental data for calibration and validation. Typically, experimental data is acquired under laboratory conditions in specially designed flow loops, designed to carefully control all slurry transport parameters. Of these parameters flow velocity and mixture concentration are very important, and the aim is to keep these as steady as possible during an experiment. Typically a data point is acquired by averaging measured pressure losses over a period of several minutes at fixed concentration and steady flow velocity. This results in models calibrated with steady-state data, which are best used to design a pipeline based on evaluating a maximum load case, and always based on the assumption of a relatively steady mixture velocity and particle concentration.

1.2.2. STEADY-STATE PIPELINE DESIGN

DESIGNING a pipeline usually starts with a criterion for the required amount of solids it needs to transport, the pipeline production. A pipeline diameter and pump size is selected, the concentration is chosen based on the production requirement, and the energy added by the pump is weighted against the energy losses in the pipeline. This process is iterative, where various pipe diameters, pump sizes and pump revolutions are evaluated, and a final decision is made based on the concentration in the pipeline and the mixture velocity. The pipeline should be efficient, by ensuring that the velocity is not too high and the concentration is not too low. Also, safe continuous flow should be

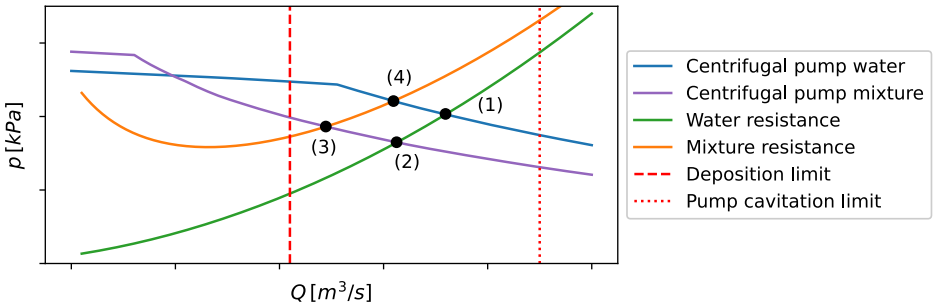

Figure 1.5: An example of a centrifugal pump curve and pipeline resistance curve. Both are given in case of water and in case of a mixture.

assured, therefore the velocity should not be too low (to avoid stationary particles) and the solids concentration should not be too high (to manage the risk of blockages).

The pump curve describes how much pressure a pump can generate giving a flow rate. The pipeline resistance curve represents how much pressure is lost due to friction, given a flow rate. Plotting the pump and pipeline curves in a graph gives an intersection, which is the operating velocity of the pipeline, see Figure 1.5. This operating point should be between two limits. The lower limit is the deposit limit velocity, which represents the transition below which particles form a deposit in the pipeline. The upper limit represents the mixture velocity above which the centrifugal pump will start cavitating, which is detrimental for the lifetime of the pump, and an increased risk for flow assurance, and should therefore be avoided. Operating below the deposit limit results in a significant decrease in particle mobility, and vastly increases the risk of blockages.

The pump and resistance curves can be evaluated for four scenarios, labeled accordingly in Figure 1.5:

1. The pump and pipeline are empty, pumping only water.
2. The first part of the pipeline is filled with solids up-to the pump, but downstream of the pump the pipeline only contains water.
3. The entire pipeline is filled with solids.
4. The solids feed into the pipeline is stopped, therefore the pump contains water while the rest of the pipeline still contains solids.

The above enumerated four scenarios result in four operating velocities for the pump-pipeline system. Designers evaluated this entire range of operation, and this forms the design space of the pump-pipeline system. Each scenario is calculated using empirically based steady-state models. The pump-curve contains efficiency corrections for the particles flowing through the pump, and a correction for the increased pressure that the

pump delivers at increased mixture density (while the pump revolutions remain constant). The pipeline resistance for water is based on the Darcy-Weisbach equation, while an empirical model is required for the pipeline mixture resistance. A separate model is used to estimate the deposit limit velocity. Typical inputs for the design are, particle concentration, particle size, particle density, pipe roughness, pipe diameter, pipe length and pump type.

1.3. TRANSIENT SLURRY BEHAVIOR

THE empirical models used to design hydraulic transport pipeline are calibrated using steady-state laboratory data. However, field conditions are quite different from laboratory conditions, where in the field the feed of solids entering the hydraulic pipeline system is never constant. For instance, variations in the thickness of the excavated soil layer will lead to variations in mixture density in the pipeline inlet. Or another example: variations in manoeuvring of the dredge vessels, such as the swing speed and stepping action of a cutter suction dredge, or the sailing velocity of a trailing suction hopper dredger. All these discrete processes cause fluctuations in material influx into the pipeline. The mean particle diameter can also vary locally across an excavation site, which leads to variations in frictional losses in the slurry pipeline, and changing deposit limit velocity. The effect of all these transients is expressed as fluctuations of the mixture concentration and mixture velocity in the pipeline.

Transient variations in concentration and mixture velocity can lead to flow instabilities. This became apparent during the expansion of the Prins Claus Plein highway junction (the Hague, the Netherlands) in 1981, where sand was delivered in a 650 mm diameter pipeline over a distance of 10 km. Sand was injected into the system with mixture densities varying between 1250 kg/m^3 and 1350 kg/m^3. After traveling through the ten kilometer long pipeline the density fluctuations amplified into density waves. Density waves are in essence the unintended clustering of particles, caused by a spatial redistribution effect while particles flow through the pipeline. The density waves exited the pipeline intermittently as only water or as thick sediment plugs with densities of over 1500 kg/m^3 (Matoušek (1995), Matoušek (1996b), Talmon (1999), Matoušek (2001)). In this case of long distance slurry transport, the self-amplifying density waves transients led to an unstable system. The density waves caused strain on the pump drives and increased the risk of blockages. An unsteady out-flux at the end of the pipeline is also undesirable, because the bulldozing capacity required to distribute the sediment is not constant. The cause of the Prins Claus density waves, was related to the mixture velocity being too close to the deposit limit velocity, and at times dropping below it, which is now understood to cause density wave amplification.

The fear of blockages and density waves causes designers of long dredging pipelines to be conservative. A typical design particle concentration for long pipelines is ~ 0.15 by volume (van den Berg, 2013). While in short pipelines, onboard of dredgers, concentrations up-to ~ 0.35 are an everyday occurrence. Due to the conservative design approach of long dredge pipelines, the transport process is relatively inefficient due to the low concentration. Thus, there is potential for further optimization, to improve energy and cost

efficiency by increasing the concentration, if the risk of density waves can be mitigated. To enable this, a better understanding of density waves is required.

Another case where transients caused flow instabilities, was during vertical hydraulic transport experiments conducted for European Union funded Blue Mining project, by a team of TU Bergakademie Freiberg and Royal IHC in Halsbrücke, Germany. All details are available in the Blue Mining public report (van Wijk, 2018). In short, a flow loop was built having 242 meters of vertical pipes together with 57 meters of horizontal pipes. These experiments were subject to heavy transient behavior resulting in self-amplifying density waves. These waves grew to severe amplitudes and eventually lead to an unstable system, causing the operators to intervene and stop the pipe system within an hour of operating to avoid clogging of the system. This system was designed using the conventional steady-state design methodology, by designing an operating velocity well above the deposit limit velocity. Regardless, the system was unstable as density waves formed and amplified. However, these density waves were different from those encountered in the Prince Claus Plein pipeline case, as the Freiberg density waves formed at velocities well above the deposit limit velocity. At times even twice the deposit limit velocity. This is the main issue related to the Freiberg case: the traditional steady-state design method, which aims at designing an operating velocity above the deposit limit, did not guarantee a stable system. As such the steady-state design method failed in this case.

1.4. Motivation and Objectives

The Freiberg experiments demonstrated that current steady-state design methods do not always guarantee transient stability of a pipeline system. However, these steady-state methods has been applied successfully for decades. Such it is unclear when the steady-state method falls short, and when transients should be considered. Therefore, one of the first objectives of this research is to identify the sources of (unstable) transients. This is to enable the further development of new design methods and philosophies to take into account these unstable transients.

A second objective is to determine the root cause of density wave amplification, as the existing theories are not fully established. Furthermore, the Freiberg density wave case seems to be caused by an unknown effect, as the Prins Claus Plein density waves were caused by a mixture velocity too close to the deposit limit, while the Freiberg pipeline operated far above the deposit limit.

What is clear, is that a different design approach is needed to consider unstable transients, by considering time domain effects in the design phase. A good approach is applying numerical simulations, specifically by Computation Fluid Dynamics (CFD). Instabilities may be caused by local microscopic effects in the pipeline, but could affect the stability of the entire system. As such, both the local transients and the entire pipeline should be simulated in the transient model. The entire domain of the pipeline can be many kilometers long, this requires the simulation of several hours of slurry flow. Such large domains and simulation times, makes modelling using 2-dimensional (2D)

or 3-dimensional (3D) CFD impractical, due to large computational costs. The use of 1-dimensional (1D) Driftflux modelling for vertical hydraulic transport pipelines has already been explored by van Wijk (2016), with the 1D Vertical hydraulic Transport model (1DVHT). The 1DVHT model has shown the ability to capture effects such and differential particle velocities, which entails that particles of different sizes overtake each other in vertical flows. Also, centrifugal pump integration and pump failure studies were possible using the 1DVHT model by van Wijk (2016). These modelling techniques are used as inspiration for this research, and expanded to include horizontal pipes. Furthermore, another objective of this thesis is to develop a 1D-Driftflux CFD model for vertical and horizontal flows. The new model contains the same elements for vertical flows as the 1DVHT model, and will be expanded with horizontal pipe flows and will include the key physics which lead to transient flow instabilities.

The development of a 1D-Driftflux model, to simulate pipeline flows with short computational times, also fits within the vision of developing a digital twin of a pipeline. Once fully developed, a 1D-Driftflux based digital twin can run parallel to real pipelines, and give operators more insight on what is happening inside of the pipeline based on a few local sensor measurements. For instance, the 1D-Driftflux model can tell the operator that the increase of a pressure sensor value is caused by a density wave. This vision is beyond the objectives set for this thesis. However, a fast and robust functional 1D-Driftflux model, which incorporates important physical processes, such as inertia, a centrifugal pump model and coupling between the flow and pressure, is the perfect starting point to develop a digital twin of a pipeline based on constitutive relationships.

Finally, the last objective is to gain new insights on how to consider unstable transients in the pipeline design phase, and how to design the pipeline such that the risk of an unstable pipeline system is a low as possible.

1.5. Research questions

The main research question of this thesis is:

How do transients influence slurry flow stability of hydraulic transport pipelines?

To aid in answering the main research question the following sub-questions are formulated.

1. *What are the most impactful transients that affect flow stability?*
2. *What are the physical phenomena responsible for unstable transients?*
3. *How can unstable transients be simulated with a 1D-Driftflux model?*
4. *How can the risk of unstable transients be mitigated in the pipeline design?*

1

1.6. THESIS OUTLINE

THIS section explains the contents and order of the chapters and how the project was executed. The results of the work were published as journal articles, which form the chapters of this thesis. A graphical illustration of the outline of the thesis is given in Figure 1.6.

The project started with identifying which transients are important to consider, answering the first sub-research question. This part has was published as de Hoog et al. (2021) and is given in Chapter 2. The chapter starts with an analysis of instabilities like ripples and dunes found for instance in alluvial flows, and compares these to pipeline flows. Then the main sources of transients in hydraulic transport pipelines are analyzed. Thereafter, the cause of density wave amplification is analyzed using three cases studies. Specifically, density waves that form in horizontal pipes at mixture velocities u_m around the deposit limit velocity u_{dl} ($u_m \sim u_{dl}$), and density waves that form at mixture velocities far exceeding the deposit limit velocity ($u_m >> u_{dl}$).

After finishing the work of de Hoog et al. (2021), the project was split into two parallel tracks, to answer the second and third research sub-questions. The first track focused on experimental research and the second on numerical research. Two large experimental programs were designed. The first experiments of Chapter 3 aimed to study density waves at mixture velocities around the deposit limit velocity ($u_m \sim u_{dl}$). To this end a long horizontal flow loop was built, which was capable of monitoring the development of the waves. The particle size and concentration were varied as part of the study. Specifically, particle volumetric concentrations from $\sim 0.10 - 0.30$ and sizes from $242\,\mu m - 1.08\,mm$. Furthermore, Chapter 3 explains the mechanisms of two types of self-amplifying density waves in horizontal pipes. The first type is called "erosion driven density waves" and the second "sliding bed driven density waves." A secondary objective of this experiment was to generate validation data of self-amplifying density waves in horizontal pipes, to support the development of a 1D-Driftflux model (Chapter 5). This work was published in de Hoog et al. (2024b).

The second experimental program, given in Chapter 5, was specifically designed to measure the erosion of bed layers in a pipeline, to support the development of the 1D-Driftflux CFD model. This work was published as de Hoog et al. (2024a). A special experimental setup was designed where a prepared bed layer could be eroded and monitored by means of electrical resistance tomography. Specific mixture concentrations could be prepared and injected into the system, such that the effect of the concentration on the bed layer erosion could be measured. Mixture volumetric concentrations varied form $0.10 - 0.30$ and particle sizes from $150\mu m - 1.08mm$.

Chapter 4 is the first chapter that is part of the numerical research. The first step was to focus on developing a 1D-Driftflux model that could simulate the density waves encountered in the Freiberg experiments. This research was published in de Hoog et al. (2022), and provides the first clear explanation of this type density waves, and refers to these waves as "transient accumulation density waves." Chapter 4 and de Hoog et al.

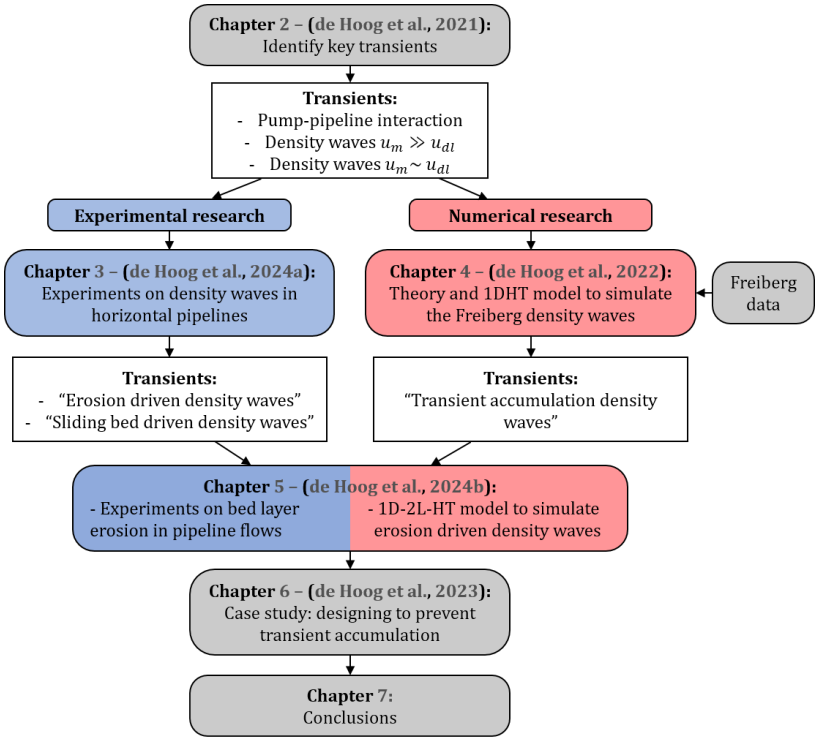

Figure 1.6: The main activities of the project and the associated publications and chapters in the thesis.

(2022) provides the first version of the 1-Dimensional-Hydraulic Transport (1DHT) Drift-flux model.

In Chapter 5 the 1DHT model was expanded with a stationary second layer, resulting in the 1-Dimensional-2-Layer-Hydraulic Transport (1D-2L-HT) model. This model was developed to model erosion driven density waves, where the presence of a bed layer is key. Therefore, the mathematical foundation of the 1DHT model had to be adapted, by incorporating temporal and spatial variations of the numerical cell volume above the bed layer. Another focus of Chapter 5 is the implementation of an erosion model. The 1D-2L-HT model was validated with data from both experimental programs and was published as de Hoog et al. (2024a), including the data of both experiments.

Chapter 6 answers the fourth research question. The validated 1D-2L-HT model is applied to numerically study the effectiveness of three density wave mitigation techniques for transient accumulation density waves, with the goal to answer the fourth research sub question. The mitigation measures are: lowering the diameter of horizontal pipes, using flow feedback control to stabilize the mixture velocity and by applying a electric power drive to the centrifugal pump. These techniques are discussed in terms of their effectiveness, costs and ease of applying the methods in the pipeline design phase.

2

DIFFERENT TYPES OF TRANSIENTS IN HYDRAULIC TRANSPORT PIPELINES

The literature on unstable transients during hydraulic transportation is very limited. Therefore, this chapter starts by analyzing any type of transient found in hydraulic transport pipelines and compares these to instabilities in other sediment transport research fields. For this end, transients are analyzed from centimeter scale ripples and dunes on top of stationary bed layers as found in alluvial flows, to density waves of several hundred meters long in hydraulic transport pipelines, to see where the similarities can be found. Thereafter, this chapter studies what causes fluctuations of the mixture velocity in pipelines, and shows how interaction between the centrifugal pump and the mixture causes velocity fluctuations at various time scales and rates. Finally, this chapter reviews the known theories and cases of density wave amplification and draws a comparison between three case studies, showing that two case studies conform with existing theories, but one case study shows an unknown type of density wave.

*This chapter has been published in the Journal of Hydraulic Engineering **147(9)** (2021).*

2.1. INTRODUCTION

HYDRAULIC transport is the backbone technology in the dredging industry for conveying sand and gravel as it allows for economic transportation of vast volumes of sediments or mining tailings compared to mechanical conveying methods, like using bulk truck carriers or (bucket) conveyors. More recently vertical hydraulic transport is often the preferred choice for transporting ore in most deep sea mining concepts van Wijk (2016), by exploiting mineral rich deposits located on the sea floor, for instance poly-metallic nodules found in the Pacific Ocean.

In horizontal pipes the mixture velocity should remain sufficiently high to avoid grains settling and forming stationary deposits at the bottom of the pipe. In the field of slurry transport the deposition limit velocity u_{dl} is often used by designers as a lower limit for safe transport. First introduced by Durand and Condolios (1952), the deposition limit velocity is defined as the transition velocity when grains first stop moving and form a stationary deposit. A huge improvement in deposition limit velocity prediction came in the form of physical two layer modelling Wilson et al. (2006), which is still being improved for coarse slurries and extended for inclined pipes (Spelay et al. (2016), Matoušek et al. (2019), Vlasák et al. (2020)). Before particles come to a complete stop, particles tend to travel as a shocking and sliding bed, especially coarse sands and gravels. Fine to coarse sand particles become suspended by turbulence at even higher flow velocities.

The design of a pipeline is based on steady state empirical models for slurry pipeline energy losses and energy characteristics for centrifugal pumps. These models are attained under laboratory conditions where mixture velocity and concentration fluctuations are allowed to dampen out. The underlying assumption for using steady state models is that any type of transient is small and does not affect flow stability. However this is not always the case, which became apparent during the construction of the Prins Clausplein motorway junction (the Netherlands) in the 1980's, where sand was transported through a 10 km long horizontal pipeline. An unknown mechanism was responsible for density wave amplification, causing large problems for the centrifugal pump drives and leading to system failures. The density wave amplification effect was studied by Matoušek (1995), Matoušek (1996b), Matoušek (2001), Talmon (1999), Talmon (2002) and Talmon et al. (2007), and now has a good foundation of the theoretical mechanisms causing it, but many questions still remain. Why is density wave amplification not experienced commonly among dredging contractors? Is the effect limited to long pipelines? What are the stability criteria and what is the influence of the centrifugal pump?

The chapter starts by explaining some hydraulic transport concepts needed for the rest of the chapter, like the slip ratio and axial particle velocity variations, and we discuss that these effects cannot lead to density wave amplification. Subsequently, a literature review is presented on small scale density waves in pipelines, which are also encountered in other fields of research, such as alluvial sediment flows. New experiments for developing deep sea mining technology, where manganese nodules are transported in vertical pipelines, show strong density wave amplification. In light of these new experiments, density wave amplification is revisited by first critically reviewing the research into density wave amplification in horizontal pipelines by Matoušek (1995), Matoušek

(1996b), Matoušek (2001), Talmon (1999), Talmon (2002) and Talmon et al. (2007). However, these sources only discuss a density wave amplification effect, which can be considered an internal microscopic slurry process. Additional transients like mixture velocity fluctuation are caused by interaction between the centrifugal pump and energy losses in the pipeline. Local density waves can influence the performance of a centrifugal pump, therefore they have the ability to affect the entire system. In the view of the authors it is important to consider microscopic and macroscopic (system wide) transients separately, since one can lead to the other. Therefore, this chapter discusses centrifugal pump induced transients. Thereafter, three case studies with density wave amplification are presented, one existing case study from literature and two new case studies. We discuss the cause of density wave amplification for each case study, using the theoretical foundation created at the start of the chapter.

2.2. Theory

2.2.1. Slip ratio and axial particle velocity variations

The slip ratio R_s is defined as the ratio between the cross section averaged particle velocity u_s and the mixture velocity u_m.

$$R_s = \frac{u_s}{u_m} \tag{2.1}$$

The mixture velocity definition used by most hydraulic transport researchers is based on the sum of the volumetric flow rate of the solid phase Q_s and the fluid phase Q_f.

$$u_m = \frac{Q_s + Q_f}{A} \tag{2.2}$$

With A being the pipe cross-sectional area. Pipeline design using steady state modelling assumes a constant slip ratio for the entire pipeline, however this is only possible in laboratory circuits and not in field conditions. A pipeline of constant diameter has no axial cross-sectional averaged mixture velocity gradients, because the mixture velocity is based on volumetric flow rate. However, the solids velocity or cross-section averaged solids flow rate can differ locally, as a function of the local concentration. Therefore, we now discuss the effect of axial concentration fluctuations on the local slip ratio in a single pipe with an arbitrary orientation.

The local solids velocity depends highly on the transport flow regime and the local concentration as shown experimentally in horizontal pipes by Matoušek (1996b). Axial variations in local solids velocity, due to concentration differences, is referred to as axial differential slip. For vertical flows van Wijk et al. (2014) show that the solids velocity and slip ratio can be estimated well using the hindered settling velocity v_{hs} Richardson and Zaki (1954), under the assumptions that friction due to particle-wall contact is low and a radial homogeneous concentration distribution of the material is present. This assumption is proven to be reasonable for coarse slurries at high concentration in a 100 mm pipe Vlasák et al. (2020), but might not be valid at low volumetric concentration (< 0.03) in very small pipes ($< 30.6\,mm$), as lift forces are shown to cause a non-uniform radial distribution of the concentration (Alajbegović et al., 1994, Messa and Malavasi,

2014). Assuming a homogeneous radial concentration distribution, the solids velocity for vertical pipes is estimated as follows:

$$u_s = u_m - v_{hs} \tag{2.3}$$

$$R_s = \frac{u_m - v_{hs}}{u_m} \tag{2.4}$$

With v_{hs} being the hindered settling velocity of the particles, which requires correction if the particle diameter d is large relative to the pipe diameter D as follows (Richardson and Zaki (1954), van Wijk (2016)):

$$v_{hs} = 10^{-d/D} v_{ts} (1-c)^n \tag{2.5}$$

The dependency of v_{hs} on the volumetric concentration c shows that the slip ratio in vertical pipes is also a function of the local volumetric concentration. For ascending vertical pipes the slip ratio is always lower than 1, while for descending pipes the slip ratio is always larger than 1. For both vertical and horizontal pipes, the limit of the slip ratio for increasing mixture velocity approaches 1.

Now we consider the axial spatial average slip ratio in pipes at different orientations that do not have axial concentration variations, thus assuming steady-state flow. This is different from what is explained above, where we considered a single pipe having axial differential slip, caused by spatial concentration variations. The spatial averaged slip ratio is higher in vertical pipes compared to horizontal pipes, at the same concentration, particle size and pipe diameter. In particular, coarse particles in horizontal pipes are subject to high frictional losses as they are transported as a sliding bed or as bed-load. In vertical pipes frictional losses are lower because particle contact with the pipe wall is much less frequent. As such, particles travel faster in vertical pipes (given the same mixture velocity and concentration), compared to horizontal pipes of the same diameter. Thus in a hypothetical circulating flow loop with a vertical ascending pipe and a vertical descending pipe, connected to each other by two horizontal pipes, where the mixture velocity is steady (in time) and no density waves are present, the particles travel fastest in the descending pipe, followed by the ascending pipe and slowest in the horizontal pipes.

Another consequence of axial differential slip, due to axial concentration waves, is a direct influence on the shape of a density waves for both horizontal (Talmon et al., 2007) and vertical pipes (van Wijk, 2016), which is a sawtooth shaped wave once fully developed. Specifically, if the particle velocity increases with increasing concentration, then the leading front of a density wave has a higher spatial density gradient than the tail. This is shown experimentally by Talmon et al. (2007), and numerically by Talmon (1999) using a modified Burger's equation and modelling the solids velocity u_s as a function of the concentration through the slip ratio R_s.

$$\frac{\partial c}{\partial t} + \frac{\partial}{\partial x}(R_s u_m c) = \frac{\partial}{\partial x}\left(\epsilon \frac{\partial c}{\partial x}\right) \tag{2.6}$$

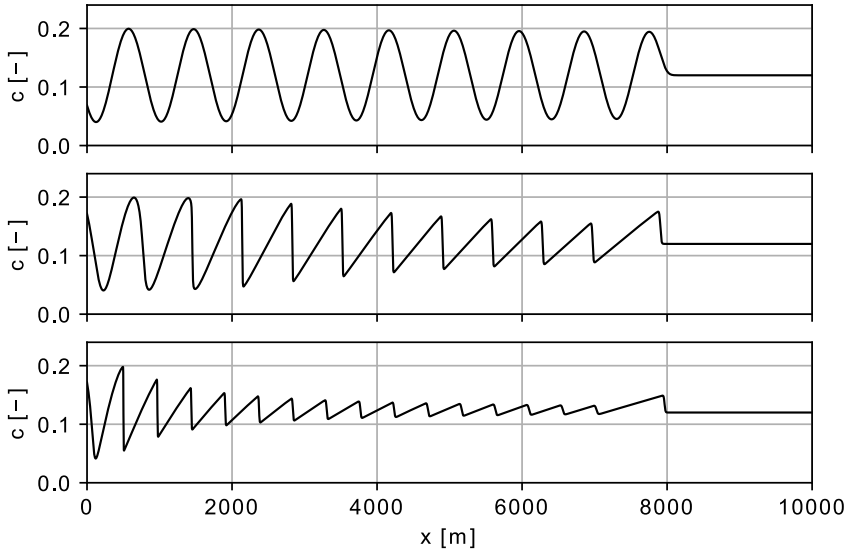

Figure 2.1: The solution of Equation 2.6. The spatial distribution of concentration at a given time, starting with a variable sinusoidal inlet on the left (average $c = 0.12$, amplitude $c = 0.08$) at a mixture velocity of $u_m = 3.5\,m/s$. Top: no variable slip. Middle: moderate variable slip, $\alpha = 0.7$ and $\beta = 0.8$ (Eq. 2.7). Bottom: high variable slip, $\alpha = 0.33$ and $\beta = 1.84$.

.

This equation provides a rudimentary method to study the development of the volumetric concentration c transported at a fixed mixture velocity u_m and with axial dispersion modeled through a diffusion coefficient ϵ. Axial dispersion can be modeled for instance according to Taylor (1954) for small particle homogeneous mixtures or according to van Wijk (2016) for vertical flows (Equation 2.5). To visualize the sawtooth shaped waves resulting from Equation 2.6, the slip ratio is modeled linearly against the data of Matoušek (1996b) using constants α and β.

$$R_s = \frac{u_s}{u_m} = \alpha + \beta c \tag{2.7}$$

Independent on the choice of slip ratio model, either linear or a more accurate nonlinear model, Equation 2.6 always produces saw tooth shaped waves under the condition that the particle velocity is a function of the local concentration (see Figure 2.1). In horizontal pipes axial variations in slip, due to concentration differences, are larger for low mixture velocities, because at high mixture velocities the variation of axial slip becomes significantly smaller Matoušek (1996b). Initially, it was thought that axial differential slip directly causes density wave amplification; however, by solving the modified Burger's of Talmon (1999) we can show that variable slip actually causes damping of density waves and modelling stronger slip causes more damping (see Figure 2.1).

Note that u_s, and therefore R_s, is based on the average velocity of all particulate

species in the mixture. van Wijk et al. (2015) shows that for vertical hydraulic transport, it is important to consider the velocity differences of mixture species, as small particles overtake larger particles, which can result in density wave growth under very specific circumstances. The difference in species velocity is also important for the minimum transport velocity in vertical pipelines, as too low mixture velocities can cause separation of species as they travel through the vertical pipeline. Density wave growth and plug formation was shown for bimodal slurries if small particles overtake larger species at extremely high volume concentrations (>0.40) and if the smaller species is too large to pass through the pores of the larger densely concentrated particles. However, under normal realistic operational velocities and concentrations, when transporting natural sediments, plug formation due to difference in mixture species velocity does not occur in vertical pipes (van Wijk et al., 2015).

2.2.2. RIPPLES AND DUNES IN PIPELINES

AXIAL density fluctuations in a horizontal pipeline are found at various scales and are caused by either fluctuating boundary conditions or internal slurry processes. Large scale fluctuating boundary conditions include changing pipeline inlet sediment flux and energy losses over time, which are especially common in dredging due to changes in excavation layer thickness, or cyclic operational maneuvers of a dredger (i.e. the stepping and swinging of a cutter suction dredger).

Microscopic slurry instabilities manifest as axial density variations, triggered by tiny perturbations of the bed height or slurry concentration. At the lowest velocities in a horizontal pipeline (far below the deposition limit velocity) coarse material at very low concentrations travels through the pipeline as tiny isolated dunes (centimeters to tens of centimeters in size). Franklin and Charru (2009) report on the formation of Barchan dunes in wide rectangular closed-conduits, but these have never been observed in pipelines, probably because pipelines are narrow and circular. However regular shaped isolated dunes are present in pipelines. Fluid shear forces over the dune cause material to travel over the dune as bed-load transport and is deposited in the low velocity wake of the dune. New material is eroded at the front of the dune, thereby propagating the dune forward. In dredging and mining pipelines sediments are transported almost exclusively at high volumetric concentrations (> 0.20), therefore at low velocities isolated dunes connect and form a continuous bed layer with a wavy surface (Matoušek and Krupička, 2013), which can be described as ripples which are of similar scale as the isolated dunes. Kennedy (1969) described ripple formation to be caused by an "orderly pattern" of erosion and sedimentation over height differences in the bed layer. Kennedy (1969) and Charru and Hinch (2006) attributed this instability to a phase lag component of the fluid shear stress over a wavy surface, as inertia dictates that the fluid cannot instantaneously follow the shape of a wavy surface. This causes a wake and deposition of material behind the crests, while most material is eroded from the top of the crest where shear is highest.

The microscopic density fluctuations explained above can occur in both closed conduits or open channel flows and in steady or unsteady flows when certain conditions for the bed shear stress versus particle diameter are met (Southard, 1991). However, these processes in pipelines only occur for velocities far below operational conditions and are

of small insignificant scale to affect the stability of the pipeline operation. The ripples and dunes are limited in size and amplitude, and once the fluid velocity is increased to operational levels, either the bed layer fully erodes or starts sliding when the bed's static friction with the pipe wall is overcome. The sliding bed conditions differ significantly from ripple or dune related instabilities. In addition, the scale of ripples and dunes is very small compared to large scale density waves found in pipelines, which can be hundreds of meters long (depending on the system's length). Therefore, comparing pipeline instabilities at high flow velocities with those encountered in alluvial flows at low velocities is not trivial.

2.2.3. LARGE SCALE DENSITY WAVE AMPLIFICATION IN PIPELINES

LARGE scale density wave amplification is known to occur in horizontal hydraulic transport pipelines. The first well researched case was the Prins Clausplein pipeline system, a 10 km long and 650 mm diameter pipeline delivering medium sized sand (more details further in the chapter). The system was fed with a relatively stable supply of sand at an average volumetric concentration of ~ 0.18. The sediment was redistributed as it traveled through the pipeline, becoming concentrated in density peaks with a wave length of ~ 680 m and an amplitude of over 0.30. This case was first studied by Matoušek (1995) and Matoušek (1996a), the mathematical instability was hypothesized by Talmon (1999) and Talmon (2002), and experimentally investigated by Talmon et al. (2007). The instability is referred to as the erosion and sedimentation imbalance.

Erosion and sedimentation balances are used to study and predict the growth or erosion of sediments layers on large scales like in river and coastal flows (van Rijn et al., 2019), and are also found to be useful in other applications in the dredging industry, for instance the sedimentation of sand in hopper suction dredgers (van Rhee, 2002). The erosion and growth of the bed layer can be described as a vertical sedimentation velocity of the bed top v_{sed}, which is governed by an erosion and sedimentation balance.

$$v_{sed} = \frac{S - E}{\rho_s(1 - n_0 - c_{nb})} \tag{2.8}$$

With S being the sedimentation flux, E the erosion flux, ρ_s the grain density, n_0 the porosity of the bed layer and c_{nb} the volumetric concentration of the suspended sediment flow above the bed layer, the near bed concentration. When the erosion flux is smaller than the sedimentation flux, the bed grows, and the bed erodes when the opposite is true. The sedimentation flux can be estimated as follows:

$$S = \rho_s v_{ts} c_{nb} \tag{2.9}$$

Where v_t is the terminal settling velocity of a particle. The erosion flux can be estimated using empirical relationships; for instance those found in van Rhee (2010), Bisschop (2018) and van Rijn et al. (2019). These relationships show that erosion is a function of the bed shear stress, which is mainly a function of the flow velocity over the bed and the particle size. Equation 2.9 is only valid for very low concentration suspensions. Furthermore, both sedimentation and erosion fluxes are increasingly limited for higher

concentrations of the suspension. For the sedimentation flux the hindered effect is often modeled using the Richardson and Zaki (1954) hindered settling principle:

$$S_h = S(1 - c_{nb})^n \tag{2.10}$$

where S_h is the hindered sedimentation flux and m is the hindered settling exponent with a value between $2.36 < n < 4.7$ Rowe (1987). The hindered sedimentation flux rises quickly with increasing concentration up to a maximum value of around 0.20, after which the sedimentation flux drops, due to hindered settling (see Figure 2.2 top). Hindered erosion E_h can be modeled as presented by van Rhee and Talmon (2010):

$$E_h = E\frac{1 - n_0 - c_{nb}}{1 - n_0} \tag{2.11}$$

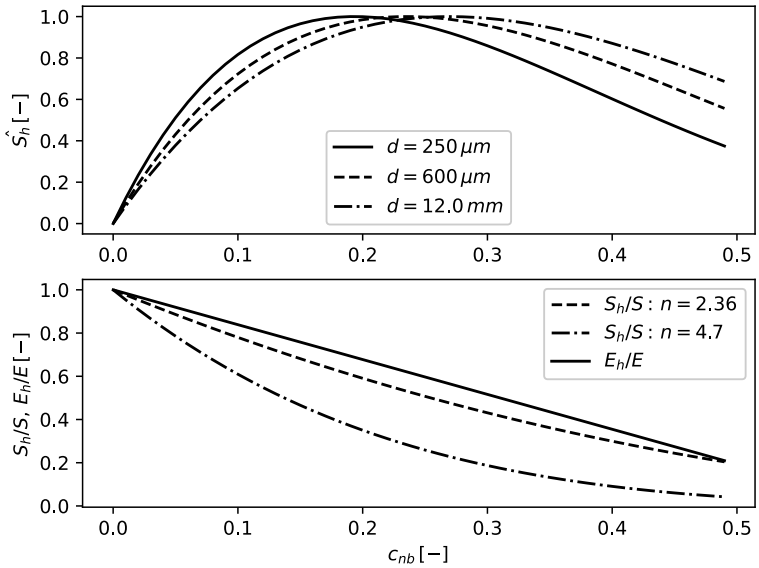

Figure 2.2: Top: the normalized sedimentation flux ($\hat{S_h} = S_h/max(S_h)$) for three particle diameters d. Bottom: the particle concentration hindered effect on the erosion and sedimentation fluxes, where the sedimentation flux is a function of the Richardson and Zaki (1954) settling exponent n.

Without knowing the exact value for E, we can still compare the effect of the hindrance terms in Equations 2.10 and 2.11. This is shown in Figure 2.2 (bottom), where the ratio's $\frac{S_h}{S}$ and $\frac{E_h}{E}$ are plotted as a function of c_{nb}. Figure 2.2 shows that the hindrance terms of Equation 2.10 are always smaller than the hindered effect in Equation 2.11, for all values of n (n modeled according to Garside and Al-Dibouni (1977)).

To summarize, erosion is a function of mixture flow related parameters: the flow velocity and the concentration, whereas sedimentation is only a function of particle parameters and the concentration. Therefore, at high flow velocities erosion will always dominate sedimentation and as a result no deposition will occur in a pipeline. The balance between erosion and sedimentation becomes more interesting at lower velocities where the concentration determines which is highest. Miedema et al. (2003) show how in a two layer pipeline model the bed shear stress, and consequently erosion, increases as a function of the amount of transported material. Combined with the fact that the sedimentation flux drops beyond a concentration of ~ 0.20 and the effect of hindered sedimentation is always larger than hindered erosion (as explained above), this creates a situation where erosion is higher than sedimentation for high suspended concentrations. This means that, depending on the local concentration in a pipeline, the flow can favor either erosion or sedimentation. More specifically, at low concentration ($<\sim 0.20$), sedimentation is dominant and density waves are damped out, as material settles out of suspension. At high concentration ($>\sim 0.20$) erosion is dominant and density waves tend to grow, as material is entrained from the bed layer into the flow. The underlying cause of density wave amplification in pipelines was first theorized to be the sedimentation and erosion imbalance by Talmon (1999) by means of linear stability analysis of a system with a stationary bed and suspended flow. Talmon (2002) stated that density wave amplification is also possible in case of a sliding bed layer. In conclusion, the density wave amplification mechanism is only possible when two conditions are met. The first condition is a high suspended concentration, while the second condition requires a source of material for the density waves to grow in the form of a stationary or a sliding bed layer. Once the stationary or sliding bed layer is fully eroded the density wave cannot grow further and amplification ceases.

So how does the density wave amplification mechanism express itself in hydraulic transport? Obviously density wave amplification through the erosion and sedimentation imbalance, requires a horizontal or inclined section in the pipeline where stationary deposits can be formed. Matoušek and Krupička (2013) described a smooth transition from a stationary to sliding bed for low concentrations. However, for high concentrations the bed starts shocking and sliding intermittently, with parts of the bed in motion and other parts being stationary. This type of density wave mimics the movement of a caterpillar, with the crest of the wave being mobile and troughs being stationary. This transient behavior is caused by the imbalance between sedimentation and erosion as explained above. At high concentration, erosion is dominant over sedimentation and because the eroded material is suspended, it experiences less friction and travels faster. This eroded material is transported forward and increases the concentration further down the pipe, which again triggers the imbalance and propagates the crest of the density wave forward. The bed layer height behind the crest is lower due to the local heavy erosion. The thinner bed experiences a smaller bed shear force and the bed stops sliding. The motion of the caterpillar density wave can also be explained by the deposition limit velocity, which decreases with increasing concentration. This inverse relationship of the deposition limit velocity with the local concentration can be predicted mathematically using two-layer modelling Wilson et al. (2006) and has also been observed during experiments

Matoušek (1997). Thus the crest of the density wave has a higher concentration, therefore a lower deposition limit velocity and can become mobile, while the low density tail remains stationary.

The initiation of the density wave amplification was measured specifically in Talmon et al. (2007), where intense density waves formed at high concentrations, when the mixture velocity was decreased slowly to just above the deposition limit velocity. The density waves were saw tooth shaped (due to variable slip) and had a wave length similar to the system length. At higher velocities the bed layer was fully eroded and the system was stable. A characteristic of these experiments was the rapid onset of the density waves, as the amplitude grows to an equilibrium maximum in just three to four passes through the closed circuit loop. The equilibrium maximum of the wave amplitude was also experienced by Matoušek and Krupička (2013).

2.2.4. CENTRIFUGAL PUMP INDUCED TRANSIENTS

IT is a well known fact that the energy provided by a centrifugal pump, in an idealized case and if the drive has sufficient power, increases when the density of the mixture increases. In contrast when the drive has insufficient power, the mixture velocity reduces (Wilson et al., 2006). This interaction between density waves and energy delivered by the pump has to date never been mentioned nor analyzed in the density amplification literature, but can definitely contribute to the initiation of the density wave amplification. Therefore, it is important to analyze in detail the contribution of the centrifugal pump(s) to pipeline transients. The following analysis is valid for both vertical and horizontal pipes.

The energy delivered by a centrifugal pump is converted into potential energy (pressure) and kinetic energy (velocity) and balances the energy lost due to friction over the pipeline, resulting in a certain flow rate referred to as the system's operating point (see Figure 2.3). The pressure and flow rate changes frequently, as the material flux injected into the system varies over time due to varying operating conditions. Variable field conditions, such as the thickness of the layer excavated by the dredger, will result in mixture density variations flowing into the system. More material influx will cause higher frictional losses in the pipeline as the material flows through the pipe, decelerating the mixture. Additionally, a change in mixture density in the pump accelerates the mixture, as the increased density results in higher pump pressure, a fundamental principle of centrifugal pump operation (Wilson et al., 2006). Summarizing, the mixture velocity in a hydraulic transport system changes due to interaction with the centrifugal pump in two ways: a shift of the operating point due to changing frictional losses and a change of operating point due to increase of density in the pump. But which of the two is dominant and more frequent?

To answer this question, let us consider a system with a length L, a centrifugal pump close to the inlet and an average flow velocity of u_m. Initially the system is only filled with water at density ρ_f. At some point in time grains are injected at the inlet and the mixture density rises to ρ_m. As the mixture is advected through the pipeline, resistance and en-

ergy losses increase over time. This can be expressed as a change in pressure needed to pump the slurry through the pipeline, dp_m/dt, which is proportional to the change in density and the time required for the material to travel through the system T. Moreover T is a function of the system length L and the mixture velocity u_m. Illustrative values are $L = 5\,km$, $u_m = 5\,m/s$, $\rho_f = 1000\,kg/m^3$, $\rho_m = 1200\,kg/m^3$. The order of magnitude of the pipeline frictional pressure drop p_m changing over time is as follows:

$$\frac{dp_m}{dt} \propto \frac{\rho_m - \rho_f}{T} \propto (\rho_m - \rho_f)\frac{u_m}{L} \sim \mathcal{O}(10^{-1})\,\frac{Pa}{s} \tag{2.12}$$

It must be noted that Equation 2.12 is accurate for suspended mixtures (in a vertical or horizontal pipe), but for coarser horizontal sliding bed mixtures the change of friction losses is higher than $(\rho_m - \rho_f)/T$ due to additional Coulomb friction. However, it is not an order of magnitude higher, and therefore the results of this analysis remain valid. Furthermore, once the pipeline is filled, $\frac{dp_m}{dt}$ practically reduces to zero if the average mixture density is constant, regardless of the magnitude of the frictional pressure losses.

The change in pressure due to a density wave passing through the pump is directly proportional to the change in density and the typical period of density waves. In dredging the period of density wave fluctuation T_w is related to for instance the swinging motion of a cutter suction dredger, or to the thickness change of the excavated layer, thus in the order of seconds to minutes. When these fluctuations pass through the centrifugal pump the pressure is affected instantaneously. The order of magnitude of the pump pressure p_p change over time equals:

$$\frac{dp_p}{dt} \propto \frac{\rho_m - \rho_f}{T_w} \sim \mathcal{O}(10^1)...\mathcal{O}(10^2)\,\frac{Pa}{s} \tag{2.13}$$

This shows that the change of the pump pressure over time is significantly larger than the change of pipeline resistance over time with a fluctuating inlet density, especially for very long pipeline systems. This analysis is valid for a slurry system which starts with water, but once filled with sediments the average mixture density can be said to be constant in time, with some variations in space due to varying pipe inlet density. As a result, the average pipeline resistance is also constant in time. Consequently, a change in mixture velocity is dominated by density fluctuations passing through the centrifugal pump. Do note that the magnitude of mixture velocity changes is also influenced by the inertia of the slurry.

A density wave will only increase the pump pressure if the drive of the pump has sufficient power to maintain the impeller speed as the density wave passes. Drives can either be diesel engines with variable speed control or electric engines. When a diesel engine operates at maximum load it is characterized by delivering constant torque; therefore as the density wave passes the impeller speed will decrease, together with a decrease of mixture velocity. An electric drive has the advantage of operating at constant mechanical power at maximum load; therefore, as a density wave passes the hydraulic power is sustained, assuming the efficiency is unaffected. Consequently, even if the impeller speed drops, the mixture velocity remains unaffected with a electric driven pump Wilson et al. (2006), again assuming the pump efficiency remains unaffected. However, the

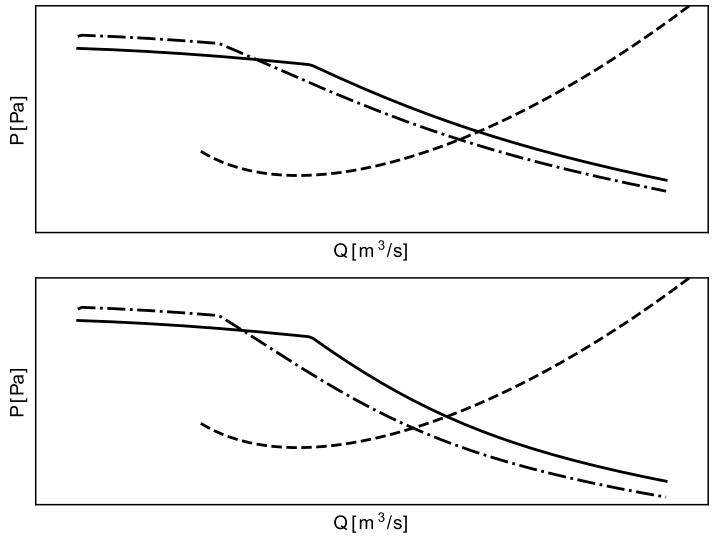

Figure 2.3: Pipeline resistance curves (dashed) and pump characteristics at high concentration (dash-dotted) and low concentration (solid). Top: pump with an electric drive (constant power). Bottom: pump with a diesel drive (constant torque).

efficiency of the pump is also affected by the increase of particles in the pump known as head reduction, see for instance Stepanoff (1965). Therefore, even for electric drives the mixture velocity reduces as a density wave passes, but the reduction is still not as large in comparison with a diesel drive. These effects can be seen in Figure 2.3 where pump curves are calculated using the Stepanoff (1965) head reduction factors.

2.3. Cases Studies: Density wave amplification in pipelines

2.3.1. Case study: Prins Clausplein

In 1981 the highway intersection Prins Clausplein was constructed close to the Hague, the Netherlands. Medium to fine sand was provided by means of a 10 km long, 650 mm diameter hydraulic transport system. A cutter suction dredger was positioned at the pipeline inlet and three additional pump booster stations were needed along the pipeline to overcome friction losses. The sand was injected into the system with inlet concentrations varying between $0-0.25$ and the mixture velocity varied between $2.5-3.5\,m/s$. The exact deposition limit velocity of the system was not measured, although Talmon (1999) did state that transport took place at velocities just above the deposition limit velocity, confirmed by later modelling Matoušek (2001). The sand had a broad distribution with 12% being smaller than 75 μm and 7% larger than 700 μm. The mass median particle diameter d_{50} varied over time, between 150 μm and 300 μm.

The system was subject to density wave amplification, measured by three density meters positioned at the dredger and diesel powered booster stations. The first density meter was onboard the dredger, the second and third density meters were positioned at a booster station located at 1866 m (Jagerplas) and 6538 m (Duinjager) along the pipeline. Figure 2.4 shows an example of data recorded during transport operations. The x-axes of the density graphs in Figure 2.4 are shifted in time to visualize the development of the waves. In Figure 2.4 the mixture velocity varied between $2.7 - 3.5\, m/s$, which is mainly caused by variations in pump pressure as explained at the start of this chapter.

Figure 2.4 shows a low density mixture entering the pipeline between 14:30h and 15:30h. At Jagerplas a noticeable reduction in density of the same part is visible and at Duinjager no material is present at all and only water passes. All material entering the pipeline between 14:30h and 15:30h is relocated to other parts in the flow. The same is occurring for the material entering at 16:30h. The material accumulates in density waves and is found in density peaks measured by Duinjager at 14:45h and 16:15h. The maximum of the density waves recorded at Duinjager were higher than 1500 kg/m^3 (the limit of the density meter). This type of flow is highly undesirable for two reasons. Firstly, the risk of blockage is very high, due to the high concentration, and secondly the diesel driven booster stations cannot cope with strong density waves. If a booster pump fails, the mixture velocity drops instantly, creating more deposits in the pipeline and intensifying the density wave growth.

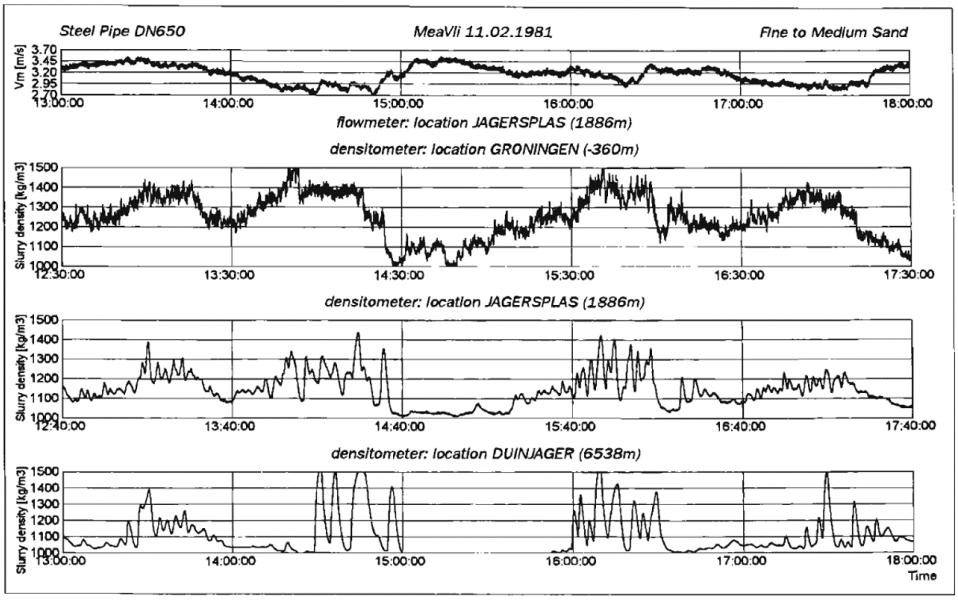

Figure 2.4: Hydraulic transport data acquired in the Prins Clausplein pipeline. Top: The mixture velocity measured and below the mixture density at three locations along the pipeline. Source: Matoušek (1996), reused with permission.

The cause of the density wave amplification was first investigated by Matoušek (1995), Matoušek (1996b) and Matoušek (1996a), and was thought to be caused by axial differential slip due to axial concentration differences. The hypothesized mechanism for density wave amplification was explained as: high concentration density waves over take lower concentrations, thereby absorbing the low concentration density wave and causing material accumulation. Equations 2.6 and 2.7 can be used to investigate this hypothesis (Talmon, 1999), which shows that axial differential slip dampens density waves (as explained in Section 2.2).

Talmon (1999) mathematically proved that the effect of erosion and sedimentation imbalance causes density wave amplification, as explained in the theory section of this chapter. Talmon (1999) modelled the slurry as two layers, with the lower layer being stationary and acting as the source for amplification. Talmon (1999) showed using linear stability analysis that perturbations of the suspended concentration lead to density wave amplification. The stability analysis also showed that density waves with a wave length of $\sim 680\,m$ amplify the most and smaller wave numbers are damped due to axial dispersion. The largest amplification wave of $680\,m$ is close to that observed in the Prins Clausplein pipeline data. Talmon (2002) extended the linear stability analysis by including a sliding bed layer, which shows the strongest amplification for $\sim 250\,m$ long waves.

As previously explained, the conditions required for density wave amplification are: A high suspension concentration (to trigger the erosion sedimentation imbalance) and a sediment source in the form of a stationary or sliding bed layer. For the Prins Clausplein pipeline the first condition is easily met as the inlet concentration is typically between $0.12-0.25$. Closed loop experiments conducted by Talmon et al. (2007) showed that density waves are formed when the mixture velocity is dropped close to the deposition limit velocity, which is also the operating point of the Prins Clausplein pipeline. A more extensive analysis of the data compared to two-layer modelling in Matoušek (2001) showed that occasionally stationary deposits were formed in the pipeline, because the mixture velocity sometimes dropped below the deposition limit velocity. The fluctuating mixture velocity can be attributed to density variation in the centrifugal pump, expressed as variations in mixture velocity and pump pressure as explained in the theory section of this chapter. Therefore, a source for density wave amplification is present in the form of sporadic deposits, caused by intermittent low mixture velocities. Both conditions for density wave amplification are met and density waves are able to grow through the erosion and sedimentation imbalance. Once these density waves have grown to a large amplitude, their interaction with the centrifugal pump can cause the system's mixture velocity to drop if the wave passes through booster pumps downstream of the pipeline. This is supported by data shown in Figure 2.4, where the mixture velocity decreased when strong density waves passed Duinjager from 14:45h to 15:00h. The mixture velocity recovers once the density waves have passed beyond Duinjager at 15:00h. A slight mixture velocity drop is also experienced around 16:20h, which coincided with density waves passing Duinjager.

This test case shows the importance of the centrifugal pump interacting with the density waves. This interaction can lead to the first density waves if the mixture velocity drops below the deposition limit velocity. In addition, once the density waves have formed, they can continue to initiate amplification if they flow through pumps farther

down the pipeline. Under these circumstance the system continues to self-excite density waves. By keeping the mixture velocity constant and above the deposition limit velocity, this self-exciting cycle can be disrupted. This can be achieved through feed back control; however, only if the pump drive is designed to cope with the added torque due to the density waves.

2.3.2. CASE STUDY: LAZY WAVE S-BEND

ONE of the challenges in the development of vertical hydraulic transport technology for deep sea mining is the slurry flow through a flexible lazy wave S-bend located at the bottom of the vertical riser. The lazy wave bend connects the excavation vehicle to the vertical hydraulic transport system and compensates for any movement of the two. Concerns regarding flow assurance require investigation of the shape of this bend and its relation to the deposition limit velocity. To this end an experimental setup was built in 2016 with an internal diameter of 100 mm. Various geometries for an S-bend were tested to study the effect of the S-bend shape on the deposition limit velocity. One of these geometries is shown in Figure 2.5, which is a scaled down and idealized geometry compared to a full size deep sea mining pipeline. The flow regime in the experiment was ensured to be the same as expected at full scale, being a sliding bed flow regime, as sliding bed flow regime is prevailed in case of particles as large as manganese nodules. As such, the experiments show the same phenomena as in the full scale deep sea mining pipeline, such as where and how deposits form in the S-bend.

Tests were conducted with two narrowly graded gravels with $d_{50} = 6.3\,mm$ and $d_{50} = 12\,mm$ (particle size distribution given in Figure 2.6). The mixture velocity was measured using a Krohne optiflux 4000 flow meter and the slurry concentration was measured using a conductivity based concentration sensor at the inlet and outlet of the S-bend. As part of the tests the mixture velocity was increased from below the horizontal pipe deposition limit ($0.75\,m/s$ and $1.28\,m/s$ for the 6.3 and 12 mm gravel, respectively) to the maximum system velocity of $5\,m/s$.

The S-bend flow loop has a considerable number of vertical and inclined segments. When decreasing the mixture velocity the first deposit is created in the lower bend of the S-bend (shown with an ellipse in Figure 2.5) at a mixture velocity of 1.9 m/s and 1.8 m/s for the 6.3 mm and the 12 mm gravel, respectively. Therefore, the deposit in the lower bend dictates the deposition limit velocity for the entire system. On several occasions density wave amplification occurred with two cases presented in Figure 2.7. During the test shown in Figure 2.7a and 2.7b the average mixture velocity (1.3 m/s) was just above deposition limit velocity of the horizontal pipes ($u_{dl} = 1.28 m/s$). Therefore, density wave amplification is possible through the erosion and sedimentation imbalance as conditions are similar to Talmon et al. (2007). The wave length of the density wave roughly equaled the system length, as also observed by Talmon et al. (2007). However, the density wave growth rate was significantly lower compared to Talmon et al. (2007). This can be explained by the presence of vertical pipes in the S-bend flow loop, which account for over half of the system length. Effectively only half of the system can

contain stationary deposits, and therefore only half of the system is involved in density wave amplification. In the Talmon et al. (2007) system, where vertical pipes were absent, the whole loop contributed to density wave amplification, therefore the growth rate is higher. Furthermore, axial dispersion in vertical pipes is low for gravels (van Wijk et al., 2014). Therefore, the density waves were relatively unaffected when flowing through the vertical pipes in the S-bend loop, neither growing or dispersing significantly. However, with fine sands the vertical parts could have created a damping effect, since fine sand experiences significant smoothing by axial dispersion.

During the tests presented in Figure 2.7c and 2.7d the mixture velocity was on average 1.8 m/s, well above horizontal pipe's deposition limit. On this occasion no deposits were present in the horizontal parts, but only a small deposit is located in the lower bend of the S-bend. This deposit was observed to cyclically erode and grow in unison with the passing of the density wave. The deposit eroded when the crest of the density wave passed and grew with the passing of the tail; behavior similar to caterpillar waves caused by the erosion and sedimentation imbalance (as explained in Section 2.2). The growth rate of the density wave was even lower compared with the previous experiment, because the only deposit feeding the density wave was small. Growing density waves were never encountered for velocities above 2.2 m/s, as above this velocity no deposit was present in the lower bend. The stability of the system was therefore directly related to the deposition limit velocity (as with the Prins Clausplein case), however the designer needs to carefully evaluate in which component the deposition limit velocity is highest,

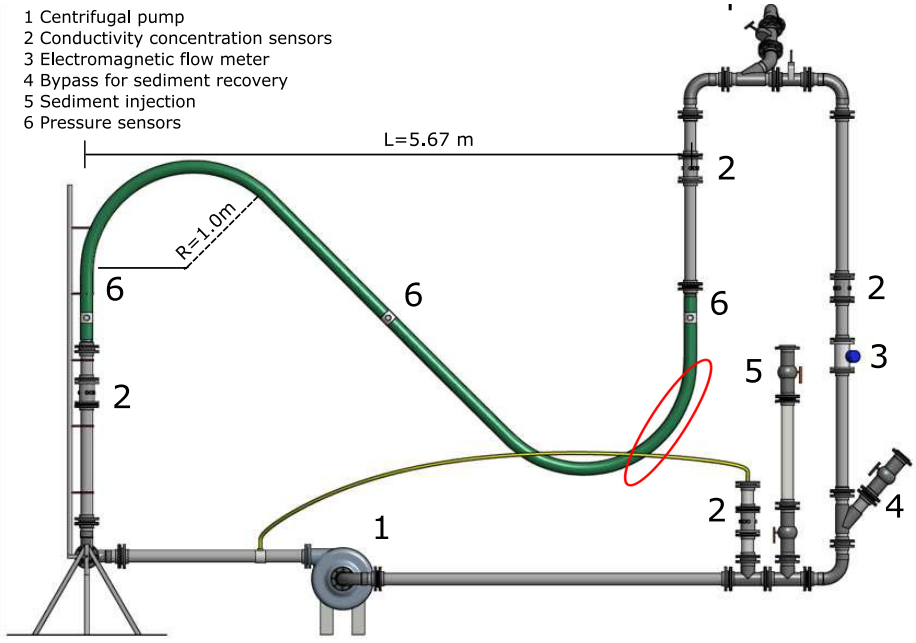

Figure 2.5: The Lazy wave S-bend flow loop. Flow is from right to left through the centrifugal pump and the ellipsis shows the location of the deposit at the highest velocity (at an upwards inclination of ~ 55°).

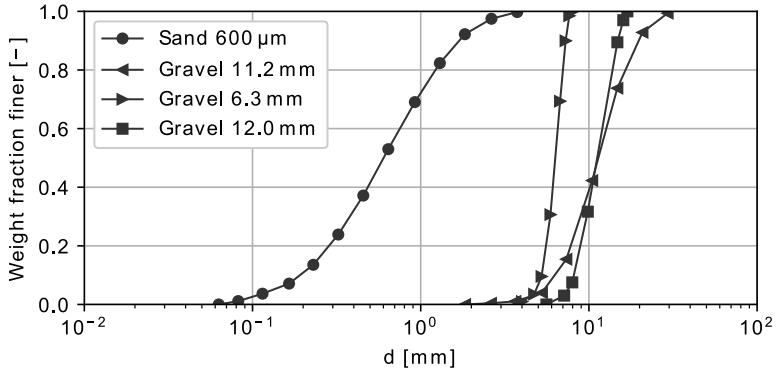

Figure 2.6: The particle size distributions used in the Lazy wave S-bend flow loop and the Freiberg system.

because even a small local deposition can lead to density wave amplification and influence the entire system.

2.3.3. Case study: The Freiberg vertical hydraulic transport experiments

Another case where transients induced flow instability was during vertical hydraulic transport experiments conducted in the summer of 2017 for Blue Mining by a team of TU Bergakedemie Freiberg and Royal IHC in Halsbrücke, Germany. The aim of the measuring campaign was validation of transport and flow assurance models to be used for deep sea mining. This medium scale setup was a closed circuit loop, built in a vertical mine shaft, consisting of a 121 m long riser and a 121 m long descending pipe with an internal diameter of 150 mm. Additionally, 57 m of horizontal pipe was needed to facilitate the pump and separation equipment. Further details of the setup can be found in Mueller et al. (2018). Tests were conducted using 600 μm sand and 11.2 mm gravel at volumetric concentrations of 0.05, 0.10 and 0.15 and their particle size distributions can be found in Figure 2.6. Measured parameters included the mixture velocity and delivered concentration c_{vd}, for which the latter is defined as the ratio of the solids volume flow rate over the total mixture flow rate.

In a flow loop consisting of a mix of horizontal and vertical pipes, the solids velocity is lowest in the horizontal pipes for coarse mixtures, because for coarse mixtures the slip ratio strongly depends on the mixture velocity, concentration and also pipe orientation. Moreover, these slurries show a degree of stratification in the horizontal pipe and, as such, energy losses are higher due to more particle-particle and particle-wall contact, lowering the solids velocity. Consequently the horizontal pipes define the lower limit of operational mixture velocities, therefore the Freiberg system was designed such that the mixture velocity could be kept far above the deposition limit velocity of the horizon-

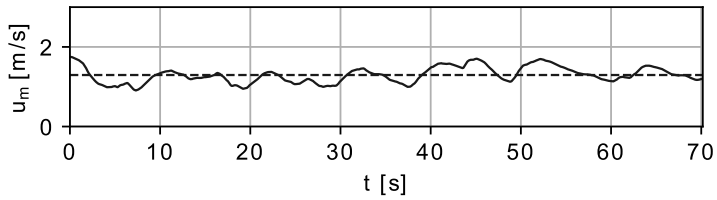

(a) Density wave growth at low velocity. Mixture velocity over time, $d_{50} = 6.3\,mm$.

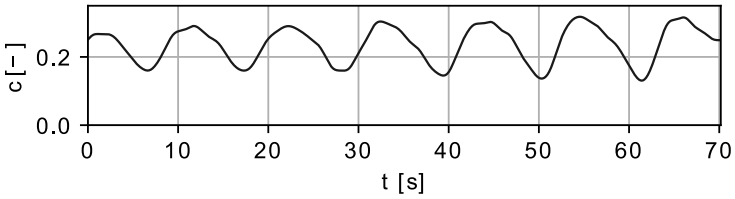

(b) Density wave growth at low velocity. Concentration over time, $d_{50} = 6.3\,mm$.

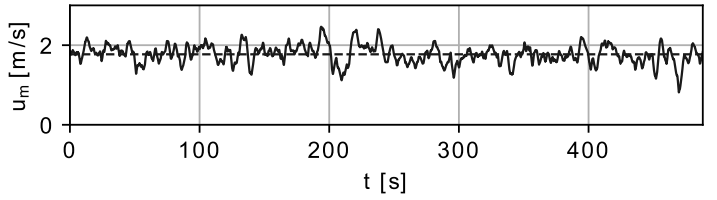

(c) Density wave growth at high velocity. Mixture velocity over time, $d_{50} = 6.3\,mm$.

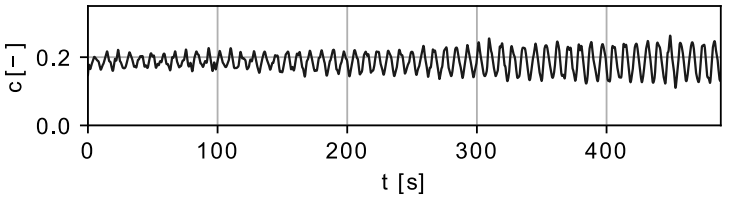

(d) Density wave growth at high velocity. Concentration over time, $d_{50} = 6.3\,mm$.

Figure 2.7: Growing density waves in the S-bend loop.

tal pipes. The horizontal deposition limit velocity of the 600 μm sand is ~ 2.5 m/s and for the 11.2 mm gravel ~ 1.5 m/s. At the beginning of each test the mixture velocity was kept at ~ 4.5 m/s and material was injected slowly to ensure a homogeneous distribution throughout the system. Despite these conditions density wave amplification took place. Figure 2.8 shows time traces of the measured velocity (measured at the riser outlet) and delivered concentration of two tests at different particle sizes. The delivered concentration was measured at the bottom of the riser and down going pipe, using a U-loop differential pressure measurement Wilson et al. (2006). Density waves formed in all tests conducted and were significantly more severe at high concentration. Each test started at the maximum velocity (~ 4.5 m/s) and the velocity was decreased gently in small increments every few minutes as part of the measuring program.

Some tests at low concentration were initially stable, until the velocity was dropped below a certain threshold and tiny fluctuations grew into large saw tooth shaped waves. In Figures 2.8a and 2.8b sand was transported at a volumetric concentration of 0.10 and amplification initiated below 3.5 m/s. Figures 2.8e and 2.8f show gravel transport at a volumetric concentration of 0.10 and density wave amplification started immediately at velocities below 4.5 m/s.

The biggest difference of the Freiberg loop compared to previous cases is the mixture velocity at which amplification is initiated. During the Prins Clausplein case amplification took place at mixture velocities close to the deposition limit velocity, like in Talmon et al. (2007). In the S-bend flow loop amplification took place when somewhere in the pipeline a deposit was still present and the mixture velocity was close to the deposition limit velocity of that particular section. However, the mixture velocities in the Freiberg case were far above the horizontal deposition limit velocity, yet amplification still took place.

A similarity between the S-bend loop and the Freiberg experiments is the growth rate of the density waves. If the cause of density wave amplification is speculated to be the same, then we would expect a small deposit to be present somewhere in the Freiberg loop. In the horizontal part of the flow loop one +45° inclined pipe (1.6 m long) was present to compensate an elevation change. It is well known that inclined pipes with an inclination angle between 30 – 45° have a deposition limit velocity up to ~ 50% higher (de Hoog et al., 2017, Matoušek et al., 2019, Spelay et al., 2016, Wilson and Tse, 1984). The deposition limit velocity in this section could not be observed during the experiment, therefore we use the Wilson and Tse (1984) method to evaluate the deposition limit velocity in this inclined pipe segment, which gives a deposition limit velocity of 3.2 m/s and 2.5 m/s for 600 μm sand and 11.2 mm gravel, respectively. As experienced in the S-bend loop, amplification should stop above these velocities, however this was not the case in the Freiberg loop, as for most experiments amplification was initiated at a mixture velocity below 4 m/s. Considering this big difference in conditions for which density wave amplification initiated between the Freiberg loop and the S-bend loop, the density wave amplification cannot be explained in the same way.

H]

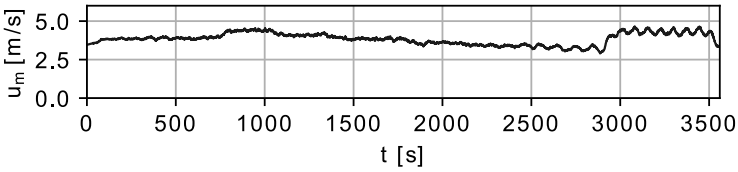

(a) Mixture velocity over time, $c = 0.10$ and $d_{50} = 600\,\mu m$

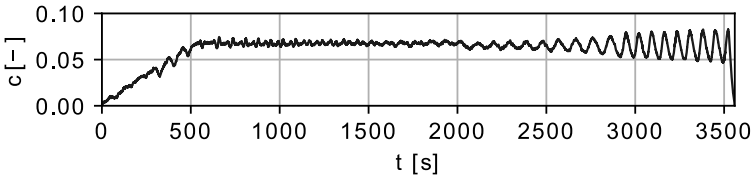

(b) Delivered concentration over time, $c = 0.10$ and $d_{50} = 600\,\mu m$

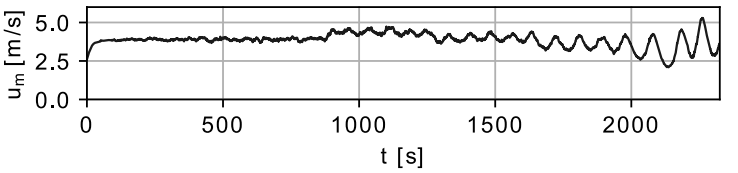

(c) Mixture velocity over time, $c = 0.15$ and $d_{50} = 600\,\mu m$

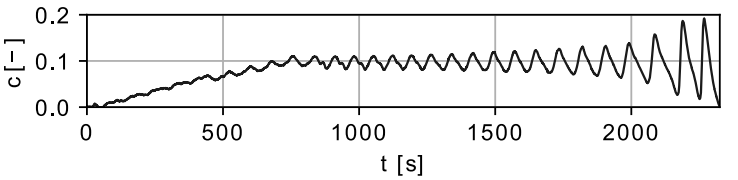

(d) Delivered concentration over time, $c = 0.15$ and $d_{50} = 600\,\mu m$

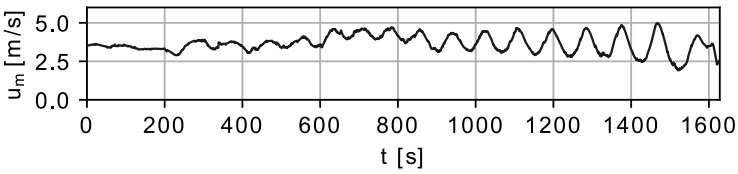

(e) Mixture velocity over time, $c = 0.10$ and $d_{50} = 11.2\,mm$

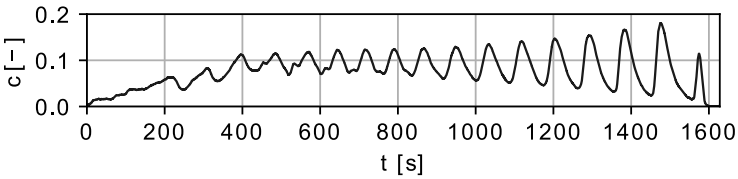

(f) Delivered concentration over time, $c = 0.10$ and $d_{50} = 11.2\,mm$

Figure 2.8: Results from experiments conducted in Freiberg.

Why density wave amplification took place in the Freiberg loop is as of yet unconfirmed, however it is very likely that another mechanism is responsible. Considering that the mixture velocity was significantly above the deposition limit when amplification occurred; the imbalance might occur in the sliding bed regime, as mathematically theorized by Talmon (2002). However growing density waves with sliding beds far above deposition limit have never been reported in purely horizontal experimental circuits, therefore this hypothesis lacks any proof to support this claim.

2.4. Discussion

Axial variations in concentration and particle velocity are common in hydraulic transport pipelines and under most circumstances are axially dispersed and do not form a significant risk to flow assurance of the system. However, the hydraulic transport system is at risk when density wave amplification occurs. Density wave amplification, through the erosion and sedimentation imbalance, is a transient phenomenon and only possible when two conditions are met. First, the concentration should be high enough to trigger the erosion and sedimentation imbalance. Additionally, a source of material is required for the waves to grow, as Equation 2.6 has shown that advection and differential slip alone are not enough.

In the case of the Prins Clausplein pipeline, stationary deposits are the source of amplification, which is evidenced by the mixture velocity sporadically dropping below the deposition limit velocity. These density waves travel through consecutive booster pumps farther down the pipeline, causing the mixture velocity to drop as they pass. This interaction with the pump creates a self exciting density wave amplification environment in the pipeline. Therefore, ensuring that the mixture velocity remains above the deposition limit velocity at all time is the best and most simple solution. This requires sufficient power from the pump drives, and preferably some reserve power to enable flow feedback control and the ability to cope with mild density waves. It has also been shown that choosing electric drives over diesel drives is most beneficial in achieving these goals.

The S-bend flow loop has the same stability criteria as the Prins Clausplein system, as amplification was never witnessed once the mixture velocity was above the deposition limit velocity in the S-bend. The deposition limit velocity in the S-bend is however more than twice as high as that of the horizontal pipes, therefore designers should design the system towards the highest deposition limit velocity of any segment in the entire system. This could be inconvenient for full scale deep sea mining systems, as in this case the system's deposition limit velocity is dictated by a very small segment and the entire system has to operate at a much higher velocity to avoid deposit formation in this segment. To better match deposition limit velocities between the pipe segments the designer has the option to reduce the pipe diameter, and therefore the deposition limit velocity, of the critical segments like the S-bend.

In case of the Freiberg system, amplification cannot be attributed to the conventional erosion and sedimentation imbalance. The key condition for stability of the erosion and

sedimentation imbalance is the absence of stationary deposits. The segment with the largest deposition limit velocity in the Freiberg system was a 1.6 m long, 45° inclined pipe with a deposition limit velocity of 3.2 m/s and 2.5 m/s for 600 μm sand and 11.2 mm gravel, respectively. Nonetheless, amplification still occurred for velocities up to 4.5 m/s, which poses a significant problem as the stability criterion cannot be based on knowledge gained from the S-bend and Prins Clausplein system.

What we do know for a fact is: given the same mixture velocity in the Freiberg system, the solids velocity in the vertical pipes is higher compared to the horizontal pipes, as explained earlier in this chapter. This difference in particle velocity can be expressed as a difference in the spatial averaged slip ratio between the vertical and horizontal pipe (at the same mixture velocity and concentration). To provide an estimate of the magnitude of this spatial averaged slip ratio difference, we consider slip ratio data acquired in a 100 mm flow loop of 12 mm gravel from de Hoog et al. (2017). No slip ratio data of the same gravel or pipe diameter is available for vertical pipes, therefore to estimate the slip ratio of the vertical ascending pipe we use Equation 2.4. The results can be seen in Figure 2.9.

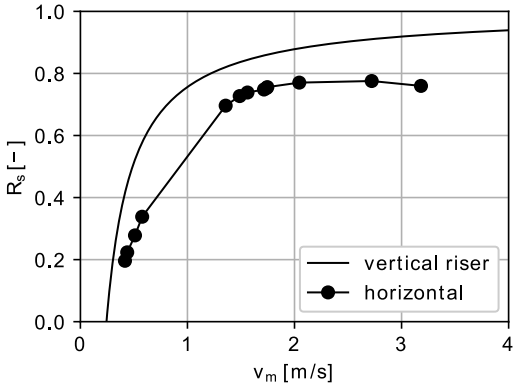

Figure 2.9: The spatial averaged slip ratio in a 100 mm pipe and 12.0 mm gravel. The horizontal data set is from measurements (de Hoog et. al 2017) and the vertical plot is calculated from Equation 2.4.

In the same 100 mm flow loop the reported horizontal deposition limit velocity was 0.8 m/s and Figure 2.9 shows that a large difference in spatial averaged slip ratio is possible for velocities significantly above the deposition limit velocity. The material in the horizontal pipe travels slower, therefore must increase in concentration. Consequently, material temporarily accumulates in the horizontal pipe as it flows from the vertical pipe into the horizontal pipe. ...

Addendum to de Hoog et al. (2021): *This is called transient accumulation. The theory given on transient accumulation in the remainder of this paragraph can now be considered as outdated. See Chapter 4 (Section 4.2) for the up-to-date theory on transient accumulation. For sake of transparency the original text of the article (de Hoog et al., 2021) is given unaltered below.*

...If at this moment a density wave passes, the hypothesis is that this density wave will erode the accumulated material and through the sliding bed erosion-sedimentation imbalance the density wave grows. This will result in a cyclic build-up and erosion of material in the horizontal pipes. This transient accumulation mechanism is however only a hypothesis and requires further validation. The proof supporting the transient accumulation hypothesis is the difference in solids velocity (a proven fact) and mathematical proof of sliding bed erosion and sedimentation imbalance at high flow velocity. The sliding bed erosion and sedimentation imbalance (Talmon, 2002) has never been observed in purely horizontal flow loops, where for high velocities sediment is well dispersed through the system. However, when combining horizontal and vertical pipes, with largely different solids velocities, transient accumulation does in fact cause differences in local concentration, and therefore material buffers from which density waves can grow and the perturbation needed to trigger the sliding bed imbalance. This is the underlying assumption of the transient accumulation hypothesis.

It must be stated that the transient accumulation hypothesis is presented here as a working hypothesis, which will be investigated as part of future research. If this hypothesis is valid, matching slip ratio by means of pipe diameter variation is a plausible solution to avoid the problem.

2.5. Conclusions

The presented study provides an analysis of transients affecting flow assurance in hydraulic two phase transport. The main sources of transients encountered in hydraulic transport are caused by the centrifugal pump, but these transients by itself do not cause an unstable system or density wave amplification. The amplification of density waves can however be initiated by the centrifugal pumps, but the main mechanism is an imbalance between erosion and sedimentation at high pipeline concentrations and at mixture velocities close to the deposit limit. Furthermore, amplification is not caused solely by axial differential slip for both horizontal (Talmon, 1999) and vertical pipes (van Wijk, 2016) under realistic operational conditions. Rather, amplification is only possible in conjunction with a source of material from which the waves can grow. These sources can be created if the pipeline velocity drops below the deposition limit velocity, even for a short period, as seen in the Prins Clausplein pipeline. The S-bend experiment showed that even a small segment containing a stationary deposit can cause density wave amplification, but at a much lower amplification rate. However, the Freiberg experiment showed that amplification is also possible for velocities far above the deposition limit velocity, and thus in this case not caused by the same erosion and sedimentation imbalance. The working hypothesis for amplification is a transient material accumulation effect between pipes with a large difference in solids flow rate (slip ratio).

3

EXPERIMENTS ON DENSITY WAVE AMPLIFICATION IN HORIZONTAL PIPES: EROSION- AND SLIDING BED DRIVEN DENSITY WAVES

This chapter contains a detailed experimental study into the influence of particle size and concentration on self-amplifying density waves that amplify by feeding from a stationary bed layer, typical for horizontal pipes. Chapter 2 describes only a single type of density wave that occurs under these circumstances. However, these experiments show that in fact two distinct separate mechanisms can lead to density wave amplification, both amplifying by feeding from the material of a stationary bed layer. The two separate waves types are explained in this chapter. They are called: erosion driven- and sliding bed driven density waves. The two types of density waves show different behavior in wave amplitude, celerity, wave length and amplification rate. In addition, a strong correlation between the wave amplitude and the mean concentration was found, independent of the particle size, and specific to each density wave types. These experiments are also used to validate the CFD model reported in Chapter 5.

This chapter has been submitted to the International Journal of Multiphase Flow (2024).

3.1. INTRODUCTION

Hydraulic transportation is the main technology to transport sediment in many industries like dredging, mining and deep sea mining. Pipelines can be many kilometers long and in case of coarse sediments, centrifugal pumps are often the preferred pump type to drive the system (Visintainer et al., 2023). Flow assurance studies for these pipelines apply steady-state methodologies and mainly involve comparing the operating velocity of the pipeline with a minimum threshold velocity to avoid stationary sediment deposits in the pipeline. This threshold velocity is generally called the deposit limit velocity among academics and engineers.

Even though pipeline designers utilize steady-state methods, the slurry flow in the pipeline is by its nature unsteady. Fluctuations of the mixture velocity are caused by temporal variations in mixture density entering the pipeline through three mechanisms. Firstly, by the unsteady nature of feeding the pipeline, especially in the dredging industry (i.e. the stepping and swaying of a cutter suction dredger). Secondly, by fluctuations in energy losses in the pipeline. Thirdly, due to pump pressure variations, caused by an unsteady mixture density flowing through the centrifugal pump(s). Under the right conditions the aforementioned transients can lead to the spatial redistribution of sediment within the pipeline. In other words, solid particles can agglomerate into density waves, which self-amplify once formed (de Hoog et al., 2021, Matoušek, 1996b, Talmon et al., 2007).

Horizontal long distance pipelines can be many kilometers long. When transporting settling slurries, which show a significant non-uniform solids concentration profile over the pipe cross-section, these pipelines are typically designed at a volumetric solids concentration not exceeding 0.15. This upper limit is purely based on field experience in the dredging industry (van den Berg, 2013). Higher concentrations are avoided out of fear of density waves and blockages. While in shorter pipelines, for instance found onboard of dredge vessels, volumetric concentrations easily reach 0.35 without any issues. Therefore, much can still be gained in longer pipelines, since the most efficient transport process in terms of energy consumption is at the highest possible concentration, while transporting at the lowest possible mixture velocity. Additionally, increasing concentration will make the transport process more energy efficient and shorten the duration of projects, which constitutes as a gain in cost efficiency. Thus, a better understanding of how self-amplifying density waves form, potentially enables transportation at high concentrations in long pipelines and leads to a more optimized transport process.

The first publicly reported case of self-amplifying density waves was by Matoušek (1996b). These waves were $\sim 700\,m$ long at peak concentrations over 0.30 by volume. The pipeline was 10 km long and 650 mm in diameter. Due to the long wave length and high peak concentrations, the waves seriously impeded the safety of the pipeline, and pump drives had difficulties coping with the strong density waves. The pipeline transported sand with a particle size ranging from fine to medium sand (the average particle size varied in the range of 100-300 μm) with a wide particle size distribution (with 0.07 of the volume larger than 700 μm). The pipeline was used to construct the Prins Claus

highway junction in The Hague, the Netherlands, and will be referred as such in the remainder of the chapter. Matoušek (1996b) was the first to publish research on these density waves. During this research Matoušek (1996b) discovered that the particle velocity is a function of the local particle concentration, being higher at high concentration, and related this physical phenomenon to the development of density waves. However, now it is understood that this variable particle velocity is not the mechanism behind density wave development (de Hoog et al., 2021, Talmon, 1999).

Talmon (1999) developed a theory to explain the Prins Claus pipeline density waves, and attributed the wave formation mechanism to an adverse relationship between erosion and sedimentation of the bed layer, using a linear perturbation analysis. This mechanism is referred to as the erosion and sedimentation imbalance, which entails that high concentration flows erode stationary particle deposits, and low concentrations create deposits (at velocities around the deposit limit velocity). As a consequence, local high concentrations cause erosion of the deposit layers. The eroded sediment is transferred to the turbulent suspensions, increasing the local concentration more and flows farther down the pipeline. This increased concentration causes even more erosion in the next pipe section, a continuous cycle that allows the wave to self-amplify. Talmon et al. (2007) dedicated experiments to support the developed theory, and noted that within a closed circular laboratory flow loop a single wave forms with the same length as the flow loop.

Matoušek and Krupička (2013) did experimental research on various unsteady processes in a laboratory flow loop, including density waves. The flow loop had an internal diameter of 100 mm and tests were conducted with 530 μm glass beads. It was observed that at low concentration the regime transition from flow with a stationary to flow with a sliding bed was smooth. In contrary, at high concentrations the transition was observed to be unstable. Specifically, at high concentration the bed layer had a shocking sliding behaviour, intermittently stationary and mobile, referred to by Matoušek and Krupička (2013) an "unstable slip point" of the bed. Note, Matoušek and Krupička (2013) did not mention what is considered a low and a high concentration. The most important observation by Matoušek and Krupička (2013) was that the development of density waves is associated with the occurrence of the shocking sliding bed behaviour, but does not explain how exactly the waves are formed. Additionally, multiple waves were detected in the flow loop, therefore the wave length of these waves was shorter than the flow loop, which is in contradiction with the experimental findings by Talmon et al. (2007).

From this research it became clear that Talmon et al. (2007) and Matoušek and Krupička (2013) were looking at two separate density wave mechanisms (more details in Section 3.2). The only difference concluded by Matoušek and Krupička (2013) was the difference in wave length, but does not mention the possibility that the density wave mechanism might be different compared to Talmon et al. (2007). The experiments in this research clearly show the same distinctions in wave length and shows that the density waves are linked to the transport regime. The waves measured by Talmon et al. (2007) were caused by the erosion-sedimentation imbalance, which we call "erosion driven density waves." While the waves encountered by Matoušek and Krupička (2013) are formed by a differ-

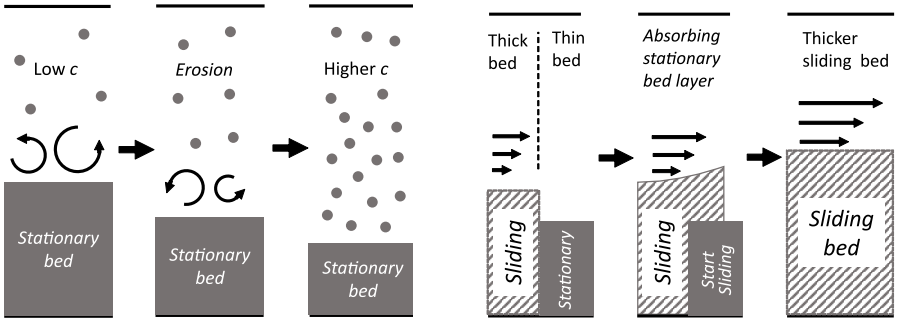

(a) Erosion driven density waves. (b) Sliding bed driven density waves.

Figure 3.1: An illustrative representation of the two density wave amplification mechanisms.

ent mechanism, which we choose to call "sliding bed driven density waves", since these waves are in fact sliding bed layers which amplify by absorbing stationary beds. In Section 3.2 the mechanisms are explained further.

No dedicated study on the effect of the particle diameter on density waves has ever been conducted. In addition, the conflicting reports on the wave lengths between Talmon et al. (2007) and Matoušek and Krupička (2013) was one of the motivations for this experimental research. Therefore, the original research question for these experiments was: What is the influence of particle size and concentration on the formation of self-amplifying density waves?

The chapter starts with a Theory section (Section 3.2), explaining the two density wave mechanisms. After which the Methods (Section 3.3) elaborates the experimental setup and the techniques used to compute various density wave properties like: mean concentration, peak concentration, wave length and wave celerity. In the Results and Discussion (Section 3.4) the measurements are shown and discussed.

3.2. THEORY

The two density wave amplification mechanisms identified in this research are theoretically explained. In support, a graphical explanation is given in Figure 3.1.

3.2.1. EROSION DRIVEN DENSITY WAVES

When the mixture velocity exceeds the deposit limit velocity (starting from low velocity) a bed layer of fine sand tends to fully erode and get into the suspension. In terms of flow regime changes we state that the flow regime changes from "stationary bed" to "suspended" mixture flow. This transition is governed by the erosion of the bed layer. The erosion driven density waves are best explained using the mathematical foundation of the theory developed by Talmon (1999). Namely, the erosion and growth of a stationary sediment bed layer can be modeled using an erosion and sedimentation balance (Biss-

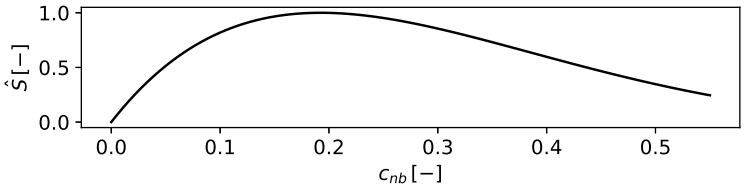

Figure 3.2: The hindered effect of the sedimentation flux (Equation 3.2) as a function of c_{nb}. $\hat{S} = S/max(S)$

chop, 2018, van Rhee and Talmon, 2010, van Rijn, 1984, Winterwerp et al., 1990):

$$v_{sed} = \frac{S - E}{\rho_s(1 - n_0 - c_{nb})} \tag{3.1}$$

In Equation 3.1 v_{sed} is the vertical sedimentation velocity of the bed top interface, S is the sedimentation flux of particles, E the erosion flux, n_0 the bed porosity and c_{nb} the near bed volumetric concentration of particles responsible for the erosion process. When S and E are equal, the bed does not grow or erode. S is often modeled using the established hindered settling approach by Richardson and Zaki (1954):

$$S = \rho_s v_{ts} c_{nb}(1 - c_{nb})^n \tag{3.2}$$

In Equation 3.2, ρ_s is the particle density, v_{ts} the particle terminal settling velocity and n the particle size dependent Richardson and Zaki (1954) exponent ($2.4 < n < 4.65$). An important property of the settling flux is, that it rises as a function of c_{nb} up-to values of ~ 0.20 after which it decreases as a function of c_{nb}, see Figure 3.2. Meanwhile, the erosion flux E is independent of the concentration for concentrations below ~ 0.35 (then hindered erosion also plays a role, but this is outside of the scope of this explanation, for more info see Chapter 2). Moreover, erosion is dictated by inter-particle collisions in a shear layer at the top of the bed layer, which is the typical erosion mode found at high velocities in pipeline flows. Erosion due to shearing is driven by turbulent kinetic energy of the fluid and does not depend on the concentration (Keetels et al., 2023). Summarized, the sedimentation flux decreases at increasing concentration while erosion remains constant. As a consequence, Equation 3.1 dictates that at high concentrations ($>\sim 0.20$), erosion will be dominant. This mechanism allows density waves to self-amplify.

Experimental research by Talmon et al. (2007) aimed to study erosion driven density waves, in a 25 m long, 100 mm diameter flow loop using 200 μm sand. One of the main observations of this experiment was that the density wave which developed was a single wave, with the length equal to the flow loop. Waves were created at volumetric loop concentration from 0.14 to 0.30, but only with a single sand size.

3.2.2. SLIDING BED DRIVEN DENSITY WAVES

A stationary bed layer with particles of coarser sand sizes tends to start sliding, instead of fully eroding, when exceeding the deposit limit velocity (starting from a lower velocity). In other words the flow regime changes from a "stationary bed" to a "sliding bed" regime. The exact threshold particle size depends on the pipe diameter, and as an indication it is somewhere between 308-617 μm (based on the experimental results of this research), but is possibly also a function of the grading of the sediment (more in Section 3.4). The regime change threshold is called the deposit limit velocity, and is sensitive to the local cross-section averaged concentration in the pipe.

Modelling of the transition between the stationary bed and sliding bed regimes, can be achieved using steady-state two-layer models (Matoušek et al., 2018, Visintainer et al., 2023, Wilson et al., 2006). These two layer models evaluate a force balance between the hydrodynamic bed shear stress, (which pulls on the bed layer) and the Coulombic friction of the bed layer against the pipe wall (which resist the bed layer from sliding). If the bed shear force exceeds the static friction force the bed layer starts sliding. Local higher cross-section averaged concentrations have thicker bed layers, which experience more bed shear stress. This is caused by the reduced cross-section above the bed, which causes a higher velocity above the bed at equal flow rate, thus increasing the bed shear stress. The bed shear force is a higher order effect than the friction of the bed layer against the pipe wall, thus as a function of increasing bed thickness the bed shear stress increases at a faster rate than the bed friction. As a consequence, thicker beds will slide while thinner beds remain stationary, at equal flow rates. Summarized, a bed layer can slide at local high concentrations, which remains stationary at lower local concentrations.

Figure 3.3 shows the deposit limit velocity u_{dl} as a function of the cross-sections average concentration c, computed with a steady-state two-layer model (Wilson et al., 2006). In Figure 3.3 we see that for concentrations above ~ 0.10 bed layers will slide for higher concentrations. Thus a local high concentration can initiate a sliding bed, while other parts of the flow remains stationary, as shown by 3.3. This sliding bed will quickly travel down the pipe, and absorb any stationary bed layer in its path, and consequently increase in concentration further. Since the deposit limit velocity is lower for higher concentration (Figure 3.3), the sliding bed layer will continue to slide and grow as it absorbs more stationary bed layers. In the view of the authors this is the second mechanism that causes density wave amplification, and is related to the inverse proportionally between the deposit limit velocity and the local concentration (at concentrations above ~ 0.10, see Figure 3.3). Since this mechanism is directly related to the slipping of the bed layer, and the mobile wave is in the sliding bed regime, these waves are called "sliding bed driven" density waves in the remainder of the chapter.

Figure 3.3 also helps explaining one of the main observations by Matoušek and Krupička (2013). Specifically, at low concentration a stable transition towards a sliding bed was observed, and at high concentration the transition was unstable with a sliding and shocking bed layer. Furthermore, density waves were associated with the sliding shocking

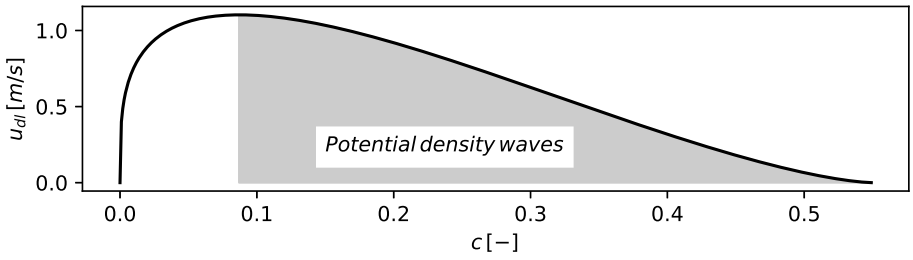

Figure 3.3: The deposit limit velocity u_{dl} as a function of the cross-section averaged concentration in the pipe c, computed with the Wilson two layer model (pipe diameter $D = 42\,mm$ and the particle diameter $d_{50} = 1.08\,mm$). If the mean concentration in the pipe is higher than the concentration maximum in the u_{dl} curve, sliding bed driven density waves can be formed if the mixture velocity is close to the deposit limit.

behaviour. It makes sense that the shocking bed occurs at concentrations above 0.10 according to Figure 3.3, since tiny changes in local concentration can cause the bed to slide or not, and when these local gradients are small enough they will be damped by turbulence and will not grow into large waves, but still cause the shocking sliding bed behaviour. Additionally, in Figure 3.3 the deposit limit velocity increases with concentrations below 0.10. Thus, under these conditions instabilities cannot lead to density waves, nor a shocking bed, which explains why the transition to a sliding bed is smooth.

3.3. Methods

3.3.1. Experimental setup

To study density waves and the effect of the particle diameter and concentration, a dedicated experimental flow loop was built. The philosophy behind the flow loop design was to build a flow loop with the largest length over pipe diameter ratio as possible, longer than previous experimental research (Talmon et al. (2007): $L/D = 250$, Matoušek and Krupička (2013): $L/D = 520$), within constrains of the laboratory size. The philosophy was to test if the density wave length indeed equals the system length like found in Talmon et al. (2007) and de Hoog et al. (2021), or perhaps a limit to the wave length is possible, which would explain the density waves found in Matoušek and Krupička (2013). A secondary reason for a long flow loop is to avoid damping of the waves. More specifically, axial turbulent dispersion dampens waves and increases with the local longitudinal concentration gradient (Taylor, 1954). In shorter circuits the longitudinal concentration gradient of a wave is higher, assuming the same wave form and that the wave length equals the system length. As such, shorter circuits have a stronger damping effect on density waves, which can prevent waves from developing. The above design criteria resulted in a flow loop with an inner diameter of 42 mm, and a total length of 45.5 m, which is 1083 pipe diameters. See Figure 3.4 for a schematic of the loop.

The loop was built using transparent PVC to be able to visually observe the density waves in the entire flow loop, which is required to detect a sliding bed layer. A 22 kW

pump was used to drive the system. Two vertical U-loops were used to measure the delivered concentration c_{vd} at two locations in the loop (Clift and Manning Clift, 1981). The delivered concentration is defined as the solids flow rate Q_s over the volumetric mixture flow rate Q_m:

$$c_{vd} = Q_s / Q_m \tag{3.3}$$

Dispersion due to bends was kept to a minimum by using the U-loops and centrifugal pump to make major directional changes, and a long radius bend ($R = 1.5\,m$) was used to complete the loop. The mixture velocity was measured using an Electromagnetic Flow Meter (EMF) of type Krohne Optiflux 4000, 0...12 m/s, with an accuracy of ±0.5% full range. The pressure sensors in the U-loop were of the type Druck, Unik 5000, -50...+50 kPa differential pressure transducers with an accuracy of ±0.04% full range. All sensors were calibrated at the start of experimental program. The sensor signals were logged at a sampling rate of 2 kHz using a 24 bit data logger.

Four sieved quartz sand types were used for the experiments. The sand types are Zilverzand (Zz) with a particle diameter of $d_{50} = 242\,\mu m$ and Dorsilit types 7, 8 and 9 (D7, D8 and D9 respectively), with particle diameters of $d_{50} = 1.09\,mm$, $d_{50} = 617\,\mu m$ and $d_{50} = 308\,\mu m$, respectively. These sand types have a very narrow grading, see Figure 3.5.

Nineteen tests were conducted with the four sand types by varying the average loop volumetric concentration of solids between 0.10 and 0.25. Each test started by filling the flow loop to a desired concentration, and at high mixture velocity ($>> u_{dl}$) such that any concentration variations could dampen out. After this initial period the pump revolutions, and therefore flow rate, were slowly lowered over a period of several minutes until a bed layer formed. From that point on the pump revolutions were kept constant, and the density waves were allowed to develop. After some time the waves reached a steady-state amplitude, these steady-state periods were used for the data analysis, like determining peak concentration, wave lengths and the celerity. See Figure 3.6 for an example of an experiment.

3.3.2. COMPUTING WAVE PROPERTIES

The focus of these experiments was to measure as many density wave related parameters as possible, such as the wave length, celerity, and peak concentration. The measuring principles and algorithms used to extract these properties from the data are explained.

The wave celerity was computed by cross-correlation of the measured time traces of the two U-loops. This results in a time lag between the signals, and with the known distance between the U-loops, the wave celerity could be computed using the cross-correlation. The best results were obtained by first normalizing both measurements. Specifically, the measurements are normalized with respect to their average and maximum concentration value. This results in traces with values between 1 and -1. Without this procedure the correlation is not always successful. Figure 3.7 shows an example of the time shift computed using the cross-correlation technique. Figure 3.7a shows the

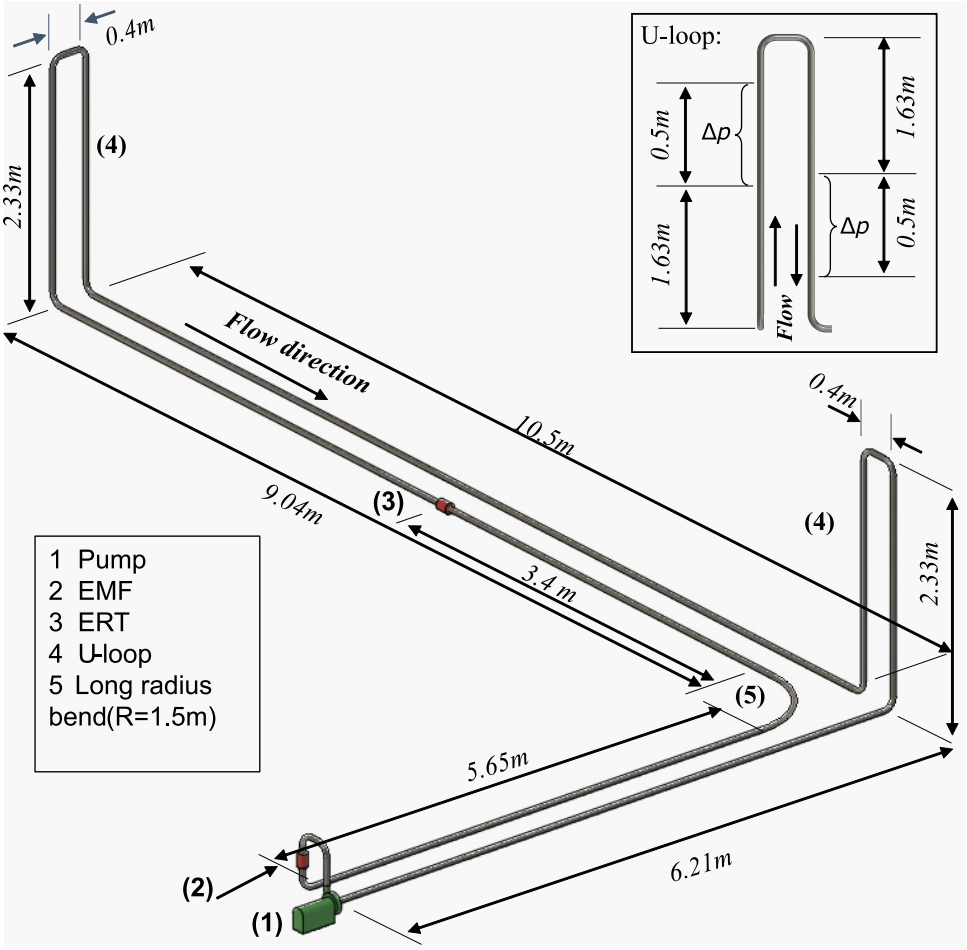

Figure 3.4: A schematic of the flow loop, showing sensor locations and dimensions on the pipe segments.

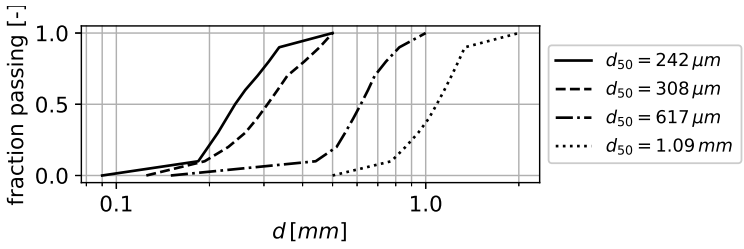

Figure 3.5: The particle size distribution of the sand types used for the experiments.

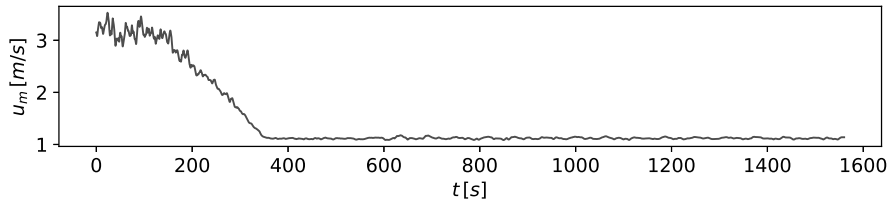

(a) Mixture velocity.

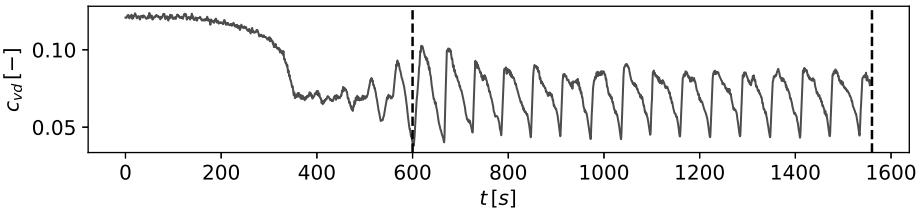

(b) Delivered concentration. The two vertical dashed lines indicate the part used for the data analysis.

Figure 3.6: Test Zilverzand (Zz), nr. 1, $d_{50} = 242\,\mu m$. This is an example of erosion driven density waves.

original U-loop time traces, and 3.7b shows the same traces where U-loop 2 is shifted in time based on results attained using the cross-correlation method, making the signals overlap. From experience of using this algorithm, we deduced that the correlation is highest at the steep upwards gradient at the wave front. The correlation is computed from an entire steady-state section of an experiment which can last several minutes. During this time the waves have recirculated many times, and sometimes develop and merge into new waves. As such, the computed wave celerity represent the average celerity of all waves in the loop, temporally averaged over an experiment.

The wave length is straight forward to measure in case of erosion driven density waves, since these produced a very clear single periodic wave. As such, the wave period is simply computed from the time between peaks of the U-loop c_{vd} measurements, and the wave length is computed as the product of the wave celerity and the wave period. However, in case of sliding bed driven density waves the wave length is not periodic. Multiple waves in a loop were present, and at times they merge into a larger waves with twice the length (see Figure 3.8a). Therefore, a different approach was taken to measure the wave length of the sliding bed driven density waves.

An three step algorithm was developed to detect the flat sections between the sliding bed driven waves. These flat sections occurred in all experiments with sliding bed driven density waves. The first step was to reduce noise, by passing the time traces through a low pass filter with a cut-off frequency of 2 Hz. Secondly, the derivative of the entire trace was computed. The condition $\frac{\partial c}{\partial t} < 1^{-5}$ was applied to detect the flatter sections, which was chosen by trail and error such that the waves were successfully isolated. Thirdly,

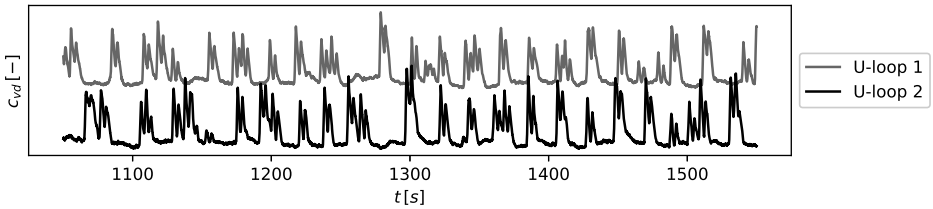

(a) Original time traces.

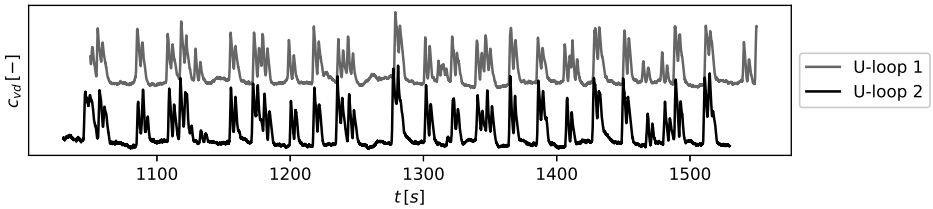

(b) U-loop 2 shifted in time based on the cross-correlation method.

Figure 3.7: An example of the cross-correlation technique to measure the velocity of both wave types.

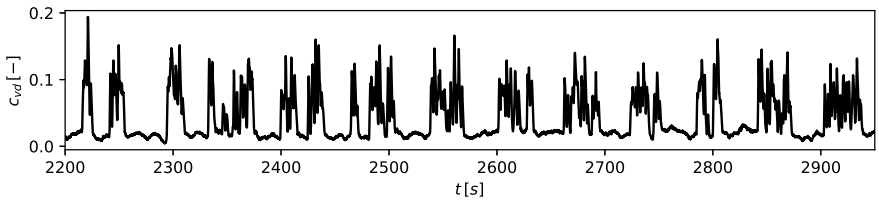

(a) A closer view of sliding bed driven density waves.

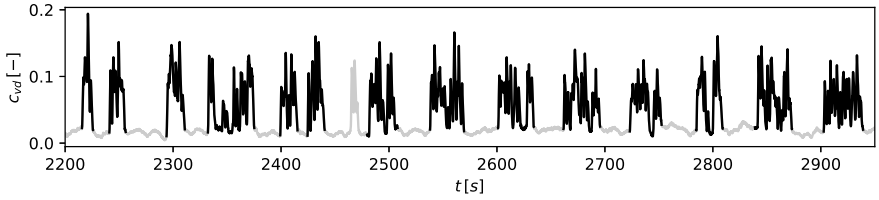

(b) Isolation of the waves using an algorithm that detects the flat sections between the waves.

Figure 3.8: An example of sliding bed driven density waves.

a condition was applied to filter out very small low gradient sections of only a few time samples. The shortest flat spot allowed was 1000 samples (=0.5 seconds), again this value chosen by visually judging that the waves were successfully isolated. With the flat sections isolated, the waves were said to be anything that is not a flat section, see Figure 3.8b. From an isolated wave, the wave period and the wave length could be determined. Applying this method for all waves in a time trace, resulted in a distribution of wave periods (see Figure 3.9a). From this distribution the average wave period was computed and considered to be the average of the entire experiment. From this average wave period the wave length could be calculated by multiplication with the wave celerity. Note that sometimes the isolation algorithm fails to isolate a wave, for example at 2475 seconds Figure 3.8b. However, enough wave samples are found in an experiment (samples sizes ranging from 13–167 waves, depending on the experiment) that such irregularities are not frequent enough to significantly influence the final averaged value.

The wave maxima, minima and average concentrations were again straight forward to determine in case of the erosion driven density waves. A peak finding algorithm available in the Python Scipy library was applied to find local maxima and minima in the U-loop time traces (*scipy.signal.find_peaks()*). In case of the sliding bed driven density waves, the wave peak concentration was computed from the maximum from each isolated wave, using the aforementioned wave isolation algorithm. The minima were computed from the minimum of the flat sections in between the sliding bed driven waves. This produced three normal distributions for the maxima, means and the minima of the isolated sliding bed waves (see Figures 3.9b, 3.9c, 3.9d, respectively). The average of each distribution was taken as the average of the entire time trace.

3.4. Results & Discussion

All properties of the experiments and the density waves can be viewed in Table 3.1 and 3.2. The time traces of the mixture velocity and delivered concentration of all experiments can be viewed in Figure 3.6 and in Appendix A. Only the delivered concentration of the first U-loop is plotted, to avoid clutter in the graphs. The figures highlight the data analysis sections within two vertical dashed lines. Some experiments have two or three sections that were used to analyse the density waves. These are numbered in the graphs, and respectively named in Tables 3.1 and 3.2. The bed height y_b was determined visually from camera footage. This represents an average bed height, since it slightly fluctuates as different concentration parts of a wave passing the camera. Unfortunately, the water during experiment D9, 2.2 and 2.3 was too turbid to observe the bed layer on the camera footage.

The main highlight of this chapter is the clear distinction in behaviour of the two wave types. The 242 μm and 308 μm sand produced erosion driven density waves. These waves developed relatively slowly, requiring several circulations through the flow loop to reach a steady amplitude. A tiny stationary bed layer was always present at the bottom of the pipe, thus not all sediment was eroded and suspended into the density waves.

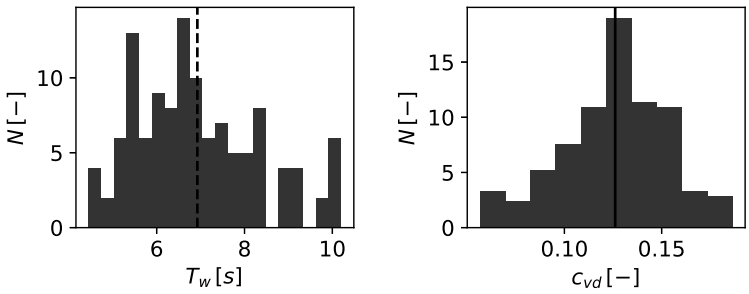

(a) Wave periods.

(b) Wave maxima.

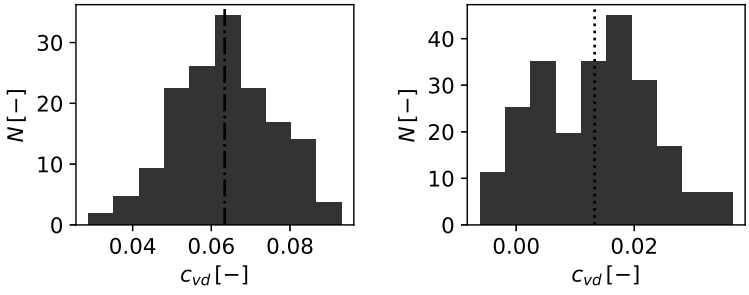

(c) Wave means.

(d) Wave minima.

Figure 3.9: An example experiment, showing the distribution of the wave periods T_w, the concentration maxima, means and minima. The average of the distribution was considered as the average wave length of an experiment.

Table 3.1: All density wave properties that were computed from the experiments, part i.

	d_{50} $[mm]$	c_{loop} $[-]$	$u_{m,0}$ $[-]$	$c_{w,mean}$ $[-]$	$c_{w,peak}$ $[-]$	$c_{w,min}$ $[-]$	c_{mean} $[-]$
Zz 1	0.242	0.10	2.94	0.05	0.09	0.04	0.05
Zz 2.1	0.242	0.15	2.07	0.08	0.13	0.06	0.08
Zz 2.2	0.242	0.13	1.54	0.14	0.17	0.08	0.14
Zz 3	0.242	0.18	2.38	0.13	0.18	0.09	0.13
D9 1.1	0.308	0.10	2.31	0.08	0.10	0.03	0.08
D9 1.2	0.308	0.08	1.81	0.05	0.07	0.01	0.05
D9 2.1	0.308	0.16	2.17	0.07	0.09	0.02	0.07
D9 2.2	0.308	0.15	1.93	0.03	0.04	0.01	0.03
D9 2.3	0.308	0.12	1.59	0.01	0.01	0.00	0.01
D8 1	0.617	0.12	3.41	0.06	0.13	0.01	0.05
D8 2	0.617	0.19	3.04	0.06	0.10	0.02	0.04
D8 3	0.617	0.17	1.26	0.15	0.31	0.06	0.12
D8 4	0.617	0.19	1.56	0.14	0.30	0.05	0.12
D7 1	1.08	0.13	3.10	0.07	0.14	0.02	0.05
D7 2	1.08	0.12	2.36	0.07	0.15	0.02	0.05
D7 3	1.08	0.19	2.86	0.10	0.19	0.01	0.07
D7 4	1.08	0.24	1.92	0.13	0.23	0.06	0.12
D7 5	1.08	0.20	1.09	0.13	0.24	0.06	0.12

The 617 μm and 1.08 mm sand showed sliding bed driven density waves. These waves developed to full amplitude very quickly, usually within one circulation of the loop. These waves were also able to fully absorb the bed, leaving behind sections with only water. This was observed visually and also measured in the delivered concentration measurements. Although, the zero concentration periods are not very pronounced in the time traces of c_{vd}. Furthermore, these periods also occurred within a wave, and should not be confused with the long flat sections as seen in for instance Figure 3.8. These zero concentration periods were very short and as such the U-loop could not measure them well, since the U-loop measurement is based on spatially averaging pressure signals over a distance of 3.03 m. As such, for zero concentration period to be fully measured, it should be at least be 3.03 m long, which was not often the case. The video footage shows the zero concentration sections best. The zero concentration water only sections were also a key observation in the Prins Claus pipeline (de Hoog et al., 2021, Matoušek, 1996b). The shocking bed behaviour was predominant as reported by Matoušek and Krupička (2013), however these shocking bed layers were usually quickly absorbed by a density wave.

Some interesting relationships between the density wave parameters (Table 3.1) have been discovered. For instance, Figure 3.10 shows that the wave peak concentration $c_{w,peak}$ correlates strongly with the average concentration of the wave $c_{w,mean}$, for both wave types. Interestingly, the peak concentration of erosion driven density waves is roughly 1.5 times the average concentration. The data from Talmon et al. (2007) is also plotted in

Table 3.2: All density wave properties that were computed from the experiments, part ii.

	$u_{m,w}$ $[m/s]$	u_w $[m/s]$	L_w $[m]$	$\frac{y_{b,mean}}{D}$ $[-]$	$u_w^{'}$ $[m/s]$	$L_w^{'}$ $[m]$
Zz 1	1.12	0.79	49.3	0.06	0.77	47.9
Zz 2.1	1.00	0.82	48.7	0.14	0.75	44.0
Zz 2.2	1.24	1.09	47.4	0.08	1.04	45.4
Zz 3	1.17	1.06	47.6	0.11	0.99	44.4
D9 1.1	1.33	1.08	50.2	0.07	1.04	48.4
D9 1.2	1.05	0.73	52.0	0.16	0.65	46.0
D9 2.1	0.84	0.65	50.6	0.11	0.61	47.2
D9 2.2	0.64	0.40	53.2	n/a	n/a	n/a
D9 2.3	0.50	n/a	52.8	n/a	n/a	n/a
D8 1	1.06	1.03	7.2	0.16	0.91	6.3
D8 2	0.68	0.77	6.3	0.29	0.56	4.6
D8 3	0.64	0.99	36.8	0.41	0.57	21.0
D8 4	0.62	0.95	40.9	0.39	0.57	24.4
D7 1	0.89	0.80	29.4	0.21	0.67	24.3
D7 2	0.85	0.82	25.4	0.20	0.69	21.4
D7 3	0.71	0.87	35.3	0.30	0.62	25.3
D7 4	0.61	0.91	44.1	0.41	0.52	25.1
D7 5	0.62	0.85	40.6	0.43	0.46	22.0

Figure 3.10a, which shows that this trend also continues for erosion driven waves measured in a 100 mm diameter pipe, with mean concentrations up to 0.3. Apparently, the erosion driven wave mechanism shares common properties, which also applies to the larger 100 mm pipes, and is not very sensitive to the particle diameter. However, at this point we do not have an explanation for the $c_{w,peak} \approx 1.5 \cdot c_{w,mean}$ property.

In case of the sliding bed waves the wave peak concentration is twice the average, $c_{w,peak} \approx 2.0 \cdot c_{w,mean}$, as seen in Figure 3.10b. If the peak is twice the average, the minimum equals zero, which simply results from the fact that sliding bed driven density waves are able to absorb the whole bed and leave behind only water, unlike the erosion driven density waves. The ability of the density waves to leave behind only water was also witnessed in the Prins Claus pipeline (de Hoog et al., 2021, Matoušek, 1996b). Based on this property, the Prins Claus pipeline could have been subject to sliding bed driven density waves, even though the average particle diameter in the pipeline was relatively low between 100-300 μm. More on this discussion can be found at the end of Section 3.4.

The next interesting property is that the wave celerity u_w is a function of the mean wave concentration. In Figure 3.11a the measured wave celerity over the mixture velocity u_w/u_m is plotted against the mean wave concentration, for both wave types. Interestingly, the sliding bed driven density waves consistently propagate faster than the mixture velocity. It is physically impossible that the particles flow faster than the carrier fluid, therefore another effect must be responsible for the high wave celerity. This

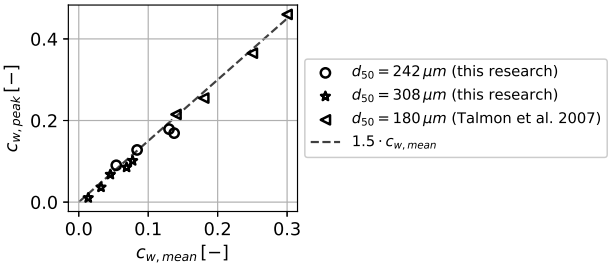

(a) Erosion driven density waves.

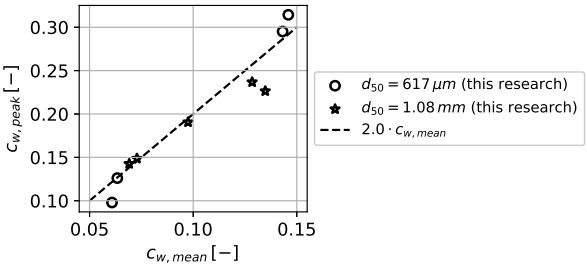

(b) Sliding bed driven density waves.

Figure 3.10: The measured wave peak concentration as a function of the wave mean concentration.

phenomena was also mentioned by Matoušek and Krupička (2013) and the idea came that the reduced cross-section above the sliding bed layer increases the velocity above the bed and therefore also the velocity of the wave. The reduced cross-section raises the wave velocity above the mixture velocity, because the mixture velocity is measured in a vertical pipe, which cannot contain a bed layer. To test this hypothesis, the wave celerity was corrected for the reduced cross-section above the sliding bed layer. The corrected wave celerity

$$u_w^{'} = u_w \frac{A^{'}}{A} \tag{3.4}$$

is computed from the reduced flow area above the bed layer $A^{'}$ and from the observed bed height y_b. Figure 3.11b shows all corrected wave celerities $u_w^{'}$ as a function of the mean wave concentration. The corrected wave celerity forms a linear trend, regardless of the wave type. To quantify how good the linear trend is, the normalized-root-mean-square-error e_{NRMS} was computed, which very suitable to compare different data sets, and is zero for a perfect linear fit. The resulting e_{NRMS} is given in Figure 3.11a and 3.11b. By applying the reduced cross-section correction, the e_{NRMS} improved from 0.2 to 0.08, suggesting that the hypothesis of the reduced cross-section is indeed a plausible mechanism which increases the wave celerity above the mixture velocity.

Another notable property is the measured wave length, given in Figure 3.12a. This

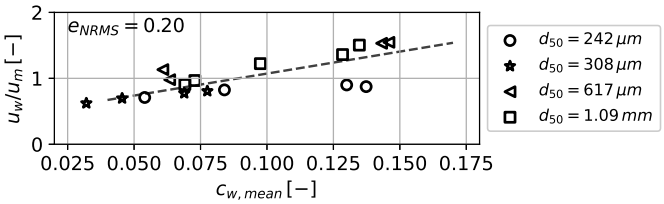

(a) Without correcting for the reduced flow cross-section.

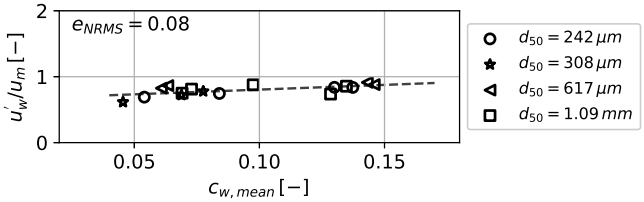

(b) After correction for the reduced flow cross-section.

Figure 3.11: The wave celerity as a function of the mean concentration. e_{NRMS} is the normalized root means square error of the fitted linear curve.

shows that the measured wave lengths are consistently above the length of the flow loop (45.5 m), in case of the erosion driven density waves. Naturally this is not possible, since the longest wave that can be contained in the flow loop must have the same length as the loop. This error comes from the fact that the wave length is computed from the wave period, and more importantly, from the wave celerity. As mentioned before, the wave celerity is higher due to the reduced cross-section above the bed. Correcting the wave length from the corrected wave celerity $u_w^{'}$, allows us to compute a corrected wave length $L_w^{'}$, which is plotted in Figure 3.12b. The average value of the corrected wave lengths is $46.2 \pm 4.2\,m$, and the loop length now falls within the spread of the data points. The wave length of the sliding bed driven density waves as a function of the mean wave concentration is plotted in Figure 3.13. No clear trend can be deduced from this, other than that the 1.08 mm sand produces longer waves than the 617 μm sand. Why sliding bed waves are longer for larger particles is currently still unknown, and is worth investigating in future research.

The new insights on how the wave peak concentration is related to the wave average concentration is very valuable for pipeline designers, assuming these trends are also valid for larger pipeline diameters. This assumption is not far fetched, as the flow regimes dictating the density wave types also occur in larger pipe diameters (i.e.the stationary bed, sliding bed and the suspended flow regimes). The average wave concentration is the same and the mean slurry concentration in case of erosion driven density waves, and 0.01 to 0.02 higher in case of sliding bed driven density waves. Therefore, as pipeline designer a rough estimation of the wave peak concentration can be made based on the average design concentration of the pipeline.

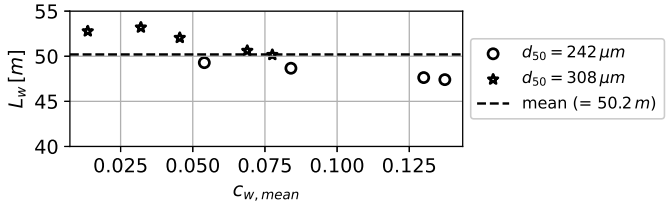

(a) Without correcting for the reduced flow cross-section.

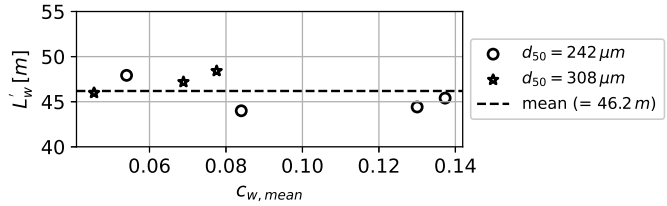

(b) After correction for the reduced flow cross-section.

Figure 3.12: The wave lengths of the erosion driven density waves.

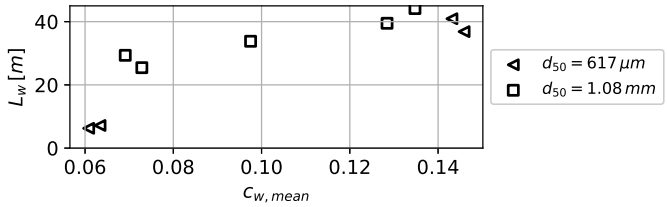

(a) Without correcting for the reduced flow cross-section.

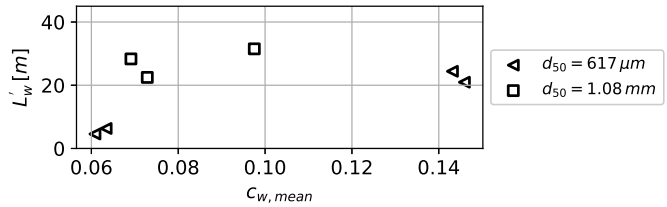

(b) After correction for the reduced flow cross-section.

Figure 3.13: The wave lengths of the sliding bed driven density waves.

With this knowledge designers can estimate the amplitude and effect of density waves if waves are expected, for instance when the pump and drive are power limited and the estimated design mixture velocity is close to the deposit limit velocity. Or for instance when a wide range of particle sizes is expected, where the average particle diameter will change in time, and as such u_{dl} fluctuates as a function of the particle size.

The new insights also put into perspective why long distance dredging pipelines are traditionally designed at concentrations below 0.15. Namely, if a sliding bed density wave forms the peak could grow to twice the average concentration, thus 0.30. This is still on the safe side. If for instance the pipeline average concentration is designed at 0.20, and the mixture velocity drops below the deposit limit velocity for a short period, a density wave forms with a peak concentration of 0.4. This concentration is high enough that inter-particle and particle-wall forces start dominating frictional losses, and basically the wave becomes a mobile sediment plug (van den Berg, 2013). The plug has high resistance with the pipe wall (Visintainer et al., 2023), slowing down the mixture in the pipe, and if the wave is long enough this could lead to a pipeline blockage.

Erosion driven density waves form less risk to long pipelines that operate close to the deposit limit velocity. The argument is twofold. Firstly, if density waves are formed, their amplitude will grow to $c_{w,peak} = 1.5c_{w,mean}$, which is less than sliding bed waves. This also suggests that long pipelines transporting fine sand can be designed for slightly higher concentrations, perhaps to an average concentration of 0.2 (then waves will grow to 0.30, which is still considered safe). Secondly, the erosion driven density waves need more time develop to full amplitude, compared to the sliding bed driven density waves. Therefore, if the pipeline mixture velocity drops below u_{dl} for a short period, the wave might not have the time to fully develop and become large enough to impede the safety of the pipeline. In contrary, the sliding bed driven density waves develop very quickly, and could grow to full amplitude if the mixture velocity temporarily drops below u_{dl} for a short period. Exactly how short this period may be, is still difficult to estimate with the current knowledge.

One question remains: What density wave mechanism was predominating the Prins Claus pipeline? The arguments for sliding bed driven waves are: i) The wave peaks are ~ 2.0 times the mean concentration. ii) The Prins Claus pipeline data clearly shows long sections (up to an hour in time) with only water and all sediment was absorbed into the waves. The arguments for erosion driven waves are: i) the mean particle diameter in the Prins Claus pipeline is in the range of 100-300 μm, and from the experiments of this research that would indicate erosion driven waves. ii) The growth rate of the Prins Clause pipeline seems low, requiring tens of minutes to develop, and do not seem to grow almost instantly as seen in the sliding bed driven waves of this experiment. This last argument however is not that solid, since it is not known how much time the Prins Claus pipeline actually operated below u_{dl}. If the pipeline would have constantly operated below u_{dl} then sliding bed driven waves would formed rapidly, based on lessons learnt in this research. However, if the pipeline only sporadically operated below u_{dl} than even the growth rate of sliding bed density waves would seem low.

A strong counter argument against sliding bed driven waves in the Prins Claus pipeline is the particle size, being similar to particle sizes that showed erosion driven waves in this research. However, it was reported that the distribution of particle was very broad with 0.07 by volume larger than 700 μm, which is large enough to cause sliding bed driven waves. The experiments of this research were well graded sands, thus a direct comparison of mean particles sizes might not be valid. If sliding bed driven density waves were indeed the main mechanism in the Prins Claus pipeline, then the waves were caused by the larger fractions of the particle size distribution. Whether this is possible is a important research question for future research, since broadly graded sediments are very common in practical applications.

3.5. CONCLUSIONS

THIS chapter was dedicated to study the effect of the particle diameter and concentration on the formation of self-amplifying density waves in horizontal hydraulic transport pipeline. The experiments revealed that Talmon et al. (2007) and Matoušek and Krupička (2013) were studying two different density wave mechanisms, while describing the same traditional theory by Talmon (1999). The experiments of this research clearly distinguish the two wave types.

Erosion driven density waves developed in case of finer sands, in this research 242 and 308 μm. Erosion driven density waves develop relatively slowly, and can reach a peak amplitude 1.5 times the average concentration of the mixture, as found in this research.

Sliding bed driven density waves, are caused by the inverse proportionality between the deposit limit velocity and the concentration, at mean mixture concentrations above ~ 0.1. These waves form the highest risk for hydraulic transport pipelines compared to the erosion driven density waves, since the sliding bed driven density waves reach their peak amplitude very rapidly, and their amplitude can grow to twice the average mixture concentration, as found in this research.

The density wave data generated is very useful for future numerical modelling of these processes. First steps toward numerical modeling have already been made in (de Hoog et al., 2024b). Furthermore, the new knowledge already provides valuable insights for pipeline designers today. Long distance pipelines are always designed conservatively with concentrations not exceeding ~ 0.15. The new insights in the mechanisms responsibly for density waves, explains how this conservative limit came to be. In addition, we know that erosion driven density waves are not as risky as sliding bed driven density waves, therefore the design limit can be chosen less conservatively. An open question remains: What is the influence of the particle size distribution on the type of wave that develops? Can a broad distribution lead to sliding bed driven density waves, while the mean particle size is low ($\sim< 300\,\mu m$)? This question should be answered as part of future research.

4

TRANSIENT ACCUMULATION DENSITY WAVES: EXPERIMENTS AND THE 1DHT MODEL

This chapter presents the 1-Dimensional-Hydraulic-Transport (1DHT) CFD model. This model was developed to simulate transient accumulation density waves as encountered in the Freiberg experiments and developed as a transient pipeline design tool. The traditional steady-state pipeline design method (see Chapter 1) was insufficient to assure safe flow in the Freiberg pipeline, as the transient accumulation waves self-amplified at mixture velocities far above the deposit limit velocity. This chapter contains the mathematical foundation of the 1DHT model and applies the data of the Freiberg experiments for calibration and validation. The 1DHT model shows its ability to predict transient accumulation density waves. This chapter also contains a sensitivity analysis of the model and ends with a discussion on the application range of the 1DHT model.

*This chapter has been published in Powder Technology **400(3)** (2022).*

4.1. INTRODUCTION

DENSITY variations in hydraulic transport pipelines are very common, caused by fluctuating solids influx. These fluctuations are caused by the nature of the excavation process typically feeding these pipelines, and by the dredge operators actions. In the 1980's it was discovered that density waves could amplify while flowing through the pipeline, when the bulk velocity was too close to the deposition limit velocity, defined as the threshold velocity at which particles settle out of suspension and form a deposit in the pipeline. Research by Matoušek (1996b, 1997), Talmon (1999), Talmon et al. (2007) laid the foundation for understanding density wave amplification for horizontal pipelines, caused by an inverse relationship between sedimentation and erosion of sand deposits in a pipeline when the pipeline operates close to the deposit limit velocity. This is referred to the "erosion and sedimentation imbalance", and as a result high concentration zones of a slurry erode deposits and low concentration parts form deposits (de Hoog et al., 2021, Talmon, 1999). As such, a spatial redistribution occurs with sediment redistributing from low density parts to high density parts of the flow. Density wave amplification in horizontal pipelines can be avoided by remaining well above the deposit limit velocity, preferably with a safety margin to compensate for inaccuracies in deposit limit velocity predictive models and to account for velocity variations due to pipeline-pump dynamics (de Hoog et al., 2021), see Chapter 2.

Recent experimental research into vertical hydraulic transport technology for deep sea mining (Mueller et al., 2018) showed density wave amplification occurring far above the deposition limit velocity. These experiments, referred to as the "Freiberg experiments," were conducted in a closed loop pipe circuit, containing long vertical sections and some horizontal pipes to facilitate a centrifugal pump and soil injection and separation equipment (more details can be found in Section 4.3.1). A combined vertical and horizontal loop is designed based upon the deposit limit velocity of the horizontal pipes, as the minimum design velocity of vertical pipes is typically lower (which is typically two or thee times the terminal settling velocity of the largest particles (van Wijk, 2016)). The Freiberg experiments showed density wave amplification in all tests at mixture velocities significantly above the deposit limit velocity of the horizontal pipes (sometimes double). The amplification rate seemed to depend on the particle size, the average volumetric concentration and the mixture velocity relative to the deposit limit velocity (more details in Section 4.3.1). The origins of the mechanism behind amplification was explored by de Hoog et al. (2021) and was thought to be caused by a different and new mechanism as opposed to the erosion and sedimentation imbalance. The authors of de Hoog et al. (2021) hypothesized that amplification can be caused by a reduction of the particle velocity when particles flow from vertical to horizontal pipes resulting in an increase in concentration, referred to as "transient accumulation." This chapter continues with work of de Hoog et al. (2021) (Chapter 2) and explains transient accumulation and presents the Freiberg vertical transport experiments which were subject to this new type of density wave amplification. Amplification through transient accumulation is caused by local particle velocity differences (as a function of pipe orientation) and interaction between the centrifugal pump load and changing pipeline resistance (more details in Section 4.2). These interactions are difficult to isolate and study experimentally, since

they occur simultaneously and the interaction is two way. Due to the complex nature of the interaction, the problem is best investigated using transient modelling. Therefore, this chapter presents a 1D Driftflux CFD model, which accounts for the pump-pipeline interaction and particle velocity variations and is capable of predicting density wave amplification. The 1D model shows very satisfactory agreement with the Freiberg experiments.

4.2. Theory - transient accumulation

The mechanism causing density wave amplification at mixture velocities far exceeding the deposit limit velocity, as experienced in the Freiberg experiments, was first discussed in de Hoog et al. (2021). It was speculated that amplification was caused by a velocity difference of particles when flowing from the horizontal into and vertical parts of the circuit. The reasoning was based on studying the Freiberg data, observing that density waves grew faster at lower velocities (but still above the deposit limit) and at higher concentrations, which increases the spatial particle velocity difference. The volumetric mixture velocity

$$u_m = u_s c + u_f (1 - c) \tag{4.1}$$

is by its definition spatially constant

$$\frac{\partial u_m}{\partial x} = 0 \tag{4.2}$$

With u_s = the cross section averaged particle velocity, u_f = the cross section averaged fluid velocity and c = the volumetric concentration of solids. The solids velocity u_s and fluid velocity u_f may change locally, for instance due to the pipe orientation, or a difference in the local mixture concentration. Regardless, u_m remains the same throughout the pipeline, as u_m is based on a volume flow balance. The transport of particles in a pipe can be described with a 1D advection-diffusion equation (de Hoog et al., 2021, Talmon, 1999, van Wijk, 2016):

$$\frac{\partial c}{\partial t} + \frac{\partial}{\partial x}(u_s c) = \frac{\partial}{\partial x}\left(\epsilon \frac{\partial c}{\partial x}\right) \tag{4.3}$$

Where x = the axial coordinate along the pipe (regardless of orientation) and ϵ = a diffusion coefficient. As mentioned before, the cross section averaged particle velocity u_s can differ locally, as a function of the local concentration and pipe orientation. Particles travel faster in vertical pipes, because frictional losses are lower compared to horizontal pipes. Assuming a temporal steady-state, and the effect of diffusion is low, Equation 4.3 reduces to:

$$\frac{\partial}{\partial x}(u_s c) = 0 \tag{4.4}$$

As such, when particles flow from a vertical riser into a horizontal pipe and the particle velocity decreases, the concentration increases simultaneously. Specifically, equation 4.4 shows that $u_s c$ should remain constant between the vertical and horizontal pipe,

and as such the concentration increase in the horizontal pipe is inversely proportional to the particle velocity decrease:

$$\frac{c_1}{c_2} = \frac{u_{s,2}}{u_{s,1}} \tag{4.5}$$

In Equation 4.5, subscript 1 denotes the vertical pipe, and subscript 2 the horizontal pipe.

The particle velocity in the horizontal pipe can be estimated from the slip ratio R_s (Wilson et al., 2006), which is a commonly used concept by hydraulic transport researchers, although it is difficult to measure and therefore data and models are scarce.

$$R_s = \frac{u_s}{u_m} \tag{4.6}$$

For vertical pipes van Wijk (2016) showed that the cross section average particle velocity u_s can be modeled well using the hindered settling principle Richardson and Zaki (1954), under the assumptions that the particles are homogeneously distributed in the pipe cross-section. Note, for very low concentration this assumption might be invalid, as Messa and Malavasi (2014) show that for coarse particles at $c < 0.03$ the concentration profile is non-uniform. The hindered settling principle is as follows:

$$u_s = u_m - v_{ts}(1-c)^n 10^{-d/D} \tag{4.7}$$

In the Equation above v_{ts} = the terminal settling velocity of a particle and n = the Richardson & Zaki settling exponent (calculated using Garside and Al-Dibouni (1977)). For large particles relative to the pipe diameter, the d/D term is required, which is usually neglected by most researchers. The terminal setting velocity can be calculated using Ferguson and Church (2004).

Figure 4.1 shows the ratio of the particle velocity u_s over the volumetric mixture velocity u_m as a function of u_m at a volumetric concentration of $c = 0.15$, for a vertical riser and a horizontal pipe. For the horizontal pipe the slip ratio model from Sobota and Kril (1992) was used (for more details see Section 4.3.2).

The magnitude of the particle velocity difference between the vertical and horizontal pipes is shown well in Figure 4.1. The spatial particle velocity difference is higher at lower mixture velocities. Thus from this trend, if amplification is indeed caused by a spatial particle velocity change, one expects that amplification would be more severe at lower mixture velocities, which was indeed observed in the Freiberg experiments (more details in Section 4.3.1).

However, de Hoog et al. (2021) (Section 3.5) does not manage to explain how a spatial velocity change actually leads to amplification of density waves. Imagine a vertical riser, followed by a horizontal pipe and another riser. At a constant mixture velocity, a density wave first flows from the riser into the horizontal pipe. As a results, the particle velocity decreases going from (1) to (2) in Figure 4.1, accompanied by an increase in concentration. Once the mixture flows out of the horizontal pipe and into the second riser, the

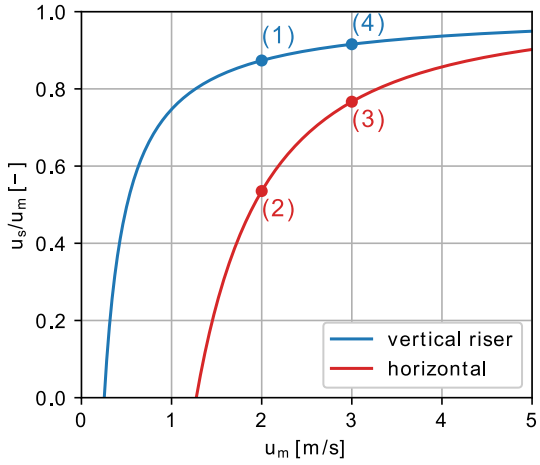

Figure 4.1: The cross section averaged particle velocity in a vertical riser and a horizontal pipe, calculated using Equations 4.25 and 4.7. $D = 150\,mm$, $d = 11.2\,mm$, $\rho_s = 2650\,kg/m^3$, $c = 0.15$.

mixture velocity increases (from (2) to (1) in Figure 4.1) and the concentration recovers. The transient accumulation in the horizontal pipe was temporary.

However, if the mixture velocity increases when the density wave flows through the horizontal pipe, the concentration recovers less when flowing into the second riser, from (3) to (4) in Figure 4.1. In other words, when the mixture velocity increases, the spatial particle velocity change is less when the wave flows out of the horizontal pipe compared to when the wave flowed into the horizontal pipe. Mathematically, the absolute value of the spatial velocity gradient when the wave flows from the first riser (1) into the horizontal pipe (2), is greater than the gradient when the wave flows out of the horizontal pipe (3) into the second riser (4), if the mixture velocity accelerates when the wave was flowing through the horizontal pipe:

$$\left|\left(\frac{\partial u_s}{\partial x}\right)_{1,2}\right| > \left(\frac{\partial u_s}{\partial x}\right)_{3,4} \tag{4.8}$$

and

$$\left(\frac{\partial c}{\partial x}\right)_{1,2} > \left|\left(\frac{\partial c}{\partial x}\right)_{3,4}\right| \tag{4.9}$$

if

$$\left(\frac{\partial u_m}{\partial t}\right)_{2,3} > 0 \tag{4.10}$$

Note that the concentration of the wave does not increase when flowing through the horizontal pipe, because there is no spatial velocity change (caused by a pipe orientation change) and only a temporal mixture velocity change (i.e. $\frac{\partial u_s}{\partial x} = 0$).

Concluding, when the mixture accelerates the mixture concentration does not recover to its original when the wave flow out of the horizontal pipe and the density wave remains amplified. The mixture velocity increases when the density wave flows into the horizontal pipe, because a centrifugal pump does not operate at constant flow rate, and the hydrostatic pressure required to lift the wave in the riser is lost. As such, the system accelerates while the pump revolutions remain constant.

4.3. Methods and Materials

4.3.1. Experiments

In 2017 a vertical hydraulic transport flow loop was constructed in a vertical mineshaft by a collaboration of Royal IHC and Bergakademie Freiberg located in Halsbücke, Germany. The goal of this flow loop was to investigate and validate wall resistance models, particle slip models, plug formation for vertical hydraulic transport used for deep sea mining applications. The flow loop, with a 152 mm inner diameter, consisted of a 121 m vertical descending pipe, a 121 m long riser and 57 m of horizontal pipelines at the top side. The top side pipes were to facilitate the centrifugal pump and the soil injection and separation equipment. See Figure 4.2 for a schematic overview of the flow loop and the instrumentation. For more details a reference is made to Mueller et al. (2018).

The flow loop was instrumented with a magnetic flow meter (Krohne Optiflux 4000) to measure the mixture velocity, a pressure differential meter measuring the centrifugal pump manometric pressure and a u-loop delivered concentration measurement system Clift and Manning Clift (1981). The delivered concentration

$$c_{vd} = \frac{Q_s}{Q_m} \tag{4.11}$$

is defined as the ratio of the solids flow rate Q_s over the mixture flow rate Q_m Wilson et al. (2006) and is measured based on differential pressure according to the technique described in Clift and Manning Clift (1981). The corresponding differential pressure measurement over $p1 \rightarrow p2$ and $p3 \rightarrow p4$ was placed 7.5 m apart at the bottom of the two vertical pipes, see Figure 4.2.

The researchers used sand and gravel with a d_{50} particle diameter of 600 μm and 11.2 mm respectively (distribution in Figure 4.3) and the volumetric concentration of sediment was varied as an experimental parameter, between 0.05 and 0.15. The deposition limit velocity of these two sediment types was estimated to be $\sim 2.5\, m/s$ and $\sim 1.5\, m/s$, for the 600 μm sand and 11.2 mm gravel respectively. The mean particle diameter

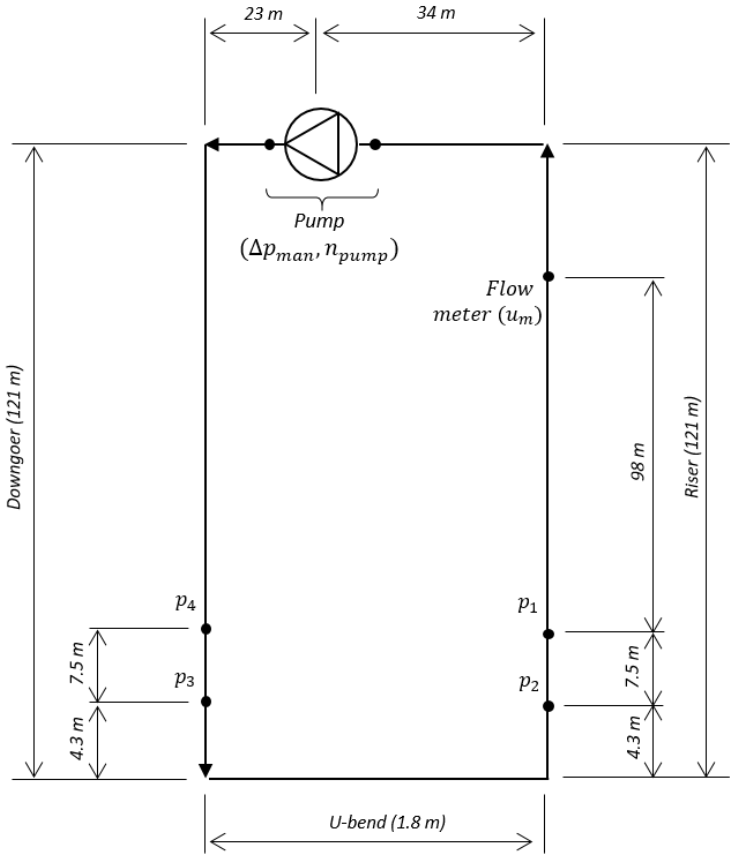

Figure 4.2: A schematic of the flow loop built in Freiberg.

$$d_m = \frac{d_{10} + d_{20} + ... + d_{90}}{9} \tag{4.12}$$

of the sand and gravel are $d_m = 741\,\mu m$ and $d_m = 12.1\,mm$, respectively.

The experiments were set up to measure the steady state pressure losses of the mixture. As such, the test started at the highest velocity, thereafter the velocity was lowered in increments of $0.5\,m/s$ every few minutes. The results of four notable experiments can be viewed in Figures 4.4, 4.5, 4.6 and 4.7, showing time traces of the mixture velocity, delivered concentration, pump pressure and pump revolutions. At the start of the experiment the system was empty, as shown by the concentration time traces, and was filled up to the desired sediment concentration. Each experiment was preceded by a water experiment, which were used to determine wall friction coefficients. The relative wall roughness $\frac{k_s}{D}$ changed throughout the course of the experimental program, varying between $4.7 \cdot 10^{-4} \leq \frac{k_s}{D} \leq 9.5 \cdot 10^{-4}$. The roughness was determined using differential pressure measurement along the riser, as part of water-only-experiments conducted be-

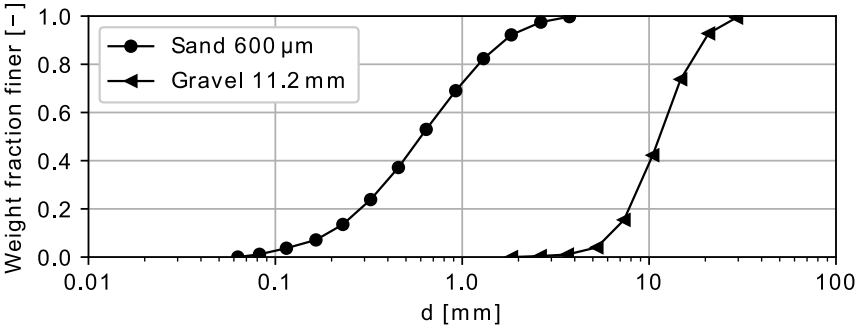

Figure 4.3: The particle size distribution of the 600 μm sand, and the 11.2 mm gravel.

fore and after each mixture experiment. The wall roughness was found to change over time, likely due to degradation of the pipe wall.

nr.	$d_m\,[mm]$	$d_{50}\,[mm]$	$c\,[-]$	$u_{dl}\,[m/s]$	$u_{th}\,[m/s]$
1	0.741	0.600	0.05-0.10	~ 2.5	~ 3.7
2	0.741	0.600	0.07	~ 2.5	~ 3.5
3	12.1	11.2	0.05	~ 1.5	~ 2.5
4	12.1	11.2	0.14	~ 1.5	~ 3.2

Table 4.1: Parameters of the conducted experiments.

The density wave amplification effect is clearly demonstrated in Figures 4.4, 4.5, 4.6 and 4.7 and occurred in all conducted experiments. No additional sediment was added and the system was a closed loop, therefore amplification is in essence a material redistribution effect. Also note that amplification occurred even when the pump revolutions were constant over long periods. Also notable is the fact that the mixture velocity at which amplification took place was well above the deposit limit velocity, which is a stability criterion to avoid amplification through the erosion and sedimentation imbalance as described in de Hoog et al. (2021). The threshold velocity at which the first significant wave was formed (which continues to grow) is given in Table 4.1 as u_{th}, which is between 40% and 110% higher than the deposit limit velocity. In addition the wave length of the density waves was roughly equal to the system length (the total length of all pipes). Furthermore, the shape of strong density waves is saw-tooth like (Figures 4.4b and 4.7b) and skewed towards the front of the wave. The saw-tooth shape is caused by the fact that at high concentration the cross section averaged particle velocity is higher than at low concentration (de Hoog et al., 2021, Talmon et al., 2007).

The mixture velocity varies in unison with the density waves. This is a result of the working principle of a centrifugal pump. Namely, the mixture velocity is a result of both

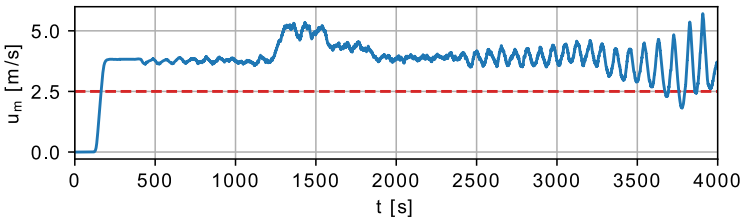

(a) Blue solid: The measured mixture velocity. Red dashed: estimation of u_{dl}.

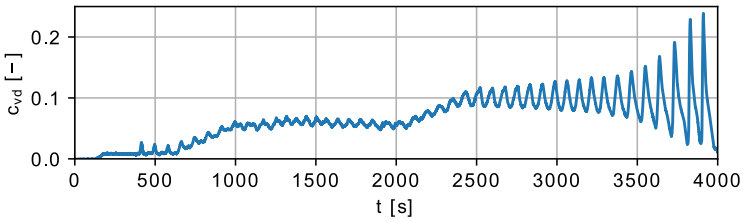

(b) The delivered concentration.

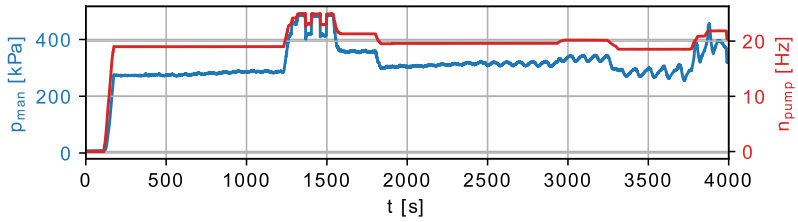

(c) The pump manometric pressure (blue) and the pump revolutions (red).

Figure 4.4: Experiment nr. 1, with sand, $d_m = 741\,\mu m$, $c = 0.05 - 0.10$.

the pump revolutions and the resistance of the pipeline (Wilson et al., 2006). At constant pump revolutions, the pipeline resistance continues to change and depends on the position of the density wave in the pipeline. The pipeline resistance is highest when the density wave travels up the riser, due to the hydrostatic mixture gradient. And the resistance is lowest when the wave travels down the downgoer and the hydrostatic gradient accelerates the mixture. When the waves flows out of the riser into the horizontal pipes, the mixture accelerates and the conditions are met to initiate amplification through the transient accumulation mechanism as explained in Section 4.2.

The experiment shown in Figure 4.4 was initially at an average volumetric delivered concentration $c_{vd} = 0.05$, and small waves were constant in amplitude, however once the system was filled further up to $c_{vd} = 0.10$ the density wave grew with each circulation through the loop, while the average mixture velocity had not changed significantly ($u_m \approx 3.7 m/s$), but still remained well above the deposit limit velocity ($u_{dl} \approx 2.5 m/s$).

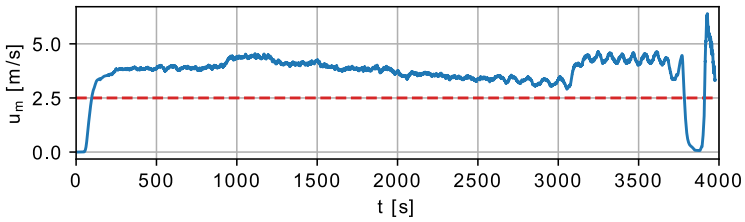

(a) Blue solid: The measured mixture velocity. Red dashed: estimation of u_{dl}.

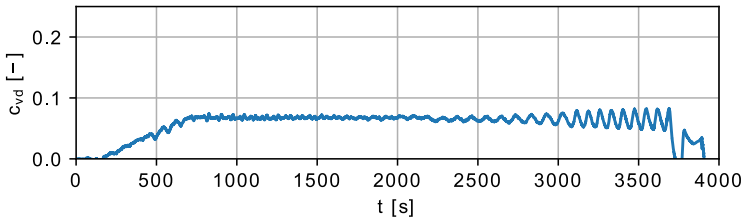

(b) The delivered concentration.

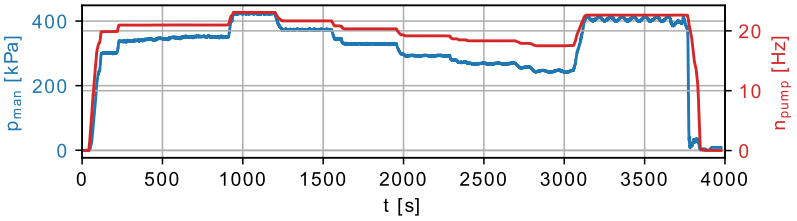

(c) The pump manometric pressure (blue) and the pump revolutions (red).

Figure 4.5: Experiment nr. 2, with sand, $d_m = 741\,\mu m$, $c = 0.07$.

This demonstrates that the concentration influences the onset of amplification and the amplification rate. This concentration dependency is further demonstrated in the experiments of Figures 4.6 and 4.7, where $11.2\,mm$ gravel was transported at an average volumetric concentration of 0.05 and 0.15, respectively. The low concentration experiment was initially stable, until the mixture velocity was reduced to around $u_m = 2.5 m/s$ and amplification sets on very rapidly, while still being above the deposit limit velocity $u_{dl} \approx 1.5 m/s$. The high concentration gravel experiment however (Figure 4.7) was unstable from the start ($u_m \approx 3.2 m/s$, $u_{udl} \approx 1.5 m/s$), regardless of the high velocity, demonstrating the concentration influence on amplification. Section 4.2 explains how density waves can amplify due to a spatial particle velocity change. The magnitude of the velocity change is a function of the concentration, being larger at higher concentration. A larger spatial velocity change therefore leads to a higher amplification, which explains the concentration dependency amplification.

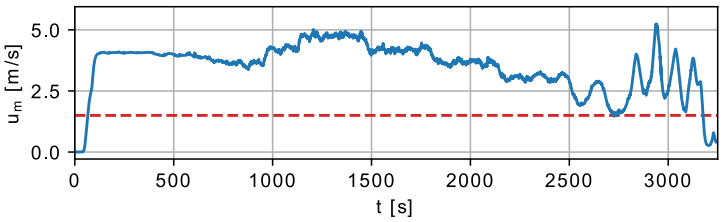

(a) Blue solid: The measured mixture velocity. Red dashed: estimation of u_{dl}.

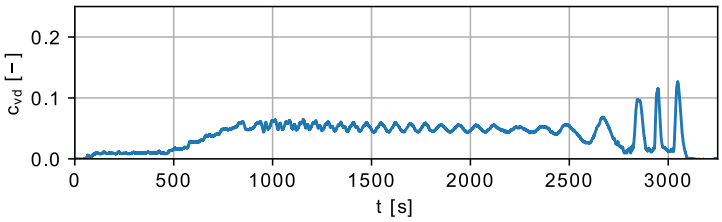

(b) The delivered concentration.

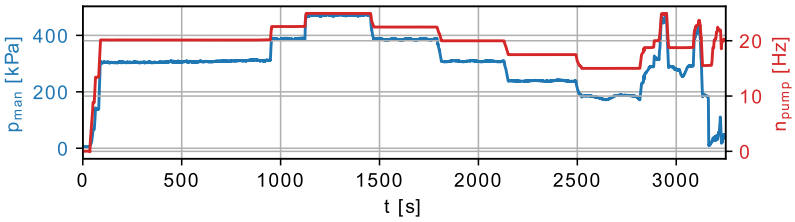

(c) The pump manometric pressure (blue) and the pump revolutions (red).

Figure 4.6: Experiment nr. 3, with gravel, $d_m = 12.1\,mm$, $c = 0.05$.

Figure 4.5 and 4.6 also demonstrate that the average mixture velocity influences the onset of amplification as both experiments were stable at high velocity, and amplification started below a certain velocity, even though the mixture velocity was still well above the deposit limit velocity ($\sim 2.5\,m/s$ and $\sim 1.5\,m/s$, for the $600\,\mu m$ sand and $11.2\,mm$ gravel respectively). This can again be explained because at lower mixture velocities, the spatial velocity change of particles between the horizontal and vertical pipes, is higher than at high velocity. As such the concentration change is also higher at low mixture velocities (see Figure 4.1).

4.3.2. 1D CFD Driftflux Model

A 1D CFD Drift-flux model is proposed to study and model the density wave amplification as witnessed in the Freiberg flow loop. For the model to predict density

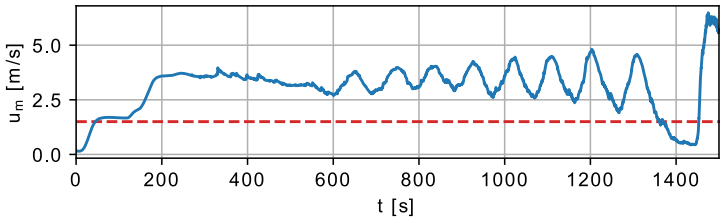

(a) Blue solid: The measured mixture velocity. Red dashed: estimation of u_{dl}.

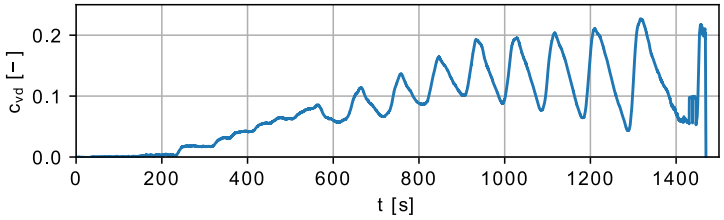

(b) The delivered concentration.

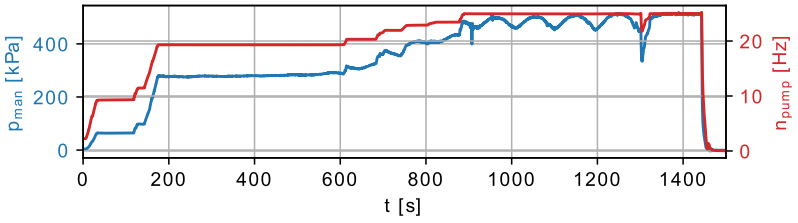

(c) The pump manometric pressure (blue) and the pump revolutions (red).

Figure 4.7: Experiment nr. 4, with gravel, $d_m = 12.1\,mm$, $c = 0.14$.

wave amplification, the particle velocity should be a function of pipe orientation (vertical or horizontal) and of the concentration (see Section 4.2). Furthermore, the model should be pressure driven and the pressure source should be representative of a centrifugal pump, where the pressure is a function of the volumetric flow rate, particle diameter and concentration. With such a pressure driven model, the variations in pipeline resistance will lead to mixture velocity variations.

MODEL STRUCTURE

For the 1D model presented below all scalar values are cross section averaged values. In the Driftflux model a distinction is made between two types of mixture velocities. The first mixture velocity u_m is based on the volumetric flow rate of all phases (Equation 4.1). Another mixture velocity $\hat{u}_m$ can be defined based on the mass flow rate of the phases (Ishii and Hibiki, 2011):

$$\hat{u}_m = u_f \frac{\rho_f}{\rho_m}(1-c) + u_s \frac{\rho_s}{\rho_m} c \tag{4.13}$$

With ρ_s = the solids density, ρ_f = the fluid phase density and ρ_m = mixture density. u_m is often referred to as the volumetric flux j and $\hat{u}_m$ the Favre average mixture velocity in Drift-flux literature (Goeree, 2018, Ishii and Hibiki, 2011). The Drift-flux model is based on a single continuity equation taking into account all phases (Goeree, 2018, Ishii and Hibiki, 2011):

$$\frac{\partial \rho_m}{\partial t} + \frac{\partial}{\partial x}(\rho_m \hat{u}_m) = 0 \tag{4.14}$$

The 1D mixture momentum equation is based on the assumption that the mixture can be modeled as a single fluid with density ρ_m and is based on the work of Goeree (2018), van Wijk (2016). Note that x is the axial coordinate along the pipeline, whether the pipe is horizontal or vertical.

$$\begin{aligned} \frac{\partial}{\partial t}(\rho_m \hat{u}_m) + \frac{\partial}{\partial x}(\rho_m \hat{u}_m \hat{u}_m) = -\frac{\partial p}{\partial x} - \frac{4\tau_m}{D} - \rho_m g \sin(\omega) + \dots \\ -\frac{\partial}{\partial x}\left[c\rho_s(\hat{u}_m - u_s)^2 + (1-c)\rho_f(\hat{u}_m - u_f)^2 \right] + S_p \end{aligned} \tag{4.15}$$

In Equation 4.15, τ_m = mixture wall shear stress, ω = pipe inclination angle ($\omega = 0 \vee \omega = \pm\pi/2$), S_p = a pressure gradient source term to model the pressure added by a centrifugal pump and the second from last term represents the inertial coupling forces, caused by a velocity difference between the phases (Chao et al., 1978, Soo, 1976, Verloop, 1995). Pipes at different orientation (currently only vertical or horizontal) can be modeled by specifying an inclination angle for each grid cell, and as such vertical and horizontal pipes can be modeled in the same domain and solving a single momentum equation. In theory any pipe inclination could be modeled with Equation 4.15, however certain closure relationships need to be adapted to be valid for all inclinations (see below). Currently the closures presented in this work are only for horizontal and vertical pipes.

The particle transport is modeled using the finite volume method, which is best to ensure mass continuity. Since with a 1D model, small mass discontinuities are very noticeable. The finite volume method according to Hirsch (2007):

$$\int_V \frac{\partial c}{\partial t} dV + \oint_A \vec{F} \cdot d\vec{A} = 0 \tag{4.16}$$

Where c = the volumetric concentration, V = the volume of a finite volume, F = the solids flux and A = the volume surface. Using the 1D grid definition shown in Figure 4.8, allows us to rewrite Equation 4.16 to:

$$\frac{\partial c}{\partial t} + \frac{1}{\Delta x} \sum_{faces} F = 0 \tag{4.17}$$

With F = the cell face solid fluxes.

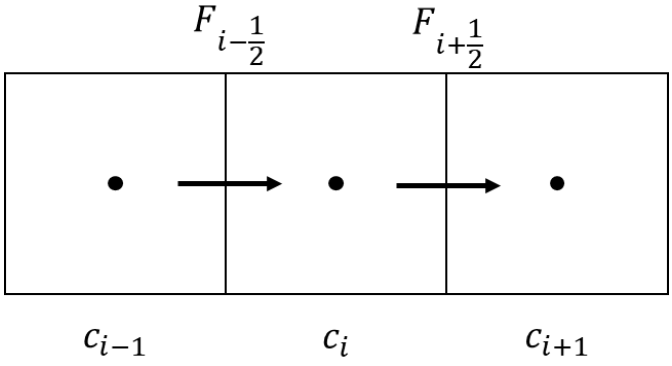

Figure 4.8: The grid definition of the 1D Drift-flux model

The cell face solid fluxes are modeled as:

$$F = u_s c \tag{4.18}$$

Typically the model is advection dominated, therefore to ensure stability c is numerically modeled using the van Leer flux limiter (Hirsch, 2007). The particle cross section averaged particle velocity u_s is modeled as:

$$u_s = u_m + u_{s/m} - \frac{\epsilon}{c} \cdot \frac{\partial c}{\partial x} \tag{4.19}$$

Where $u_{s/m}$ is the cross section averaged relative velocity of the particle with respect to the volumetric mixture velocity u_m and the last term Equation 4.19 is the diffusion velocity, modeled through the diffusion coefficient ϵ (note: $u_{s/m}$ is negative if the particle velocity is lower than the mixture velocity).

CLOSURE RELATIONSHIPS

The 1D Driftflux model as presented above requires relationships for the wall shear stress τ_m, the relative particle velocity $u_{s/m}$ and the diffusion coefficient ϵ. The wall shear stress of the mixture is the sum of the wall shear stress caused by the fluid τ_f, by the solids τ_s and minor losses τ_{ml} from system components like bends and flanges:

$$\tau_m = \tau_f + \tau_s + \tau_{ml} \tag{4.20}$$

The fluid shear stress is calculated using the Darcy-Weisbach equation:

$$\tau_f = \frac{f}{8}\rho_f u_m^2 \tag{4.21}$$

With f = Darcy-Weisbach friction factor, ρ_f the fluid density. Minor losses are to account for losses from appendages (bends, flanges and valves). The minor losses are in practice local losses, but in the solver are distributed over the entire domain, to avoid an excess amount of large pressure gradients, and associated numerical stability issues.

$$\tau_{ml} = \frac{1}{N_c}\sum_{i=0}^{N_a-1} K_i \frac{D}{8}\rho_{m,i} u_{m,i}^2 \tag{4.22}$$

With K_i = the appendage loss coefficient, N_c = the amount of cells in the 1D domain, N_a = the amount of appendages, $\rho_{m,i}$ = the local mixture density at the appendage and $u_{m,i}$ = the local mixture velocity. The solids shear stress for sand can be modeled with the equivalent liquid model concept for sufficiently high mixture velocities (Wilson et al., 2006). For sand and horizontal pipes the wall friction is calculated as:

$$\tau_s = \frac{f}{8}(\rho_m - \rho_f) u_m^2 \tag{4.23}$$

With ρ_m = mixture density and ρ_f = the fluid density. This wall sheer stress model is valid for sand slurries at high velocities ($u_m >> u_{dl}$), which is valid when applying this model for the Freiberg experiments. However, for more general cases (other than this research) keep in mind that a wall resistance model might be needed which is better suited at mixture velocities close to the deposit limit velocity, such as wall resistance models for heterogeneous slurries (Gillies et al., 2004). For the gravel slurries the wall friction is significantly higher compared to sand slurries, as the sediment is transported in a sliding bed layer. Therefore we recommend to use the sliding bed correlation used by de Hoog et al. (2017), Miedema and Ramsdell (2019), Newitt et al. (1955). For gravel and horizontal pipes the wall friction is calculated as:

$$\tau_s = \mu_{sf}\frac{D}{4} g(\rho_m - \rho_f) \tag{4.24}$$

With μ_{sf} = the mechanical friction factor between the sliding gravel bed and the pipe wall ($\mu_{sf} \approx 0.4$), D = the pipe diameter, g = the gravitational constant. This sliding bed wall friction model can be improved by applying more advanced stationary two-layer models for sliding bed flow (Matoušek et al., 2018, Wilson et al., 2006), however these are iterative in nature. Furthermore, these iterative models were found to be difficult to implement in within this numerical framework, due to instabilities in the two-layer

model results and vastly increased calculation times. The focus of this research was on developing the 1D model framework, therefore we use a less accurate, but easier to use empirical model (Equation 4.24). For vertical pipes Equation 4.23 is applied to model the wall friction, which is valid for vertical flows if the distribution of particles in the pipe cross section is homogeneous and mechanical stresses due to particle-wall contact is low.

The relative velocity $u_{s/m}$ models the velocity difference between the solids and the mixture. Empirical slurry transport research focuses mostly on wall friction losses, yet some measurements and relationships of the slip ratio (Equation 4.6) have been made during the past decades. The state of the art are physical stationary two-layer models (Matoušek et al., 2018, Wilson et al., 2006), but again these models require iterative computation. As part of this research the empirical correlation of Sobota and Kril (1992) was found to be a good alternative to simulate both sand and gravel slurries in horizontal pipes, as this model was calibrated for both sand and gravel flows. The relative velocity is calculated from the slip ratio as:

$$u_{s/m} = u_m(R_s - 1) \tag{4.25}$$

In the Equation above R_s is modeled according to Sobota and Kril (1992):

$$R_s = 1 - f_t\left(1 - \frac{c}{c_{max}}\right)^{2.16}\left(\frac{u_{crit}}{u_m}\right)^{1.7} \tag{4.26}$$

In which c_{max} = the maximum concentration of the sediment ($c_{max} \approx 0.6$) and u_{crit} = the critical velocity. Sobota and Kril (1992) does not provide a definition of u_{crit}, however in slurry transport research u_{crit} and u_{dl} typically describe a similar threshold velocity, the transition between particles in suspension and particle settling out of suspension ($u_{crit} \approx u_{dl}$). The empirical constant f_t was provided by Sobota and Kril (1992) as a graph as a function of $\log(Re_p)$. The Reynolds particle number

$$Re_p = \frac{d\,v_{ts}}{\nu_f} \tag{4.27}$$

is a function of the particle diameter d, the terminal settling velocity v_{ts} and the fluid viscosity ν_f. f_t can be approximated using:

$$f_t = \begin{cases} 0.1464 \cdot 10^{0.6031 \cdot \log(Re_p)} & \text{if } \log(Re_p) < 1 \\ 0.7858 \cdot \tanh[0.7986 \cdot \log(Re_p)] & \text{if } \log(Re_p) \geq 1 \end{cases} \tag{4.28}$$

Summarized, for horizontal pipes the relative particle velocity $u_{s/m}$ is modelled through Equations 4.25 and 4.26. While, the relative particle velocity in the vertical pipes is modelled according to the hindered settling principle (see also Equation 4.7):

$$u_{s/m} = v_{ts}(1 - c)^n 10^{-d/D} \tag{4.29}$$

The diffusion coefficient ϵ is modeled using Taylor dispersion Taylor (1954):

$$\epsilon_{Taylor} = 10.1 \frac{D}{2} \sqrt{\frac{\tau_f}{\rho_f}} \tag{4.30}$$

With D = pipe diameter, τ_f = the fluid wall friction and ρ_f = the fluid density. In van Wijk (2016), van Wijk et al. (2014) it was found that large particles experience reduced axial dispersion due to their higher inertia, and are therefore affected less by turbulent hydrodynamic forces. A modification to Taylor dispersion was proposed by van Wijk (2016), as a function of the Stokes number St:

$$\epsilon = \epsilon_{Taylor} f_\epsilon \tag{4.31}$$

$$f_\epsilon = \begin{cases} 1 - \frac{2}{3} St & \text{if } 0 < St \leq 1.5 \\ 0 & \text{if } St > 1.5 \end{cases} \tag{4.32}$$

The Stokes number is used to judge how well a particle is able to follow changes in the fluid velocity field and is a ratio of the particle reaction time t_p over the fluid reaction time t_f.

$$St = \frac{t_p}{t_f} \tag{4.33}$$

If $St << 1$ particle follows the fluid well and if $St >> 1$ particles detach from the flow. A suggested method to compute the Stokes number of large particles is given by van Wijk (2016), van Wijk et al. (2014):

$$St = \frac{4(\rho_s - \rho_f) d u_m}{3 \rho_f D v_{ts} C_D} \tag{4.34}$$

With ρ_s = particle density and C_D = the drag coefficient of a particle.

Implementation of a centrifugal pump

The centrifugal pump pressure is implemented in the momentum equation through the pressure gradient source term S_p. The source term can be applied in one grid cell, adding a pressure gradient representative of the pressure provided by the centrifugal pump. This method also supports multiple pump pressure sources along the domain, to simulate a multi-pump pipeline.

$$S_p = \frac{\Delta p_{man}}{\Delta x} \tag{4.35}$$

In the Equation above p_{man} = the manometric pressure added by the centrifugal pump, and Δx = the grid cell width. The manometric pressure of the pump is a function of the pump flow rate, this relationship is provided by the pump diagram. Figure 4.9 gives the pump diagram of the pump used in the Freiberg flow loop, and was determined by measurement.

The input of the 1D Driftflux is the rotational velocity of the pump. The pump curve of Figure 4.9 is scaled to the desired rotational velocity according to the following affinity laws (Wilson et al., 2006):

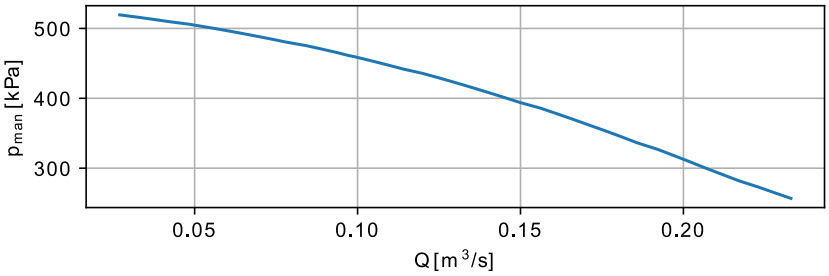

Figure 4.9: The pump curve (for water) of the 150 mm centrifugal dredge pump used in the Freiberg experiments, at a rotational velocity of 24.66 Hz.

$$\frac{Q_n}{Q_0} = \frac{n_{pump}}{n_{pump,0}} \tag{4.36}$$

$$\frac{p_{man,n}}{p_{man,0}} = \left(\frac{n_{pump}}{n_{pump,0}} \right)^2 \tag{4.37}$$

In the above Q_n and $p_{man,n}$ are the flow rate and the manometric pressure of the centrifugal pump at revolutions n_{pump}, respectively. Q_0 and $p_{man,0}$ are the respective flow rate and manometric pressure at reference revolution $n_{pump,0} = 24.66\,Hz$, see Figure 4.9.

The pressure of the pump increases proportionally with the local mixture density. However, this increase reduces slightly due to additional frictional losses caused by the particles. The pump head reduction factors of Stepanoff (1965) are applied to correct for these additional losses as shown in the Equation below.

$$\frac{p_{man,m}}{p_{man,f}} = \frac{\rho_m}{\rho_f} f_c \tag{4.38}$$

With $p_{man,m}$ = the pump manometric pressure at mixture density ρ_m and $p_{man,f}$ = the pump pressure at the fluid density ρ_f, and f_c = the Stepanoff head reduction factor.

$$f_c = 1 - c_{vd}[0.8 + 0.6\log(d)] \tag{4.39}$$

In the Equation above c_{vd} is the delivered concentration and d the particle diameter (d in $[mm]$).

Numerical implementation

The 1D Driftflux model of this research is an in-house research code and closely follows the discretization and solving techniques as described by Goeree (2018), van Wijk (2016). Summarized: The momentum equation (Eq. 4.15) was discretized on a staggered mesh. The Adams-Bashfort two time integration scheme (Hirsch, 2007) was applied to calculate an intermediate momentum, to allow for the large pressure gradients caused by the centrifugal pump source term (S_p is applied in a single cell, resulting in a large

pressure gradient). The results thus far obtained were used together with the fractional step method, giving a Pressure Poisson equation, which is solved using the Thomas algorithm. The momentum of the new time step is computed from the newly acquired pressure field, which also allows for computation of the mass based mixture velocity $\hat{u}_m$ on the new time step.

From the updated mass based mixture velocity $\hat{u}_m$, the volumetric mixture velocity u_m is updated, which is required to solve the transport equation. Firstly the relative velocity u_r is computed, which is the difference between the velocity of the solids and fluid phases (Ishii and Hibiki, 2011):

$$u_r = \frac{u_{s/m}}{1-c} \tag{4.40}$$

The relative velocity is a function of the volumetric concentration c and of the solids velocity relative to the volumetric mixture velocity $u_{s/m}$ (Eq. 4.25), which is the closure relationship as explained earlier and can be measured experimentally in laboratory circuits. The volumetric mixture velocity u_m is computed as (Ishii and Hibiki, 2011):

$$u_m = \hat{u}_m + (1-c)c\frac{\rho_f - \rho_s}{\rho_m}u_r \tag{4.41}$$

The solids velocity u_s and the fluid velocity u_f are computed as follows (Ishii and Hibiki, 2011):

$$u_s = u_m + cu_r \tag{4.42}$$

$$u_f = u_m - (1-c)u_r \tag{4.43}$$

With u_m known, the transport equation can solved using the finite volume method combined with the van Leer flux limiter for stability, as the transport equation is typically advection dominated.

4.4. Results

The interplay between spatial particle velocity, centrifugal pump load and mixture velocity changes can quickly become very complex and is difficult to investigate experimentally. The 1D Driftflux model presented in this research has the ability to simulate these effects, and investigate the magnitude of the influence of the aforementioned processes on density wave amplification, and therefore validate the hypothesis of transient accumulation.

The results of simulations using the 1D Driftflux model are presented in Figures 4.10, 4.11, 4.12 and 4.13. These figures compare the measured and simulated time traces of the volumetric mixture velocity, the delivered concentration and the pump manometric pressure.

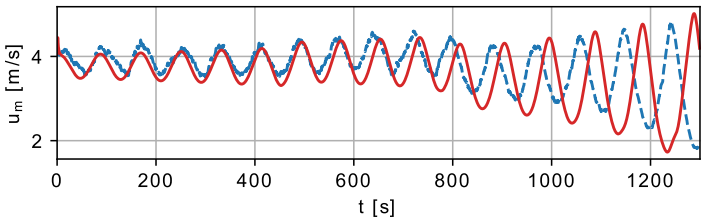

(a) The measured mixture velocity.

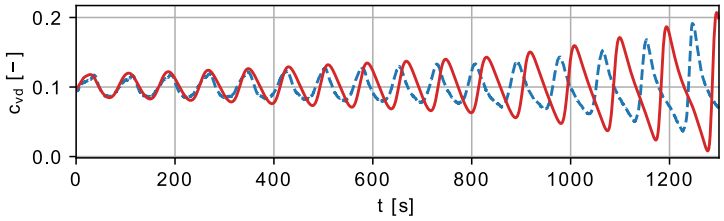

(b) Delivered concentration.

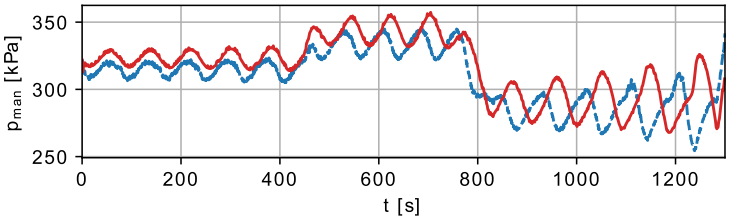

(c) Pump manometric pressure.

Figure 4.10: Simulation of the Freiberg experiment nr. 1. Blue: data, red: simulation. Sand, $d_m = 741\,\mu m$, $c = 0.05 - 0.10$.

4.4.1. Determination of model parameters

The closure relationships require two parameters, the wall roughness k_s (for the wall friction model) and the critical velocity u_{crit} (for the horizontal relative particle velocity model). All other parameters, such as particle diameter, pipe diameter, particle density, pump characteristics, etc. are known and can directly be applied. The initial conditions of the simulations were determined from the concentration data, i.e. the first wave in the data was matched with a sinusoidal wave with a mean concentration c_{mean} and an amplitude $c^{'}$, see Table 4.2. The first simulated wave is typically the first wave after the system was filled with sediment up to the desired concentration.

The wall roughness k_s was determined from the experimental data using a steady state analysis. The experimentally measured pump pressure equals the total resistance

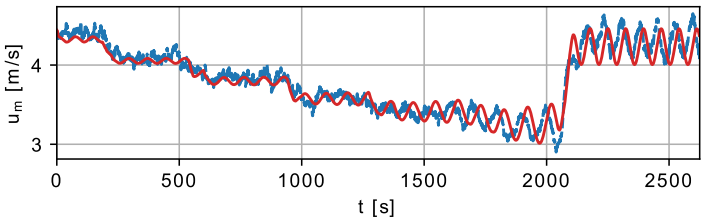

(a) The measured mixture velocity.

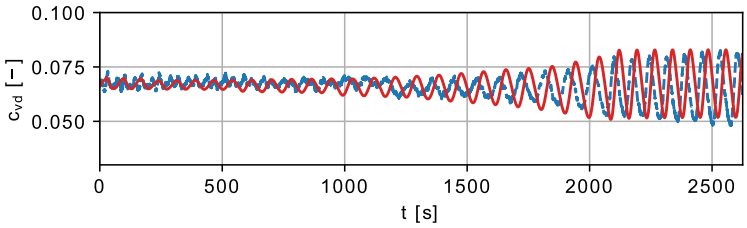

(b) Delivered concentration.

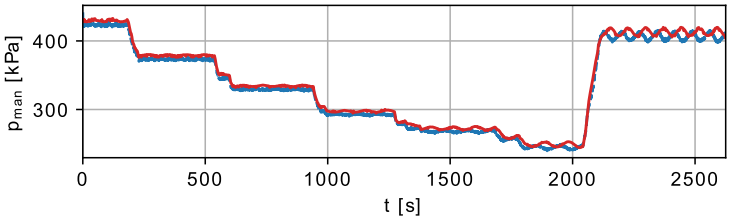

(c) Pump manometric pressure.

Figure 4.11: Simulation of the Freiberg experiment nr. 2. Blue: data, red: simulation. Sand, $d_m = 741\,\mu m$, $c = 0.07$.

losses of the pipe circuit, under steady-state conditions. Therefore, water experiments proceeding each mixture experiment were used to determine the wall roughness for the entire system (excluding minor losses), the results are shown in Table 4.2. Minor losses calculated based on the amount of bends, valves and flanges in the circuit, resulting in a total of $\Sigma K = 2.81$. The solids frictional losses were modeled as described in Section 4.3.2. In case of gravel, the mechanical friction factor between the sliding bed and pipe wall was chosen to be $\mu_{sf} = 0.4$, a typical value (de Hoog et al., 2017).

The modeled pump pressure was compared to the predicted pump pressure also using a steady-state analysis. The pump diagram in Figure 4.9 was measured accurately in a laboratory in the past, and the particle correction by Stepanoff (1965) was found to work very well.

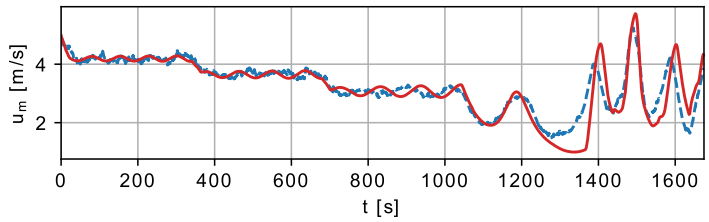

(a) The measured mixture velocity.

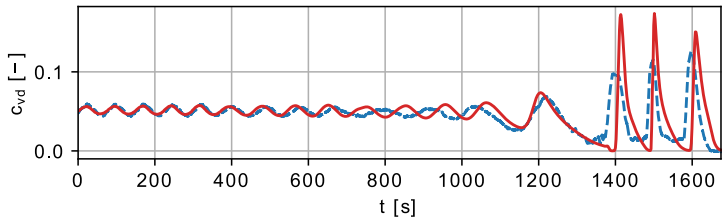

(b) Delivered concentration.

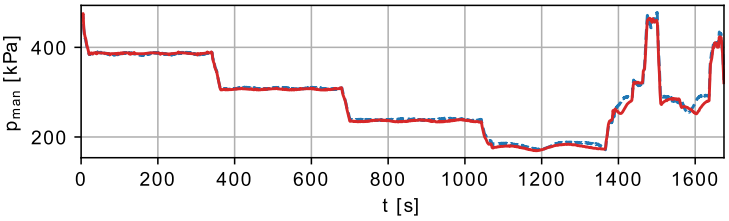

(c) Pump manometric pressure.

Figure 4.12: Simulation of the Freiberg experiment nr. 3. Blue: data, red: simulation. Gravel, $d_m = 12.1\,mm$, $c = 0.05$.

The value of u_{crit} ($\approx u_{dl}$) influences the relative particle velocity model $u_{s/m}$ in the horizontal pipes and therefore influences the simulated amplification rate. Since the relative velocity model for horizontal pipes is not exactly determined for this system and a model from literature is used, some inconstancy between the data and the simulations was experienced when using the values of the estimated deposit limit velocity for u_{crit} ($1.5m/s$ and $2.5m/s$ for sand and gravel, respectively). Therefore, the chosen value for u_{crit} was varied slightly to attain a better agreement with the data. The resulting values of u_{crit} used for each experiment are given in Table 4.2.

To judge how sensitive the results are to inaccuracies in the horizontal relative velocity model, the value of u_{crit} is varied $+/-10\%$ in the simulation of experiment 1, see Figure 4.14. Figure 4.14 shows that the amplification rate is indeed influenced slightly, however amplification is still predicted. Amplification ceases when choosing u_{crit} =

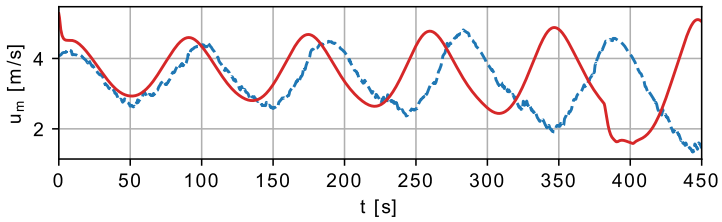

(a) The measured mixture velocity.

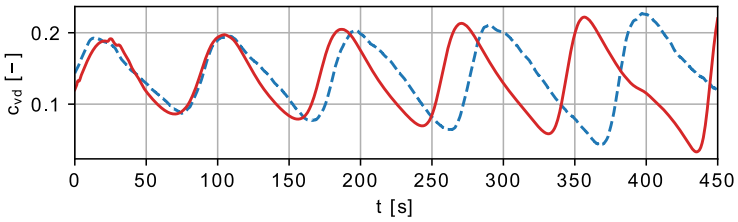

(b) Delivered concentration.

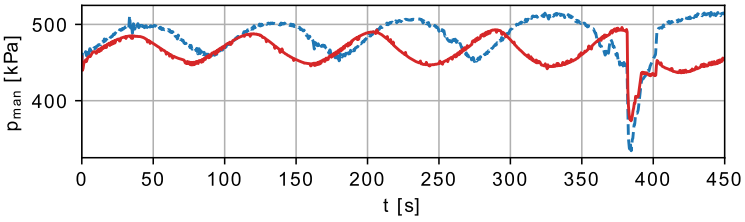

(c) Pump manometric pressure.

Figure 4.13: Simulation of the Freiberg experiment nr. 4. Blue: data, red: simulation. Gravel, $d_m = 12.1\,mm$, $c = 0.14$.

Exp. #	$d_m\,[mm]$	$c_{mean}\,[-]$	$c'\,[-]$	$\frac{k_s}{D}\,[-]$	$u_{crit}\,[m/s]$	$\mu_{sf}\,[-]$	$c_{max}\,[-]$
1	0.741	0.10	0.016	$5.1\cdot10^{-4}$	2.3	-	0.60
2	0.741	0.067	0.0020	$7.9\cdot10^{-4}$	2.2	-	0.60
3	12.1	0.052	0.038	$4.7\cdot10^{-4}$	1.8	0.40	0.60
4	12.1	0.14	0.050	$9.5\cdot10^{-4}$	2.2	0.40	0.60

Table 4.2: For the initial conditions, and k_s and u_{crit} for the simulations.

$1.6\,m/s$ (−30%), and for a $u_{crit} = 2.7\,m/s$ (+17%) the simulation cannot be completed, because the minimum concentration of the density wave drops below zero. The effect of the variations of u_{crit} on the actual value of the relative velocity $u_{s/m}$ is given in Table 4.3. From this we can conclude that to attain representative results in case of experiment

1, in the sense that the model predicts amplification and can finish the simulation, the accuracy of the relative velocity model should be within at least a +/ − 15% bandwidth.

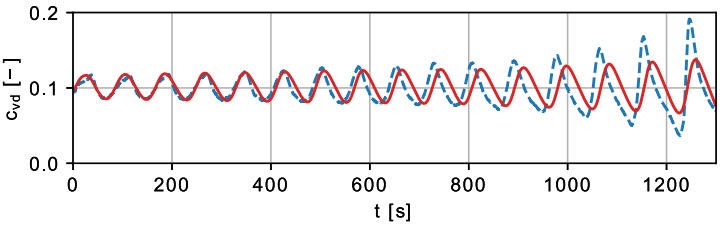

(a) Simulation using $u_{crit} = 2.5\,m/s$ (+10%)

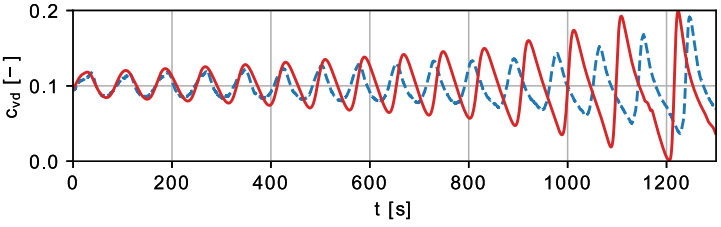

(b) Simulation using $u_{crit} = 2.1\,m/s$ (−10%)

Figure 4.14: Sensitivity demonstration of the experiment 1 simulation. Blue: data, red: simulation. Sand, $d_m = 741\,\mu m$, $c = 0.05 - 0.10$.

$u_{crit}\,[m/s]$	$\frac{u_{crit}}{u_{crit,0}}\,[-]$	$u_{s/m}\,[m/s]$	$\frac{u_{s/m}}{u_{s/m,0}}\,[-]$	Note
2.3	0%	0.93	0%	Reference, used in Figure 4.10
2.5	+10%	1.07	+15%	Used in Figure, 4.14a
2.1	−10%	0.80	−14%	Used in Figure, 4.14b
2.7	+17%	1.22	+31%	Simulation stopped $c < 0$
1.6	−30%	0.51	−45%	No amplification, but damping

Table 4.3: The results of the sensitivity analysis of the horizontal relative velocity model. Given are the average values of $u_{s/m}$ in the simulation of experiment 1, as a function of u_{crit}. Values are calculated at $c = 0.1$ and $u_m = 3.5\,m/s$.

4.4.2. Comparison of the simulation with data

The pump revolutions data of the experiments was used as input for the simulations, together with the initial conditions of the concentration wave. From that point on everything is simulated. Some notable fine details are simulated, like the saw-tooth shape of waves (Figures 4.10b, 4.13b and 4.14b), caused by the fact that the particle velocity is modeled as a function of the concentration (de Hoog et al., 2021). Furthermore, tiny kinks in the concentration and pump pressure time traces, as seen in Figure 4.10 between 1000 and 1200 s, can also be seen in the simulations (caused by rapid pump

revolutions changes). The simulation of Figure 4.12 is very notable, as the system in this experiment could be considered stable up 1050 s, even after lowering the mixture velocity several times. However, beyond 1050 s a strong density wave sets on rapidly, because the mixture velocity drops below a threshold where the particle velocity difference between the horizontal and vertical pipes becomes very large. This behavior is also simulated very well.

All simulations show an apparent phase shift when comparing the simulations with the data. This is a difference in wave velocity between the data and the simulation. The wave length equals the system length, therefore a slight discrepancy in particle or mixture velocity results in a phase shift as time proceeds. Mixture velocity deviations can be caused by pump pressure or pipe resistance mismatches between the data and simulations. These mismatches could be explained by under-performing resistance or relative velocity models, however also keep in mind that many deviations can originate from the experiments. Especially because the Darcy-Weisbach friction factor is based on the water experiment preceding the mixture experiments, and the wall roughness could change if for instance the pipe erodes during mixture experiments. This also explains the variation in measured wall roughness between the water experiments (see Table 4.2). In other words the wall roughness changed between experiments, and the water experiment preceding the mixture experiment is not exactly representative of the wall roughness during the mixture experiment. Another cause of mismatches between the data and simulations could come from the delivered concentration measurement with the u-loop measuring principle, which is known to suffer from inaccuracies ($+/-10\%$), especially for coarse sediments (Clift and Manning Clift, 1981). This data serve as input for the model, as such any discrepancies will results in deviations. The wave lengths could be matched better with manual tweaking of the wall friction factor k_s, however this was deliberately not done, to demonstrate that the resulting wave amplification rates are not very sensitive to the aforementioned variations. In the view of the authors the phase lag discrepancy is not an issue, since the 1D model still predicts the amplification rate well.

4.5. Discussion

The density wave amplification mechanism as witnessed in the Freiberg experiments is new in the sense that amplification can occur at mixture velocities far exceeding the deposit limit velocity, as explained by de Hoog et al. (2021). However, de Hoog et al. (2021) does not fully explain the transient accumulation mechanism. This chapter continues this work and provides a hypothesis and relates the mechanism to a spatial particle velocity change with a simultaneous temporal mixture velocity change. The mixture velocity change can also be attributed to the density wave as the mixture accelerates when the wave leaves the vertical riser, which is in its turn caused by the fact that the centrifugal pump does not have a constant operating point. This interaction together with the spatial particle velocity change is modeled with the 1D Driftflux model, and because this model simulates density wave amplification very well, we consider this as proof in support of the transient accumulation hypothesis.

Whether amplification occurs can now be simulated with the 1D Driftflux model. The model can be used to answer some interesting questions. Would amplification occur without the presence of the horizontal pipes? Does the pump position influence amplification. Can amplification be avoided with flow feedback control? Can amplification be avoided by better matching the particle velocity between the horizontal and vertical pipes, by decreasing the diameter of the horizontal pipes. A future study will be dedicated towards these questions (see Chapter 6).

The Freiberg flow loop was a closed loop system, while dredging and deep sea mining pipelines are open systems. In the Freiberg loop the wave could amplify during each passing through the loop, which is not possible in an open system. However, the Freiberg data also shows that once the wave is already severe, the growth in one circulation is significant. Therefore, if a strong wave already exists in an open pipeline system, it can amplify when flowing out of a vertical pipe into a horizontal pipe. This can only occur when the system accelerates significantly (see Section 4.2), moreover if the vertical pipe is long relative to the horizontal pipe. If a system contains multiple pipe orientation changes, amplification could potentially occur at each transition. To what extent, and how severely transient accumulation affects an open system pipeline requires a more detailed study using the 1D-Driftflux model, and will definitely depend on the layout of the pipeline.

The 1D Driftflux model is a transient model, but closure relationships for the particle velocity u_s are based on experimental data of laboratory circulating flow loops and attained under steady-state conditions. On top of this, u_s and c are cross section area averaged values in the 1D model, while in fact a vertical concentration distribution is present in horizontal pipes, caused by settling of the particles. Therefore we ask the question, to what extent is the 1D transient model valid?

In Keetels (2017) it was found that the steady-state vertical concentration distribution can be estimated using the integrated transient equations of the vertical sediment velocity (in a horizontal pipe). This suggests that these are stable, and any perturbation will lead to a steady-state concentration profile. How quickly this steady-state concentration profile develops was studied in Keetels et al. (2018) using a numerical analysis. A perturbed concentration profile was found to find its steady state solution within several hydraulic time unit $\frac{h}{u^*}$, with h = height of the profile and u^* = the shear velocity. Concluding, when a concentration profile is subject to changes of c and u_s that occur in a time scale several times larger than the hydraulic time unit, then the concentration profile can be considered as fully developed. Thus we can state that any empirical model of $u_{s/m}$, even when attained in the presence of density waves, is considered a valid model when the conditions as explained above are met. As such, this validity condition also defines the validity of the 1D model. A time scale for a density wave can be estimated from the wave length and the average velocity. For the 1D model to be valid the density wave time scale should far exceed the hydraulic time scale.

$$\frac{L_w}{u_m} >> \frac{D}{u^*} \tag{4.44}$$

With D = pipe diameter, u^* = shear velocity, L_w = density wave length and u_m = the average mixture velocity. The density waves studied in this research have wave lengths equal to the system length, which was also experienced in Talmon et al. (2007). Furthermore, in an open system pipeline the wave lengths are several hundreds of meters (de Hoog et al., 2021, Matoušek, 1996b, Talmon, 1999). Considering the long wave lengths of these types of density waves, the validity criterion described by Equation 4.44 is easily met and therefore the 1D model can be used to model these types of density waves.

4.6. Conclusion

The density wave amplification mechanism studied in this chapter occurs for mixture velocities far above the deposit limit velocity, and can be attributed to the transient accumulation mechanism. Transients accumulation is a complex interaction between spatial particle velocity changes (due to pipe orientation), and global mixture velocity variations due to the changing centrifugal pump load caused by density wave flowing from vertical pipes into horizontal pipes. The proposed 1D Driftflux model accounts for these effects, and is shown to be able to predict density wave amplification to great satisfactory. Since the 1D Driftflux model predicts density wave amplification so well, we consider this as further proof for the existence of a previously unknown density wave amplification mechanism. In addition the model also showed that it predicts fine details, such as the saw-tooth shape of the wave, the wave length and the systems response due to rapid pump revolution changes.

The accuracy of the closure relationships used in the 1D Driftflux model has been explored in this chapter. Resistance models and the pump related models do not effect the predictive capabilities significantly, however the particle velocity models do. The state of the art in predicting particle velocities in horizontal flows are currently iterative two layer models (Matoušek et al., 2018). The focus of this research was on the development of the 1D model framework, therefore a non-iterative less advanced empirical model was applied. Interesting follow up work would be to implement the two-layer models, to improve the predictive capabilities of the 1D transient model.

Because transient accumulation occurs at mixture velocities far above the deposit limit velocity, the conventional steady-state design method is flawed for designing systems with relatively long vertical pipes combined with horizontal pipes transporting coarse materials, for instance for deep sea mining applications. It is therefore recommended to extend the steady-state design method with a transient density wave analysis using 1D Driftflux modelling. Future work will aim at understanding which configurations of vertical and horizontal pipelines show amplification, how amplification occurs in open systems and preventive measures to avoid amplification.

5

THE 1D-2L-HT MODEL: SIMULATION OF EROSION DRIVEN DENSITY WAVES

This chapter contains the 1-Dimension-2-Layer-Hydraulic Transport CFD model (1D-2L-HT). This model was developed to simulate erosion driven density waves. The 1D-2L-HT model contains all the elements of the 1DHT CFD model (Chapter 4). Furthermore, the 1DHT model had to be extended, to allow simulation of erosion driven density waves, by adding a second layer to represent a stationary bed. This adaptation requires new time and spatial derivatives of the numerical cell volume and area in the continuity, transport and momentum equations. Moreover, the 1D-2L-HT contains a bed layer erosion model, through mass- and volume source terms in the transport- and continuity equation. The new mathematical foundation is given in this chapter. The model is calibrated and validated against two experiments. Firstly, it is validated against dedicated bed layer erosion experiments, to test the erosion part of the 1D-2L-HT model. Secondly, the model is validated against the experiments of Chapter 3 to demonstrate the ability to simulate erosion driven density waves.

This chapter has been published in the Journal of Hydrology and Hydromechanics ***72(1)*** *(2024).*

5.1. INTRODUCTION

THE dredging, mining and deep sea mining industries use hydraulic transport pipelines, powered by large centrifugal pumps, to transport sediments such as sand, rock, clay, manganese nodules and various other minerals. These pipelines are currently designed using steady-state methods. Specifically, the energy added by the centrifugal pump is weighted against the energy lost by the pipeline. This analysis results in a pipeline operating velocity. When the velocity is high, sediment is suspended by turbulence. When the velocity is low, particles form a bed layer in the pipe. The transition is called: the deposit limit velocity. Steady-state design simply aims to design a pipeline with an operating velocity above the deposit limit velocity.

The steady-state design method unfortunately has its limits, since it is based on steady state assumptions. An example of such a steady assumption is that the concentration of sediment entering the pipeline is constant. Another assumption is that the sediment concentration does not change while flowing through the pipeline. However, various field pipelines and laboratory experiments have shown that these assumptions are not always valid (de Hoog et al., 2021) (see Chapter 2). Variations in mixture concentration, either temporal or spatial, can lead to serious flow assurance issues, mainly in the form of self-excited density waves (de Hoog et al., 2021, Matoušek, 1996b, Talmon, 1999). Density waves are highly concentrated flows of sediment, that can self-amplify over time and in space. Density waves form an increased risk to safe pipeline operation, increasing the chance of pipeline blockages, failures of the centrifugal pump drive and complicate future automation of deep sea mining pipelines. In general, the longer the pipeline the greater the risk.

Density waves have so far been encountered as two mechanisms. One where the wave grows due to spatial particle velocity differences between pipes of different orientation, i.e. horizontal and vertical. This was encountered in the "Freiberg" experiments (de Hoog et al., 2021) and referred to as "transient accumulation." The key characteristic of this mechanism is, that these density waves can form despite that the pipeline operates far above the deposit limit velocity. Therefore, these transient waves cannot be predicted or considered when using steady-state design principles. The second mechanism causes the wave to grow by feeding from a stationary sediment bed layer in the pipeline, when the pipeline operates close to the deposit limit velocity. Erosion of the bed is stronger for higher suspension concentrations above the bed, therefore density waves tend to self-amplify once formed. This mechanism is referred to as the "erosion-sedimentation imbalance" (Talmon, 1999). This chapter focuses on the latter mechanism, the erosion-sedimentation imbalance.

In the case of waves formed by transient accumulation, a transient 1-dimensional Computational Fluid Dynamics (CFD) Driftflux model was developed to predict density wave amplification in Chapter 4. This type of 1D CFD is very powerful, as it allows the simulation of kilometers long pipelines in a matter of minutes on a decent laptop computer. This is currently impractical with the most state-of-the-art 2D or 3D CFD models (Messa et al., 2021), because of long computational times. Unfortunately, a 1D transient

model to predict density waves due to the erosion-sedimentation imbalance is currently not available. Since density waves due to the erosion-sedimentation imbalance are still not fully understood nor modelled, a 1D CFD model would be very valuable to further research the problem, and potentially also a great design tool for pipeline designers.

The aim of this chapter is to explore the possibility to model density waves due to the erosion-sedimentation imbalance, using 1D CFD. We propose to extended the 1D model of Chapter 4 with a second lower layer, to be able to model the erosion and sedimentation process between the suspended particles and the bed layer. The second lower layer models a stationary bed, while the upper layer models the suspended particles. A closure relationship can be used to model the transfer of sediment between the two layers. A potential candidate for this closure relationship can be found in CFD simulations of other dredging processes and morphological models, specifically empirical "erosion-sedimentation" based models (van Rijn, 1984, Talmon, 1999, van Rhee, 2010, Bisschop, 2018). However, such erosion-sedimentation models have never been applied in pipeline flows before. In this chapter we will aim to answer the following research question: Can we model density wave amplification using a 1-dimensional-2-layer (1D-2L) CFD model? A sub question is: Is an erosion-sedimentation based closure relationship suitable for modelling the sediment exchange between the stationary bed layer and the suspended flow, within a 1D-2L model?

First, we create a new numerical scheme for a 1D-2L Driftflux model. Secondly, validation experiments are conducted to validate the use of an erosion-sedimentation closure for pipeline flows. And thirdly, experiments to validate the formation of density waves in the new 1D-2L Driftflux model are conducted. These steps are elaborated in the Methods (Section 5.3) and Results & Discussion (Section 5.4). But first, the erosion-sedimentation density wave amplification mechanism is explained in the Theory (Section 5.2).

5.2. Theory

So how does the erosion-sedimentation imbalance work? A density wave can grow from a stationary bed layer in the pipeline, by erosion of the bed. This bed layer is formed when the mixture velocity drops below the deposit limit velocity. Once formed, the bed layer erodes faster for increasingly higher mixture concentrations, due to hindered sedimentation (Talmon, 1999). The concept of hindered sedimentation entails that the sedimentation rate of particles is increasingly hindered, and therefore decreases, with increasing mixture concentration (Richardson and Zaki, 1954). As a consequence, at velocities close to the deposit limit velocity, low concentration flows cause sedimentation, while high concentration flows cause erosion. This unintuitive behavior led to the name: the erosion-sedimentation imbalance (Talmon, 1999). Consequently, a local maximum of the concentration can act as a small perturbation, which locally causes more erosion than in surrounding areas. This small perturbation will grow, flows further down the pipe, erodes the bed more, and consequently grows even more. This process keeps repeating as the wave self-amplifies, until the wave is fully developed.

Mathematically, the erosion and sedimentation of a bed layer can be described with an erosion and sedimentation balance (van Rijn, 1984, Talmon, 1999, van Rhee, 2010, Bisschop, 2018):

$$v_{sed} = \frac{\partial y_b}{\partial t} = \frac{S_h - E_h}{\rho_s(1 - n_0 - c_{nb})} \tag{5.1}$$

In Equation 5.1, v_{sed} is the sedimentation velocity of the bed interface, y_b the bed height, t time, ρ_s the particle density, n_0 the bed porosity and c_{nb} the near bed concentration. The near bed concentration represents the concentration responsible for the erosion and sedimentation process, defined to be just above the bed layer (more details in Section 5.3). S_h is the hindered settling flux, which is the amount of sediment that settles out of suspension and forms a bed. E_h is the hindered erosion flux, which represents the sediment being eroded and transferred to the suspension. When E_h and S_h are equal to each other, the bed height is steady.

Hindered sedimentation is modelled using the well-known and accepted Richardson and Zaki (1954) approach:

$$S_h = \rho_s v_{ts} c_{nb}(1 - c_{nb})^n \tag{5.2}$$

In Equations 5.2 v_{ts} is the terminal settling velocity of a particle, n is the hindered settling exponent and c_{nb} is the near bed concentration. The exponent n can be modelled using Garside and Al-Dibouni (1977).

Unfortunately, hindered erosion is not as well researched as hindered sedimentation. Research by Winterwerp et al. (1992) and van Rhee and Talmon (2010) found experimental proof for hindered erosion at low bed shear stresses. While during the high shear stress experiments by Bisschop (2018) not much focus was put into hindered erosion. Recent work by Keetels et al. (2023) shows that for increasingly higher suspension concentrations erosion is dampened. This is caused by the loss of turbulent kinetic energy at high concentration ($>\sim 30\%$). Under these conditions, turbulence simply cannot pick up more sediment. Keetels et al. (2023) used multi-phase turbulent kinetic equations to derive these conclusions. They tested their theory against a wide range of experimental data, including the data from van Rijn (1984) and Bisschop (2018).

As part of this research it was found that without modelling hindered erosion in the 1D-2L model, density waves grow indefinitely in time. This is because of the $1 - n_0 - c_{nb}$ term in the denominator of Equation 5.1. This creates an additional numerically based argument, to better model hindered erosion. Specifically, erosion should be damped for concentrations approaching the bed concentration, as stated by Keetels et al. (2023). As part of this research, the following hindered erosion model is proposed:

$$E_h = E\left[1 - \left(\frac{c_{nb}}{c_{max}}\right)^m\right] \tag{5.3}$$

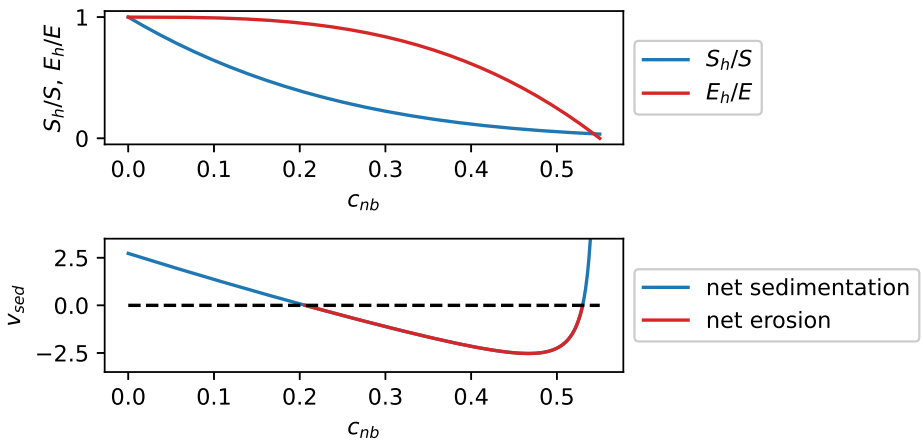

Figure 5.1: Top: a visualization of hindered erosion and hindered sedimentation as a function of the near bed concentration. Bottom: an arbitrary example of Equation 5.1, showing sedimentation for concentrations below 20% and erosion above 20%, using $S = 2.5 kg/m^2/s$, $E = 1 kg/m^2/s$, $m = 3$, $c_{max} = 0.55$.

In which E is the erosion flux without a hindered effect, thus at low near bed concentrations. For $m = 1$ and $c_{max} = 1 - n_0$ the equation equals the hindered erosion model by van Rhee and Talmon (2010). The parameters c_{max} and m require calibration, which will be elaborated in Section 5.4.

Figure 5.1 shows the results of Equations 5.1, 5.2 and 5.3, and how these can lead to density wave amplification. In this arbitrary example, the bed erodes at a near bed concentration above 20%. This can be seen in Figure 5.1 when v_{sed} is lower than zero as a function of c_{nb}. As this occurs, the flow switches from a net sedimentation to a net eroding flow. Therefore, a local small concentration perturbation will erode deposits, consequently grow, flow down the pipe, increase the near bed concentration, cause more erosion and cause the wave to grow even more. A constantly repeating cycle of erosion and density wave growth. Concluding, this causes a perturbation to self-amplify.

5.3. Methods

With the erosion-sedimentation imbalance in mind, the following steps need be taken to develop a 1-dimensional-two-layer Driftflux model, which is able to model density wave amplification. Firstly, develop a numerical scheme of a 1D-2L model. This requires implementation of the second layer. Secondly, apply the erosion-sedimentation closure relationship to model the mass exchange between the two layers. Thirdly, experimentally validate the use of an erosion-sedimentation based closure relation in pipeline flow. Lastly, experimentally validate the self-amplification of a density wave. The method section follows the steps as given above.

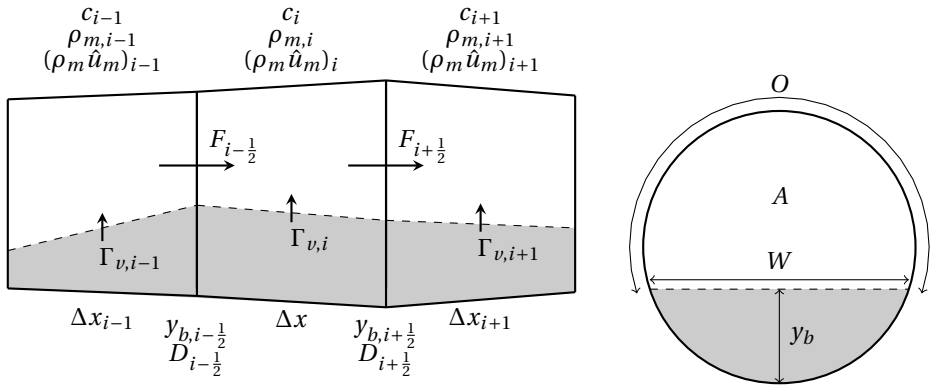

(a) Side view with variable pipe diameter and bed height on the cell faces. (b) The model cross-section.

Figure 5.2: The grid definition of the 1D-2L Driftflux model. The upper layer represents the flow of sediment and the lower layer the stationary bed. c is the sediment concentration, ρ_m is the mixture density, Δx is the cell size, y_b the bed height, D the pipe diameter, F the numerical fluxes, Γ_v the bed source term, W the bed width and O the pipe wall surface of the cell portion above the bed.

5

5.3.1. Numerical scheme of the 1D-2L Driftflux model

The 1D-2L Driftflux model is based on a self-developed in-house code. The novelty of this model is the two layers and that volume of the cells change in time and space. We use the Finite Volume Method (FVM) to discretize the model, because this method always ensures mass conservation. To further explain the model an illustration of the numerical grid is given in Figure 5.2.

The 1D-2L model is based on a circular shaped cross-section. In Figure 5.2 a numerical cell is split into an upper and a lower layer. The upper layer represents the flowing suspended mixture, while the lower layer models the stationary bed layer. The cell size is Δx and the index i denotes the cell number with $i-\frac{1}{2}$ and $i+\frac{1}{2}$ the in- and out- faces of the cell i, respectively. The pipe diameter D and bed layer height y_b are defined on the cell faces and both can change in space. Because only the upper layer flows, the momentum and transport equations will only apply to the upper layer. The volume concentration c, mixture density ρ_m, and momentum $\rho_m \hat{u}_m$ are cell averaged values of the upper flowing layer.

The 1D-2L model requires two types of mixture velocities. Firstly, the mixture velocity $\hat{u}_m$ can be derived from a mass balance of the fluid and solids phases.

$$\hat{u}_m = u_s \frac{\rho_s}{\rho_m} c + u_f \frac{\rho_f}{\rho_m} (1-c) \tag{5.4}$$

In Equation 5.4, c is the cell averaged volumetric concentration, ρ_s and ρ_f are the density of the solids and fluid respectively, and u_s and u_f their respective velocities. This mass flow based mixture velocity is referred to as the Favre averaged mixture velocity is

some Driftflux literature, and allows for a convenient way to derive the momentum equation Ishii and Hibiki (2011).

The second way to define the mixture velocity is based on a volume balance, which is required for the particle transport equation:

$$u_m = u_s c + u_f (1 - c) \tag{5.5}$$

The full derivation of the momentum and transport equations for this two-layer model, is provided in detail in Appendix B.

The continuity equation for modelling the mass flow on the entire mixture is as follows:

$$\frac{\partial}{\partial t}(\rho_m V) + \sum_{faces} (\rho_m \hat{u}_m A) = \Gamma_m \tag{5.6}$$

In which V is the volume of the upper layer cell and A the cross-sectional area of the upper cell face (the area above the bed). The volume of the upper cell V is computed numerically and is a function of D and y_b on both cell faces. This allows for a continuous grid with varying bed heights as well as varying pipe diameters. In Equation 5.6, the sum over the cell faces represents the in- and out-fluxes F over the cell faces. The mass source term Γ_m is used to exchange mass between the two layers, and is related to the volumetric source term Γ_v as depicted in Figure 5.2.

To adhere to Newton's second law, the momentum balance is as follows:

$$\begin{aligned}\frac{\partial}{\partial t}(\rho_m \hat{u}_m V) + \sum_{faces} (\rho_m \hat{u}_m \hat{u}_m A) = &- \sum_{faces} (p A) - \tau_m O - \tau_b W + ... \\ &- \rho_m g A \sin(\omega) - \sum_{faces} \left[A c \rho_s (u_s - \hat{u}_m)^2 + A(1-c)\rho_f (u_f - \hat{u}_m)^2 \right] + A S_p\end{aligned} \tag{5.7}$$

In Equation 5.7, p is the pressure, τ_m the shear stress of the pipe wall, τ_b the shear stress on top of the bed layer, O the surface area of the pipe wall (above the bed), W the surface area of the bed interface, ω the pipe inclination angle and S_p the centrifugal pump pressure source term.

The particle transport equation, which is required to model the flow of the particles only, is as follows:

$$\frac{\partial}{\partial t}(cV) + \sum_{faces} (u_s c A) = \Gamma_v \tag{5.8}$$

In Equation 5.8 u_s is the particle velocity, and Γ_v the erosion-sedimentation volumetric based source term. The particle velocity, required in Equation 5.5, is modelled as:

$$u_s = u_m + u_{s/m} - \frac{\epsilon}{c}\frac{\partial c}{\partial x} \tag{5.9}$$

This allows us to model a velocity difference, $u_{s/m}$, between the mixture velocity u_m and the particle velocity u_s. To be able to model axial diffusion due to turbulent dispersion, a diffusion velocity is modelled using the diffusion coefficient ϵ.

The relative particle velocity in the horizontal pipes is estimated with the empirical Sobota and Kril (1992) model:

$$u_{s/m} = -u_m \left[f_t \left(1 - \frac{c}{0.6}\right)^{2.16} \left(1 - \frac{u_{crit}}{u_m}\right)^{1.7} \right] \tag{5.10}$$

With f_t an empirical constant and u_{crit} the critical velocity, which is roughly equal to the deposit limit velocity. f_t is computed as function of the particle Reynolds number. This particle Reynolds number is based on the particle terminal settling velocity, v_{ts}: $Re_p = \frac{\rho_f v_{ts} d_{50}}{\mu_f}$. This particle Reynolds number should not be confused with other particle Reynolds numbers used in other fields of CFD, which are based on the slip velocity of the particle. f_t is computed as follows:

$$f_t = \begin{cases} 0.1464 \cdot 10^{0.6031 \cdot \log(Re_p)} & if\ \log(Re_p) < 1 \\ 0.7858 \cdot \tanh[0.7986 \cdot \log(Re_p)] & if\ \log(Re_p) \geq 1. \end{cases} \tag{5.11}$$

This empirical model is only applicable for mixture velocities above u_{crit}. However, we also need to model the relative particle velocity above the bed layer, thus below u_{crit}. No empirical models are available for this. Therefore, it is proposed to use the same model, but scale u_{crit} with the hydraulic diameter of the reduced flow cross-section above the bed layer, effectively modelling a smaller pipe for the cells above the bed. Since u_{crit} roughly equals the deposit limit velocity, and most empirical models of the deposit limit velocity scale with the square root of the pipe diameter (Visintainer et al., 2023), we scale u_{crit} accordingly:

$$\frac{u_{crit,h}}{u_{crit}} = \sqrt{\frac{D_h}{D}} \tag{5.12}$$

In which $u_{crit,h}$ is the critical velocity in case of a bed layer, and D_h the hydraulic diameter of the cross-section above the bed layer. This method allows for a smooth transition when computing $u_{s/m}$ once a bed layer forms, although it is not validated. Fortunately, the effect of $u_{s/m}$ was found not to be very sensitive for predicting density wave amplification, as such this proposed adaption, although not validated, seems a good placeholder until a better closure model is available.

The shear stresses, axial dispersion coefficient ϵ and pump source term S_p are modelled exactly the same way as with the 1D Driftflux model covered by de Hoog et al. (2022). The relative particle velocity $u_{s/m}$ in vertical sections of the grid is modelled differently. Specifically, the relative particle velocity in vertical pipes is based on the hindered settling velocity principle (Richardson and Zaki, 1954), which has been shown to

work well in vertical pipes (van Wijk, 2016). Since these aspects are not the focus of this chapter, we kindly refer you to Chapter 4 for these details. Rather, this research's main focus is on the two layer structure and mass exchange between the two layers.

5.3.2. Modelling erosion and sedimentation of the bed layer

To model the sediment exchange between the two layers, the erosion-sedimentation balance is used (Equation 5.1). This choice was made for the following reasons:

- The original erosion-sedimentation imbalance (Talmon, 1999) was derived using this method. As such, directly numerical modelling this is a good way to further verify the erosion-sedimentation imbalance mechanism.
- The availability of high bed shear stress erosion data from the research of Bisschop (2018). High bed shear stresses result in a shear layer above the bed, several particle diameters thick, which is different from single particle erosion (Bisschop, 2018). This erosion mechanism is the main erosion mode in pipe flows, due to the typically high velocities encountered in pipelines (in the order of meters per second).
- Erosion-sedimentation functions have successfully been applied in numerical models for various applications such as alluvial flows, coastal morphology (Delft3D) and sedimentation of sand in trailing suction hopper dredgers (van Rhee, 2002).

In the state-of-the-art 2D and 3D multiphase literature, sediment beds are modelled using rheological models or kinetic theory models. The authors are aware of these developments and discuss these further in the Results & Discussion (Chapter5.4).

The general formulation of the mass exchange terms in the CFD model need to be explained in more detail. To this end Γ_m is used in Equation 5.6 and Γ_v in Equation 5.8. These two source terms both represent the exchange of solids between the bed and the suspension, but have different units. Specifically, Γ_m is in mass flow rates, while Γ_v is in unit volume flow rates. The two are related as follows:

$$\Gamma_m = \Gamma_v \left[\rho_s - \rho_f \left(1 - \frac{1}{1 - n_0} \right) \right] \tag{5.13}$$

So how is Γ_v computed? Imagine how the top of bed layer erodes: Particles are lifted from the bed layer into the suspension. In other words, the concentration of sediment transferred to the suspension equals the change of the bed layer volume V_b multiplied by the concentration of the bed, which is equal to $1 - n_0$:

$$\Gamma_v = \frac{\Delta V_b}{\Delta t} (1 - n_0) \tag{5.14}$$

The change of the bed layer volume is computed from the change of the height of the bed layer at the cell faces.

$$\frac{\Delta V_{b,i}}{\Delta t} = f\left(\frac{\Delta y_{b,i-\frac{1}{2}}}{\Delta t}, \frac{\Delta y_{b,i+\frac{1}{2}}}{\Delta t}\right) \tag{5.15}$$

The bed height change at the faces is computed using Equation 5.1.

The pickup function to model E in Equation 5.3 needs to be defined next. The Bisschop (2018) model was chosen for two reasons. Firstly, the dataset on which this model is calibrated is of high velocity erosion. This regime is also applicable for our application, and in general suitable for pipeline flows. Secondly, the model is easy to implement numerically and does not require any iteration like a few other pickup functions do. The Bisschop (2018) model is as follows:

$$E = \frac{h_s \lambda_b (1 - n_0) \rho_s}{4 T_B} \tag{5.16}$$

In which h_s is the shear layer thickness, λ_b a coefficient to represent the amount of turbulent bursts eroding the bed layer, n_0 the porosity of the sand bed and T_B the mean bursting period of turbulent sweeps. λ_b and T_B have a physical meaning, but can be varied to calibrate the model. Bisschop (2018) recommends $\lambda_b = 1$ and $1.0 < T_b < 3.0$. Bisschop (2018) states that this model requires iterative computation. Fortunately, an explicit solution was found during this research. For further details on implementation of this pickup function, and the explicit solution, see Appendix C. To compute the erosion flux E, the following geotechnical parameters are required: the angle of internal friction ϕ, the maximum porosity of the bed n_{max}, the minimum porosity n_{min} and the permeability at the maximum porosity k_{max}.

The final piece of the puzzle is how to model the near bed concentration. The near bed concentration is the concentration just above the bed layer that dictates the erosion process, and is required for the Bisschop (2018) erosion model. At low concentration or low velocities, the concentration just above the bed layer is equal to the mean concentration of the suspension van Rijn (1984) However, at high concentrations or high velocities a shear layer develops above the bed, therefore the near bed concentration becomes a function of the height above the bed. Bisschop (2018) showed that the erosion process at high flows is governed by turbulent eddies eroding parts of the bed layer. These eddies were approximately 3 cm large. Therefore, Bisschop (2018) defined the near bed concentration to be the concentration 3 cm above the bed layer, in a 28.8 cm high conduit. This is roughly at 10% of the total height of the conduit. However, the experiments and simulations in this research are conducted in a 4 cm pipe, therefore direct application of the 3 cm height as defined by Bisschop (2018) is not viable. How to solve this problem? The largest turbulent eddy in a pipe scales linearly with the pipe diameter, or more specifically with the Stokes number (Keetels et al., 2023). Therefore, the 3 cm erosion zone is scaled linearly with the height of the conduit, 28.8 cm in the case of Bisschop (2018) and 4 cm in the experiments of this research. Using this method, an empirical relationship is derived to relate the near bed concentration to the average concentration of the suspended flow, measured from experiments, which is explained in Section 5.3.3.

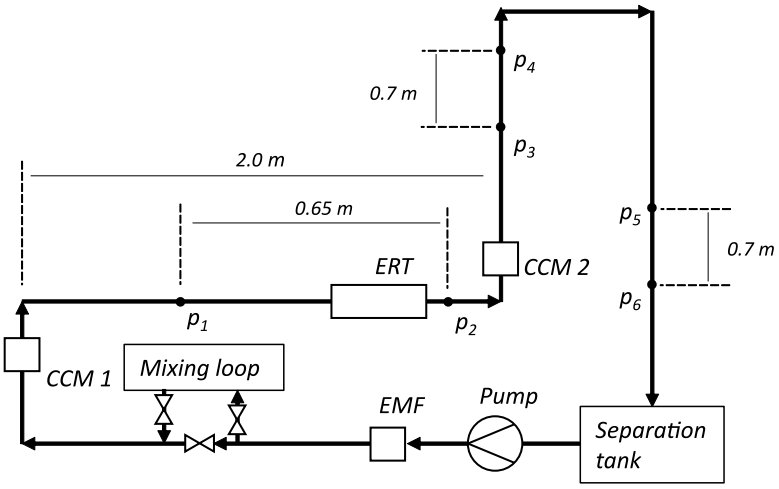

Figure 5.3: A schematic front view of the bed erosion experimental setup. ERT = Electrical Resistance Tomograph, CCM = Conductance Concentration Meter, EMF = ElectroMagnetic Flowmeter.

The resulting empirical relationship between the mean suspended concentration and the near bed concentration can be found in the Results & Discussion (Section 5.4).

5.3.3. Experiments to validate the erosion-sedimentation balance in pipe flow

A dedicated experimental flow loop was designed to study the implementation of the erosion-sedimentation balance in pipe flow. These experiments are also used to determine an empirical relationship for the near bed concentration as a function of the average concentration of the suspension. A vertically oriented 40 mm diameter pipe circuit was built. This circuit contained a 2 meter long horizontal section, with a vertical inlet and a vertical outlet. An Electrical Resistance Tomograph (ERT) was placed 1.5 meter along this section. This ERT measured the sediment concentration distribution over the cross-section of the pipe over time with a sample rate of 64 Hz. At the inlet and outlet Conductance Concentration Meters (CCM) were placed vertically. The 2-meter measuring section was prepared with a sand bed. A mixing loop, in front of the 2-meter section, was used to prepare a suspended mixture with a desired concentration, by measuring the weight of the sand and knowing the volume of the mixing loop. An Electro-Magnetic Flowmeter (EMF) was placed in front of the mixing loop to measure the mean pipeline velocity. The centrifugal pump was placed before the EMF, at the very start of the flow loop. Figure 5.3 shows a schematic overview of the experimental apparatus.

The data required to validate the erosion model is the bed height over time, the concentration above the bed layer and the mean pipeline velocity. More data was measured, like pressure losses in the pipes, inlet concentrations, outlet concentrations, however this data is not used as part of this chapter. At initiation of an experiment, the main

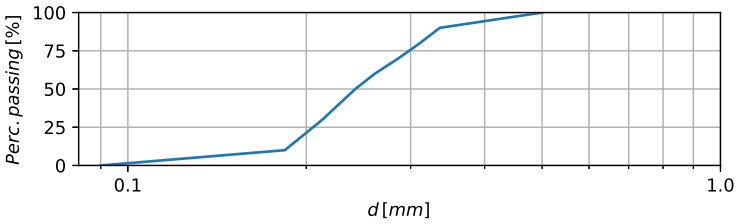

Figure 5.4: The particle size distribution of the Zilverzand used for all experiments in this research.

pump was turned on, the mixing loop was connected to the main loop and the prepared mixture was sent past the sand bed. At the end of the loop the sand was separated using a settling tank. The water was sent back into the loop to recirculate.

In total 20 experiments were conducted using five sand types at four different concentrations in the mixing loop, specifically 5, 10, 20 and 30%. The sand types ranged in size from 242 μm to 2 mm. Only the 242 μm sand showed erosion without sliding bed behavior (Zilverzand: $d_{10} = 184\,\mu m$, $d_{50} = 242\,\mu m$, $d_{90} = 336\,\mu m$, see Figure 5.4 for the particle size distribution). On the contrary, the bed layer of the coarser sand types started sliding before being fully dissolved by erosion. The sliding bed mechanism forms different density waves, and is therefore outside of the scope of this research. As such, for validation we have four experiments with 242 µm sand, at mixing loop concentrations of 5, 10, 20 and 30%.

A method is needed to determine the bed height from the ERT tomograms. Figure 5.5 shows a tomogram of a stationary bed without flow and the pipe filled halfway with a flat sand bed. Notice that at the side of the tomogram the correct bed concentration is measured, between 50-55%. However, in the middle of the tomogram the concentration is not between 50-55% as it should be. Also notice that the sharp bed interface is not well represented in the tomogram. These two issues are caused by the interpolation algorithm used to construct the tomogram from the raw sensor data, which is provided by the ERT manufacturer and tends to smear out sharp gradients. Because of the non-sharp interface in the tomogram, the actual height of the bed is located somewhere in the smeared out region. This causes an error when computing a bed height from a 1D vertical concentration profile from the tomogram (computed by horizontal integration). To correct for this error, we define that the bed interface is at a concentration of 42%, in the vertical concentration profile. This value was determined through visual observation of a half full pipe, and then interpolation of the tomogram with the method described above. Sharp gradients, like a bed interface, are not present in the suspended parts of the profiles, therefore no correction is applied in these parts of the tomogram.

The near bed concentration is also measured from the concentration tomogram. As explained earlier in Section 5.3, the near bed concentration is the concentration of the suspensions 4 mm above the bed layer, which is 10% of the pipe diameter. The near bed concentration is computed by interpolating the vertical concentration profile above the

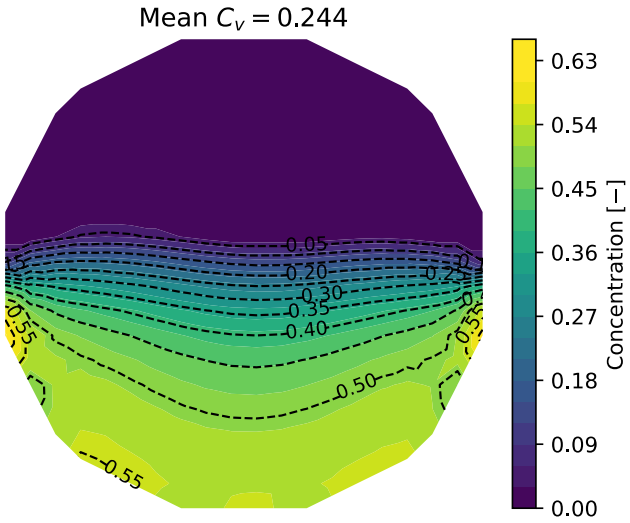

Figure 5.5: ERT tomogram of a stationary sharp flat bed interface, without flow over the top. The pipe was filled just below halfway. Notice that at the edges the correct concentration is measured, but the middle of the tomogram does not measure a bed concentration of 50-55%. This is an interpolation error.

bed. The results of the experiments are presented in the Results & Discussion (Section 5.4).

5.3.4. Experiments to validate erosion-sedimentation based density wave amplification

Another experimental flow loop was built specifically to study density wave amplification, see Figure 5.6. The loop was built to be as long as possible, in total 45.5 m long at an internal diameter of 42 mm. To measure the density wave development two vertical U-loops were constructed, to measure the delivered concentration c_{vd} (Clift and Manning Clift, 1981, Visintainer et al., 2023), spaced 15.6 m apart. The delivered concentration c_{vd} is defined as the ratio of the solids flow rate over the mixture flow rate. The two U-loops were intended to measure the development and growth of a wave between the two loops, this however was an attempt in vain. Figure 5.7 only displays the signal of the first U-loop downstream of the pump, since displaying both U-loops in one figure clutters the figure too much, and the two measurements are nearly identical. An Electro Magnetic Flowmeter (EMF) was used to measure the velocity of the mixture.

Theoretically, the U-loops affect density wave growth negatively, since these vertical parts do not contribute to density wave development, because no bed layer can form here. To check whether this was a problem, a few tests were repeated without U-loops. Fortunately, no change in wave development behaviour could be detected, thus we con-

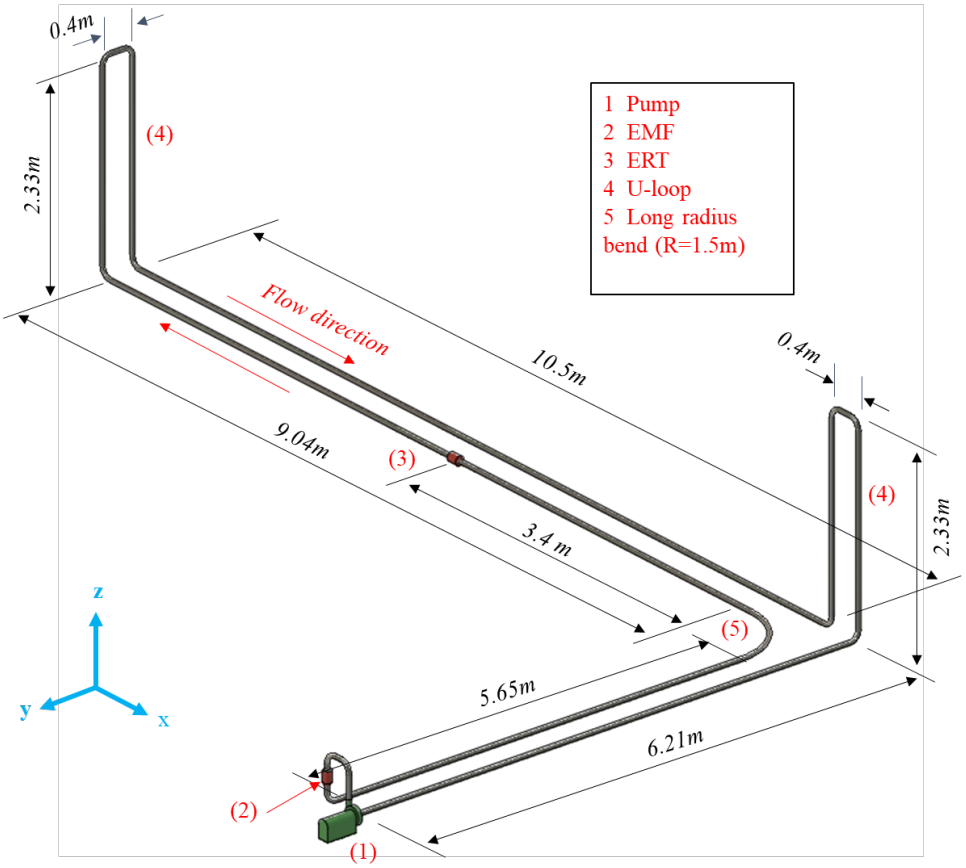

Figure 5.6: A 3-dimensional schematic overview of the density wave flow loop. EMF=Electro Magnetic Flowmeter, ERT = Electrical Resistance Tomograph.

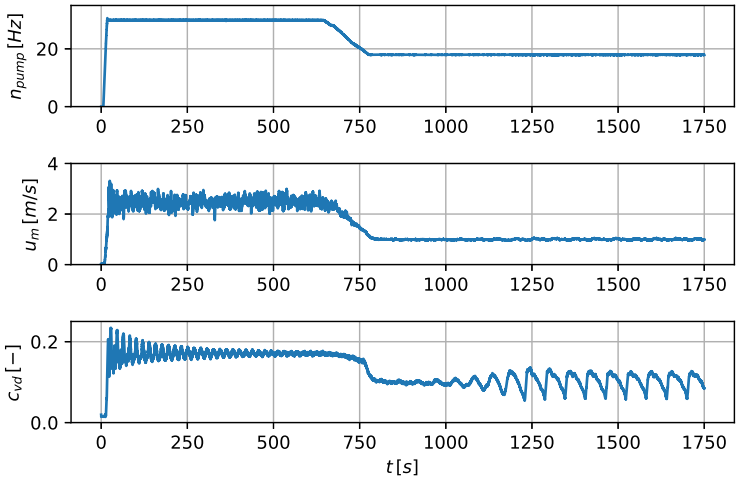

Figure 5.7: An example data set of the density wave experiments, using Zilverzand at a concentration of 18%. Top: the pump revolutions. Middle: the mixture velocity. Bottom: the delivered concentration.

cluded that the U-loops do not interfere significantly. Furthermore, the dispersive effect of the bends was kept to a minimum by limiting the use of bends only at the U-loops and at the centrifugal pump, and by building a special 1.5-meter long radius bend to complete the circuit. An ERT was also included, but unfortunately the data could not be used, since the ERT could not record data longer then the passing of a density wave. Experiments were conducted with the same Zilverzand as the erosion experiments. Three experiments were conducted with this sand type, at a mean pipeline volumetric concentrations of 10, 15 and 18%. An experiment was conducted in three stages: First, the experiment started at velocities at least twice the deposit limit velocity to disperse any waves. The second step was to slowly lower the pump revolutions until a bed layer formed. The third step was to keep the pump revolutions stable to allow density waves to grow over time. See Figure 5.7 for an example of the time (Section 5.4).

5.4. Results & Discussion

In the Methods (Section 5.3) the 1D-2L model framework was provided, and the experiments to validate the model explained. So how does the model perform against the experiments?

First the measurements of the near bed concentration are analysed, and an empirical model is derived to be able to compute the near bed concentration from the mean concentration of the suspension. The results can be seen in Figure 5.8, together with the data measured by Bisschop (2018) in the 28.8 cm conduit. The following power-law correlation can be derived from the data:

$$c_{nb} = \min(0.564 \cdot c^{0.252}, c) \tag{5.17}$$

This equation was fitted through the data in Figure 5.8, using a non-linear least squares method. The near bed concentration is bounded, to never be below the mean concentration c, since this is physically impossible. Do be aware of the spread in the data visible in Figure 5.8, caused by the concentration measurement, which will naturally affect the accuracy of the estimation of c_{nb} using Equation 5.17.

A small side note on Figure 5.8: An error was found in the data processing algorithms to determine the near-bed concentration by Bisschop (2018). The error was corrected, shown in Figure 8, which has not yet been published elsewhere. The original data can be found back in Bisschop (2018), Figure 8.12a.

Next we review the performance of the erosion-sedimentation closure by comparing the model to the experiments. The 1D-2L model was applied in a flow driven mode. This means that the volumetric flow rate is used as input for the model, and the pressure field follows as a result from the momentum equation. Additionally, the initial bed height from the experiment is an initial condition for the model. The near bed concentration was calculated from the mean concentration above the bed as measured by the ERT, using Equation 5.17.

Ideally, the erosion model should be in agreement with all four experiments using the same model settings. Figures 5.9, 5.10, 5.11 and 5.12 show the results of the erosion experiments against the model, conducted at mixing loop concentrations of 5, 10, 20 and 30% respectively. The Bisschop (2018) model was slightly adjusted, by using $\lambda_b = 0.7$ instead of the default value of $\lambda_b = 1.0$ (see Appendix B for more details). Other geotechnical parameters used in the simulation are: $n_0 = 0.44$, $n_{max} = 0.47$, $n_{min} = 0.36$, $k_{max} = 4.74e-04\, m/s$, $\phi = 34°$. These were measured by Bisschop (2018). For the hindered erosion model $m = 3.0$ and $c_{max} = 0.55$ were used for all four simulations. The exponent m was found to have a strong effect on the high concentration experiments. By comparing the time required to erode the bed, we can see that by using the above mentioned settings, all four experiments can be simulated to satisfactory agreement. Two trends were noticed during calibration of the erosion model. Firstly, for high concentrations the results are sensitive for the hindered erosion model settings, m and c_{max}. Secondly, the calibration was also sensitive to adjustment in the erosion model, λ_b, for all concentrations. A disagreement can be noticed in Figure 5.12. Figure 5.12 shows that the experiment lasts 10.5 seconds, while the model predicts a fully eroded bed after 7.5 seconds. In other words, the erosion is slightly overestimated at high concentrations. This behavior can be altered by recalibrating the hindered erosion model. Calibrating m and c_{max} to better match Figure 5.12 was attempted, however this made the calibration of Figures 5.10 and 5.11 worse, therefore m and c_{max} were left unaltered. In the introduction we asked ourselves: Is an erosion-sedimentation based closure relationship suitable for modelling the sediment exchange between the stationary bed layer and the suspended flow? We can conclude that the answer is yes, after proper calibration of the coefficients. However, if a future goal is to have a generic 1D-2L model for a large range

of pipe diameters and sand type, more experimental data is required for validation and calibration, more on this at the end of the discussion (Section 5.4).

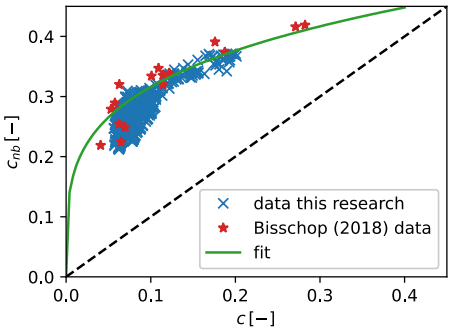

Figure 5.8: The near bed concentration c_{nb} as a function of the mean suspended concentration above the bed c. Measured values are from Bisschop (2018) and of the erosion experiments in this research.

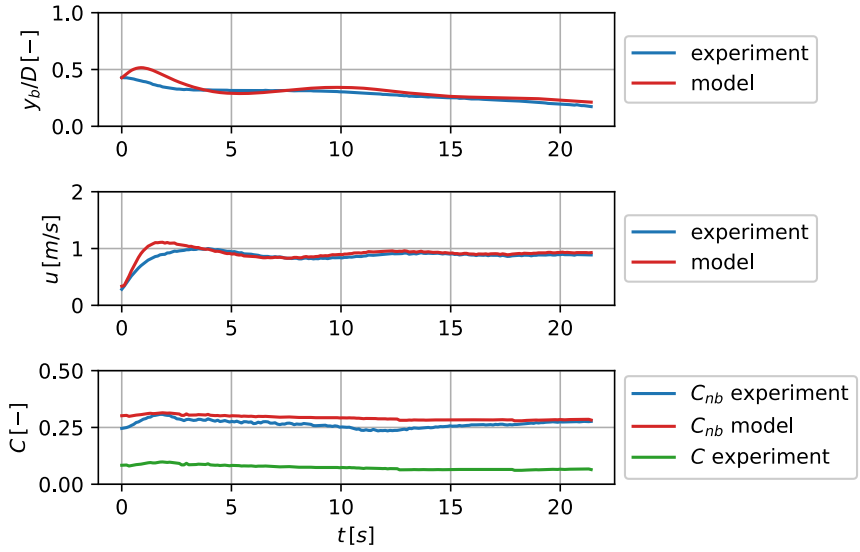

Figure 5.9: Model output against experiments, mixing loop concentration is 5%. Top: the bed height, middle: the velocity above the bed, bottom: the near bed concentration.

Now the ability of the 1D-2L model to simulate density wave amplification is analysed, using the calibrated erosion model. The full flow loop was meshed including U-loops, with a mesh resolution of 0.1 meter and a time step of 0.01 seconds. From experience using the 1D model, it is generally recommended to have several hundred grid cells

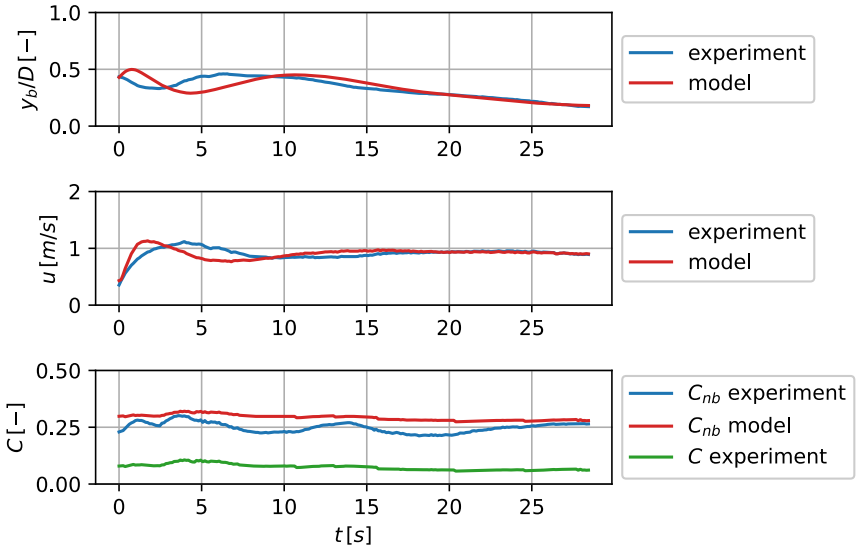

Figure 5.10: Model output against experiments, mixing loop concentration is 10%. Top: the bed height, middle: the velocity above the bed, bottom: the near bed concentration.

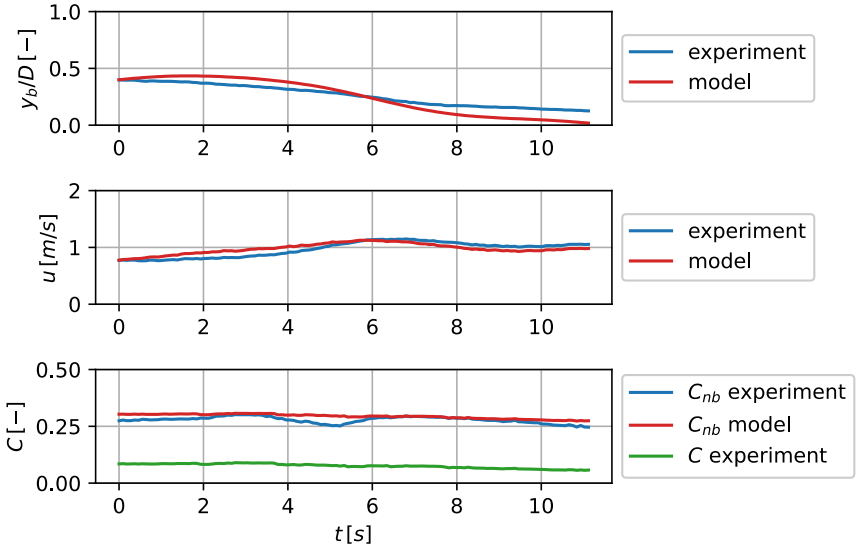

Figure 5.11: Model output against experiments, mixing loop concentration is 20%. Top: the bed height, middle: the velocity above the bed, bottom: the near bed concentration.

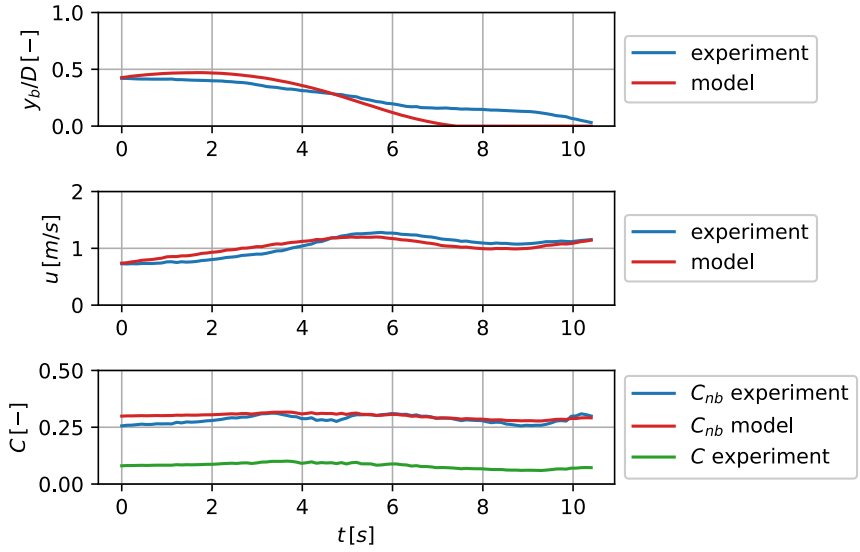

Figure 5.12: Model output against experiments, mixing loop concentration is 30%. Top: the bed height, middle: the velocity above the bed, bottom: the near bed concentration.

to represent a single density wave. These simulations typically produced two waves in the flow loop, as such we used ~ 250 cells to capture one wave. The time step is based on attaining a Courant grid number lower than 0.1. A good agreement is reached if the amplification rate and density wave amplitude are similar in the experiment and the simulation. The solver once again is used in a flow driven mode. The simulation starts at high velocity similar to the experiment. In the experiment several minutes are used to allow the wave to dampen, this is not simulated. What is simulated, is a very small initial wave with a length equal to the loop. This was to provide a perturbation for the waves to grow from, and was also present in the experiments. Thereafter, the velocity is lowered over a period of several minutes until a bed layer formed in the simulations. The formation of the bed coincides with a rapid drop of the delivered concentration measured by the vertical U-loops. The experiments showed that the effect of the waves on the mixture velocity was small, and can be considered as constant, see Figure 5.7. Therefore, in the simulations, once a bed layer formed, the simulated velocity is kept constant as well. The magnitude of the simulated velocity was chosen to attain a bed height similar as measured in the experiments.

We chose to aim for a similar bed height in the simulation compared to the experiment, because the bed height determines the amount of sediment available to create a wave, therefore this influences the final wave amplitude. This was experienced in the experiment, and also during calibration of parameters m and c_{max} for the simulations. The consequence of this choice is however, that the mixture velocity cannot be perfectly matched, since there is some discrepancy between the erosion model and the experiment at high concentrations as seen in Figure 5.12. The cause of this discrepancy was al-

ready addressed three paragraphs earlier in Section 5.4. This discrepancy directly results in the mixture velocity mismatch. It was also attempted to do it the other way around, aim for a similar mixture velocity, however then only a very thin bed, or no bed at all formed in the simulations, since the 1D-2L model slightly underestimates the deposit limit velocity. For future research, it is recommended to improve the hindered erosion model (likely not by simply adjusting the coefficients) to be able to predict the deposition limit velocity more accurately.

While calibrating the hindered erosion model, it was found that m influences mainly the amplification rate of the wave, and c_{max} the final wave amplitude. Experiment 1 and 2 (Figures 5.14 and 5.15, respectively) could be simulated well with the same settings of the hindered erosion model, using $m = 3$ and $c_{max} = 0.55$. However, with these settings simulation 3 showed waves with a 33% lower amplitude than the experiments, shown in Figure 5.15. Figure 5.16 again shows experiment 3, but now using $c_{max} = 0.56$. This gives a better match with the experiment in terms of wave amplitude, and also gives a demonstration of how changing c_{max} affects the wave amplitude.

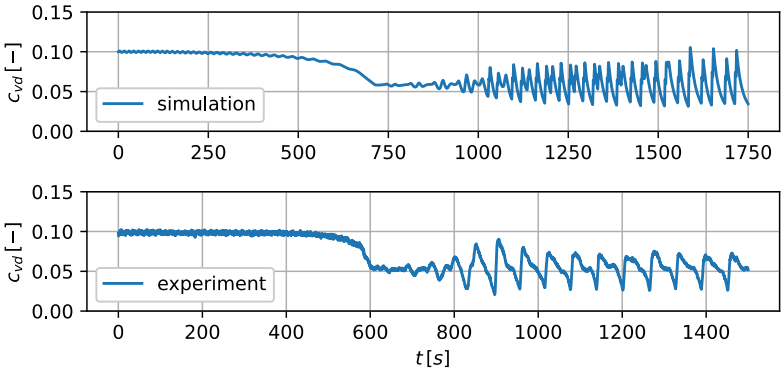

Figure 5.13: Results of simulation 1 (top) and experiment 1 (bottom), with an initial concentration of 10%.

Table 5.1 provided an overview of typical values defining the simulation and the experiments. Summarized, the following similarities can be seen between the simulations and the experiments:

(a) Wave amplitude: Simulation and experiment are within a 10% deviation for simulation 1 and 2. Simulation number 3 was slightly off when using the same model settings, a 33% deviation.

(b) The mean mixture velocity: the simulation predicts a slightly lower mean velocity, and within a 25% deviation.

(c) The average delivered concentration of the wave: Simulation and experiment are within a 10% deviation.

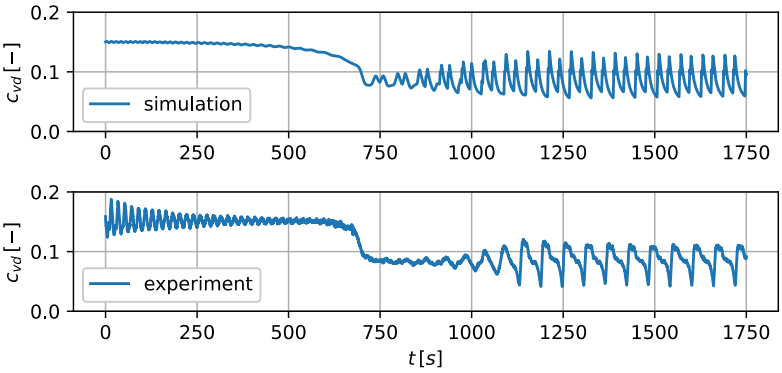

Figure 5.14: Results of simulation 2 (top) and experiment 2 (bottom), with an initial concentration of 15%.

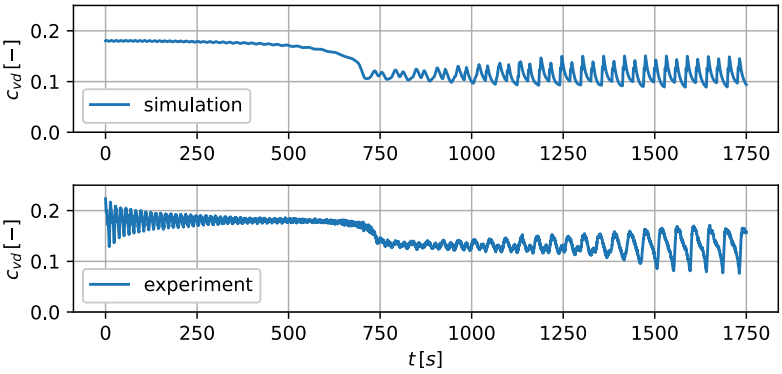

Figure 5.15: Results of simulation 3 (top) and experiment 3 (bottom), with an initial concentration of 18%.

One very obvious difference between the simulations and the experiment is the wavelength. In the experiment the wavelength always equals the length of the flow loop, which has also been observed in other density wave experiments (de Hoog et al., 2021, Talmon, 1999). These simulations however, usually end up generating two waves. Sometimes the secondary wave was small enough to be absorbed by the main wave, resulting in a single wave, but this did not always occur. Talmon (1999) stated that the relative strength between dispersive forces (ϵ in Equation 9) and amplifying forces, determines the wave length. However, changing ϵ in the model did not affect the wave length, but only the amplitude. Another hypothesis was that the U-loops affect the wave length. The idea was that the U-loops split the circuit into two sections, since in the U-loops no bed layer can form, because the pipes are vertical. Consequently, the U-loops do not contribute to the density wave amplification process. As such, the hypothesis was that the two U-loops split the flow loop into two sections, causing two waves to be initialized once a bed layer forms. However, removing the U-loops from the simulation domain

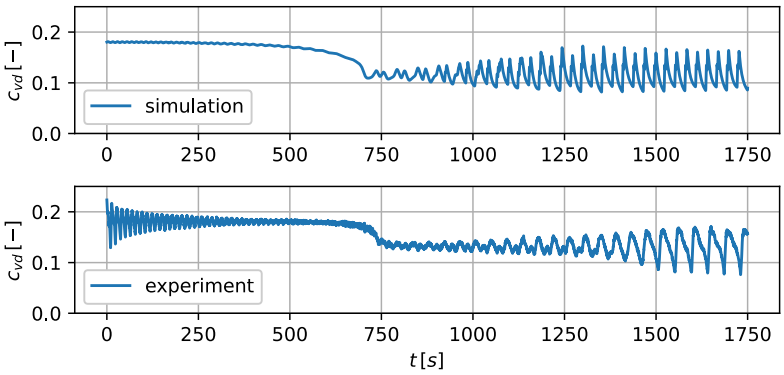

Figure 5.16: Results of simulation 3 (top) and experiment 3 (bottom), with an initial concentration of 18%. Using $c_{max} = 0.56$.

Table 5.1: The parameters defining the density wave simulations and experiments. c_{loop} is the initial loop concentration, $c_{w,mean}$ is the mean wave concentration, $c_{w,ptp}$ is the wave peak-to-peak concentration (min-max), $u_{m,w}$ is the mean mixture velocity of the wave, y_b/D is the relative bed height.

Sim/ Exp	c_{loop} [−]		$c_{w,mean}$ [−]		$c_{w,ptp}$ [−]		$u_{m,w}$ [m/s]		y_b/D [−]		m [−]	c_{max} [−]
	Sim	Exp	Sim	Exp	Sim	Exp	Sim	Exp	Sim	Exp		
1	0.10	0.10	0.058	0.054	0.052	0.048	0.82	1.1	0.05	0.06	3.0	0.55
2	0.15	0.15	0.086	0.084	0.071	0.068	0.82	1.0	0.15	0.14	3.0	0.55
3	0.18	0.18	0.12	0.13	0.060	0.090	0.81	1.1	0.12	0.11	3.0	0.55
3*	0.18	0.18	0.12	0.13	0.093	0.090	0.80	1.1	0.14	0.11	3.0	0.56

made no noticeable difference to the simulations, and still two waves formed in most simulations. Concluding, at this moment it is unclear why the simulations tend to generate two waves in the loop.

In the introduction we asked ourselves the following main research question: Can we model density wave formation using a 1-dimensional-2-layer CFD model? The answer is yes, after calibration of the coefficient. Some remarks: the method chosen in this research is very empirical. The calibration coefficients are λ_b, m, c_{max} and the coefficients related to the c_{nb} model (Equation 5.17). The Bisschop (2018) erosion model has a physical foundation, and is calibrated for sand sizes up to 562 μm, therefore has potential to scale well beyond the current use in this chapter. The hindered erosion and c_{nb} models however are purely empirical, and therefore if any user desires to apply the 1D-2L model in its current state, the user is limited to a pipe of 42 mm and sand of 242 μm.

To transform the 1D-2L model from a research model to a generic design model using the current closures, a large amount of validation data is needed of various pipe diame-

ters and sediment types. This is not advised, rather a better development path would be to use a physical based closure from literature. For example, the near bed concentration model can be improved by estimating the concentration distribution above the bed using Schmidt-Rouse type turbulent diffusion models (Matoušek and Krupička, 2014). The fact that a c_{nb} model is required, is linked to the choice of using the Bisschop (2018) erosion model, which is currently the state-of-the-art in the category of physical-empirical erosion models. Using a different closure to model erosion would eliminate the need for the c_{nb} model. An alternative for the Bisschop (2018) erosion model could be found in the state-of-the-art 3D multiphase CFD literature, where stationary sediment beds are modelled using rheological models (Chauchat et al., 2017, Goeree, 2018) or using kinetic theory (Berzi and Jenkins, 2011). Rheological or kinetic theory based models incorporate more physics, therefore these are better for scaling. This further reduced the demand for experimental data. As such, it is worth investigating the use of a 1D variation of either a rheological or a kinetic theory based model, inspired on the state-of-the-art in 3D multiphase CFD literature.

Up to this point the 1D-2L model was only used in a flow driven mode, as opposed to the pressure driven mode. In the pressure driven mode a driving pressure is applied in one of the cells (representative of a centrifugal pump), and consequently the velocity field follows from the momentum equation. The fully pressure driven mode has been verified and observed to work well, but still requires detailed validation. To verify the pressure driven mode, and therefore the full momentum equation, the energy losses of the bed layer and the mixture should match the experiments. This can be achieved with well-developed physical-empirical models from literature (Visintainer et al., 2023). A pump can be modelled to drive the system to overcome these losses. This will yield a mixture velocity similar to the experiment, and therefore also lead to density waves. This approach also allows for the ability to simulate pipeline blockages, when the density waves grows to large and forms a plug. A similar approach was used with the 1D Driftflux model in de Hoog et al. (2022). Validation of the pressure driven mode of the 1D-2L model will be conducted in the future.

Using the pressure driven mode also enables the possibility to study the role a centrifugal pump booster stations might have in triggering density waves, as hypothesized by de Hoog et al. (2021). The idea is that once a strong wave is formed, and flows through a pump booster station further down the pipe, which is not designed with enough power to handle the wave, causes a pipeline wide drop in mixture velocity. This decrease in velocity can trigger a new wave, if the mixture velocity drops below the deposit limit velocity. This effect is repeated if the new wave flows through the booster pump once more. Resulting in an unstable pipeline, constantly initiating new waves. Even through the 1D-2L model is only validated for a single particle size and pipe diameter, this wave-pump interaction can already be studied. Furthermore, the physics behind wave-pump interaction is easily scaled and translated to larger pipeline diameters, by using pump affinity laws.

5.5. CONCLUSIONS

THE main aim of this chapter was to study the possibility to model density wave amplification, caused by the erosion-sedimentation imbalance, using a 1D-2L numerical model. This model helps us understand the density wave phenomenon better, and opens the way towards using 1D transient modelling in pipeline design, to expand on the traditional steady state design methods. The 1D Driftflux model of de Hoog et al. (2022) was used as a starting point, and extended with a changing cell volume in time and space, allowing implementation of a second stationary bed layer. This 1D-2L model uses erosion-sedimentation equations to model the mass transfer between a stationary bed and the suspension, calibrated using custom erosion experiments. Finally, the 1D-2L model was calibrated against density wave experiments and shown to be able to model density wave amplification. The fact that the 1D-2L model can predict density wave amplification, further confirms the erosion-sedimentation imbalance mechanism. This result confirms that the erosion-sedimentation imbalance effect, is a driving mechanism behind density wave formation, in the presence of a stationary bed layer. Even though the model is only 1D, it shows to be able to simulate complex physical processes like bed erosion and density waves, which is a promising result on the path of further developing these type of models and using 1D modelling in daily pipeline design.

6

CASE STUDY: THE INFLUENCE OF PIPELINE DESIGN PARAMETERS ON TRANSIENT ACCUMULATION DENSITY WAVES

Whether a pipeline is subject to transient accumulation can be studied using the 1DHT model (Chapter 4). In this chapter the goal is to investigate what can be done to avoid and mitigate the effects of transient accumulation. This is achieved by simulating the same tests as in Chapter 4, with the same model settings, but introducing new mitigation measures within new simulations. For this end the 1D-2L-HT model is applied, as another feature of the model is that the mathematical framework allows the modelling of pipes of different diameters in the same simulation domain. In this case study three different mitigation measures are numerically tested.

1. *Decreasing the diameter of the horizontal pipes in the Freiberg flow loop.*
2. *Applying a constant power pump drive, in place of a constant revolutions drive.*
3. *Implementing flow feedback control on the centrifugal pump.*

Each of the three mitigation measures is evaluated for its effectiveness, but also the costs of implementation in a pipeline are discussed.

*This chapter is based on an article published in the proceedings of the 20th International Conference on Transport and Sedimentation of Solid Particles, **71–82**, 26-29 Sept., Wroclaw, Poland (2023).*

6.1. INTRODUCTION

EXPERIMENTS in various flow loops with vertical and horizontal sections have shown unsteady behavior of the slurry. Moreover, particles can redistribute spatially and form highly concentrated self-amplifying density waves. Two types of density wave amplification occurs in conjunction with the formation of a bed layer when the mixture velocity is below the deposit limit velocity, these are called erosion driven- and sliding bed driven density waves, see Chapter 3. A third mechanism occurs at velocities far exceeding the deposit limit velocity and in pipelines with vertical and horizontal sections, combined with particles having significant slip. This mechanism is referred to as "transient accumulation", see Section 4.2 for more details. Especially the transient accumulation mechanism forms a large risk for flow continuity, because wave amplification can occur far above the deposit limit velocity. Essentially it can be stated that the steady state design method (see Chapter 1) falls short in these cases.

Because of the unsteady nature of the formation of density waves, and their effect of flow assurance, a 1D CFD Driftflux model was created to predict density wave amplification (see Chapter 4), to aid in pipeline design. Chatper 4 contains the foundation of the 1DHT model, including calibration and validation with experimental data. This chapter aims to explore mitigation measured to avoid density wave amplification, using the 1D-2L-HT model from Chapter 5, with the calibrated model settings from Chapter 4.

The theory explaining the transient accumulation mechanism can be found back in 3.2, and a summary of the Freiberg experiments can be found in Section 3.3.

6.2. MITIGATION MEASURES

TRANSIENT accumulation occurs through a combination of a local particle velocity difference between two pipe sections (for instance a vertical and horizontal pipe, see Figure 6.1b), together with a transient change in global mixture velocity, see Section 4.2 for more details. As such the effect of transient accumulation can be mitigated by reducing either the spatial particle velocity difference, or avoiding the temporal mixture velocity change. This can be achieved in three ways. Firstly, by ensuring that the mixture velocity does not fluctuate in time, by using flow feedback control on the revolutions of the pump drive. This however is an economically expensive solution, since an electric motor with a frequency drive is required to enable control over the pump revolutions. In addition, the pump drive needs a reserve margin in power to prevent the pump drive from operating in a constant power regime, further increasing costs. The second option is a passive approach, by ensuring that the particle velocity difference between the vertical and horizontal pipe is minimized. This can be achieved by decreasing the horizontal pipe diameter. For example, Figure 6.1b shows the particle flow rate of a horizontal 125 mm pipe, which matches much better with the particle flow rate of the 150 mm riser, compared to the 150 mm horizontal pipe.

A third option to reduce density wave amplification, is to design the pipeline such that the centrifugal pump operates at constant power or torque. The constant revolu-

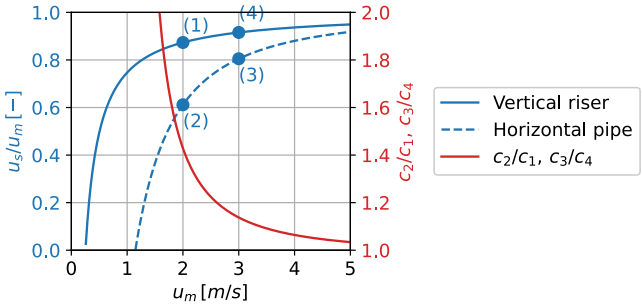

(a) Blue: vertical pipe, blue dashed: horizontal pipe, red: concentration change of a density wave (right axis).

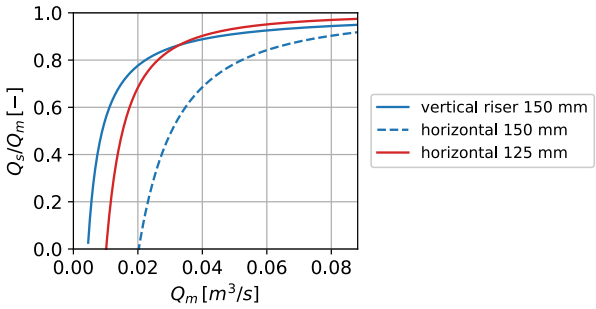

(b) Blue: vertical pipe $D = 150\,mm$, blue dashed: horizontal pipe $D = 150\,mm$, red: horizontal pipe $D = 125\,mm$.

Figure 6.1: (a) An example of the difference in particle velocity and concentration between a 150 mm vertical and a horizontal pipe, using $d_{50} = 11.2\,mm$. (b) An example of the difference in particle flow rate between a 150 mm diameter vertical pipe and a 125 mm horizontal pipe.

tions pump curve is relatively flat at lower volumetric flows (see Figure 6.2), which implicates that a small change in pipeline resistance (for instance a density wave flowing out a vertical riser) can lead to a large mixture velocity change (Wilson et al., 2006). A constant power or torque characteristic is steeper, as such potential changes in mixture velocity are smaller, see Figure 6.2. As such, a smaller change in the mixture velocity, results in less amplification.

6.3. Additions to the 1D-2L-HT CFD model

A PID controller can be implemented numerically as follows:

$$U_t = K_p\, e_t + \sum_{N=0}^{t} K_I\, e_N \Delta t + K_D \frac{e_t - e_{t-1}}{\Delta t} \tag{6.1}$$

Where U_t is the controller output at time step t, K_P the proportional gain constant K_I the integration gain constant, K_D the derivative gain constant and Δt the time step.

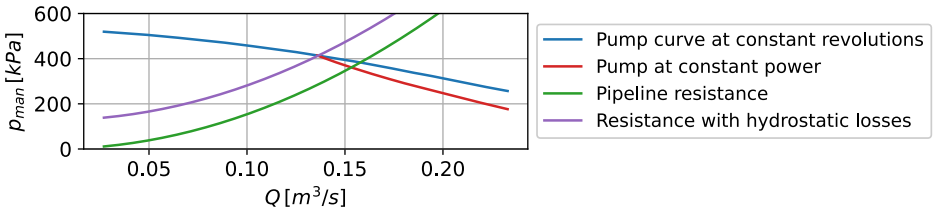

Figure 6.2: An illustrative example of a small change in pipeline operating point when the pump drive is operating at maximum power, in case of a change in hydrostatic pressure in a pipeline system.

The error e_t equals the difference between the mixture velocity at time step t, $u_{m,t}$, and the controller set point $u_{m,set}$:

$$e_t = u_{m,t} - u_{m,set} \tag{6.2}$$

Integration of the error is achieved by summation of all errors of previous time steps, N, and the derivative is computed from the error of the previous time step $t-1$. The controller output is limited to a domain of $[-100, 100]$ and mapped to the drive revolutions in the domain of zero to the maximum drive revolutions $[0, n_{max}]$.

6

The 1D-2L-HT Driftflux model contains a centrifugal pump model, furthermore the pump revolutions were the main input for the model in the Freiberg simulations. The pump reference curve in Figure 6.2 was scaled to the desired revolutions using pump affinity laws. The revolutions of the constant power curve can be computed according to the affinity laws of hydraulic power:

$$n_{cp} = \left(\eta \frac{P_{max}}{Q p_{man,cr} n_{cr}^3} \right)^{\frac{1}{3}} \tag{6.3}$$

In Equation 6.3, Q is the volumetric flow rate, n_{cp} is the revolutions of constant power drive at volumetric flow rate Q, P_{max} is the maximum drive power, η the drive efficiency at volumetric flow rate Q, $p_{man,cr}$ the pump manometric pressure at volumetric flow rate Q for a constant revolutions curve and n_{cr} the maximum drive revolutions.

6.4. Simulation results

The results of the simulation using the three wave mitigation methods as explained in Section 6.2 can be viewed in this section.

6.4.1. Differential pipe diameter simulations

Figures 6.3, 6.4 and 6.5 show the results of the simulations where the horizontal pipe diameter was reduced from a 6" (150 mm) to a 5" pipe (125 mm). As such, the particle flow rate of the two pipes is matched better (see Figure 6.1b). The initial velocity of the 125 mm horizontal pipe was taken from the experimental data (a 150 mm pipe). This results in an even lower velocity in the vertical pipes, and as such the total pressure

drop in the system is lower. Therefore, the pump pressure curve was reduced by 5% for these simulations, to get a similar velocity compared to the experiments. Just as with the simulations in Chapter 4, the pump revolutions measured during the experiments were used as input for the model. Another input of the model is u_{crit} (~ deposit limit velocity) in the relative velocity model according to Sobota and Kril (1992). The value of u_{crit} in the 125 mm pipe has been scaled according to:

$$\frac{u_{crit,125}}{u_{crit,150}} = \sqrt{\frac{0.125}{0.150}} \tag{6.4}$$

This scaling follows the Froude number type scaling found in most empirical deposit limit velocity models. The simulations show that for two cases (Figure 6.5 and 6.6) the wave amplification is reversed and the waves dampen out slowly. The simulation in Figure 6.4 is stable, not amplifying nor damping significantly. Furthermore, the simulation in Figure 6.3 still shows very slight amplification, but much less that the original case. Complete damping of the waves is only possible when the particle velocity in the horizontal pipe is equal or lower than in the vertical pipe. In the simulations of Figure 6.3 this condition was not entirely met. Reducing the pipe diameter by another standard size to 4" will solve the problem. However, there is of course a practical limit that prevents designers from lowering the horizontal pipe diameter much more. A simple example is the increased mixture velocity in the horizontal pipe will increase the wear rate of the pipe significantly. Another example in case of very coarse slurries, is that the largest particles dictate the minimum diameter of the pipe, a typical design guideline is $d_{50}/D > 1/3$ (van den Berg, 2013). How far the horizontal pipe can be reduced depends on the case.

Summarized, considering that lowering the horizontal pipe diameter is a passive and cheap solution, it is a very effective mitigation measure.

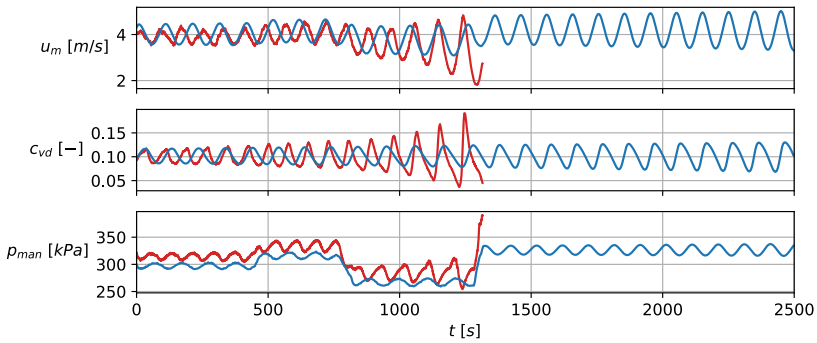

Figure 6.3: Simulation with a 150 mm riser and 125 mm horizontal pipes: Coarse sand, $c = 0.10$. Red: experimental data. Blue: simulation. Some slight amplification remains.

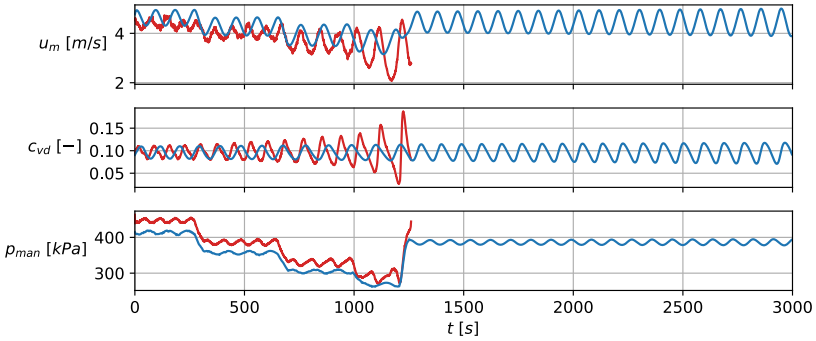

Figure 6.4: Simulation with a 150 mm riser and 125 mm horizontal pipes: Coarse sand, $c = 0.09$. Red: experimental data. Blue: simulation. The simulation is stable.

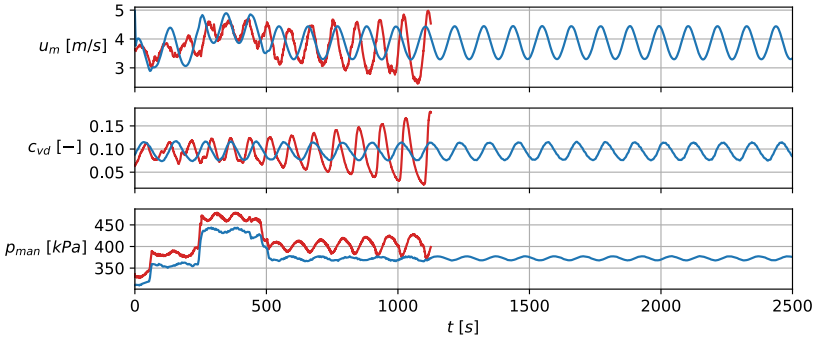

Figure 6.5: Simulation with a 150 mm riser and 125 mm horizontal pipes: Medium gravel, $c = 0.10$. Red: experimental data. Blue: simulation. The density wave dampens out.

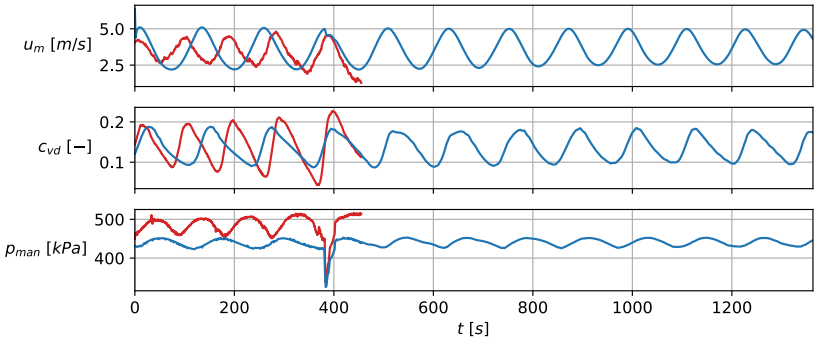

Figure 6.6: Simulation with a 150 mm riser and 125 mm horizontal pipes: Medium gravel, $c = 0.15$. Red: experimental data. Blue: simulation. The density wave dampens out.

6.4.2. CONSTANT POWER DRIVE SIMULATIONS

THE simulations in Figures 6.7, 6.8, 6.9 and 6.10 show the simulation results of using a constant power drive, compared to the original data with a constant revolutions drive. Both horizontal and vertical pipes have a diameter of 150 mm. In the original simulation of Chapter 4, the measured pump revolutions were used as input for the 1D Driftflux model. However, in these simulations this cannot be done, since the drive is limited by power. As such, the revolutions of the pump are the results of the load on the drive, see Equation 6.3. Therefore, the drive power has be chosen such that the initial velocity of the experiment is similar in the simulations of Chapter 4.

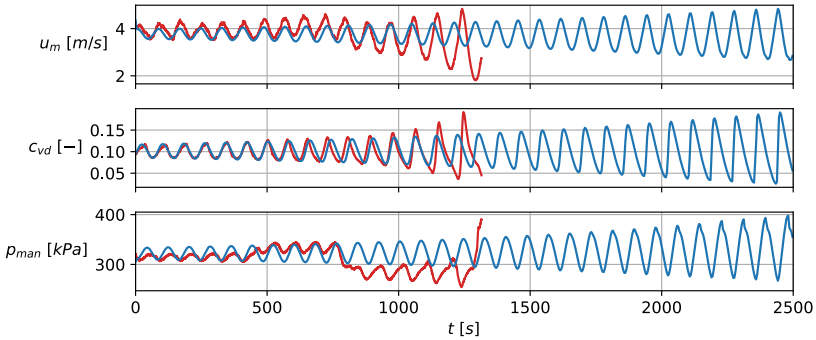

Figure 6.7: Simulation using a constant power drive: Coarse sand, $c = 0.10$. Red: experimental data. Blue: simulation.

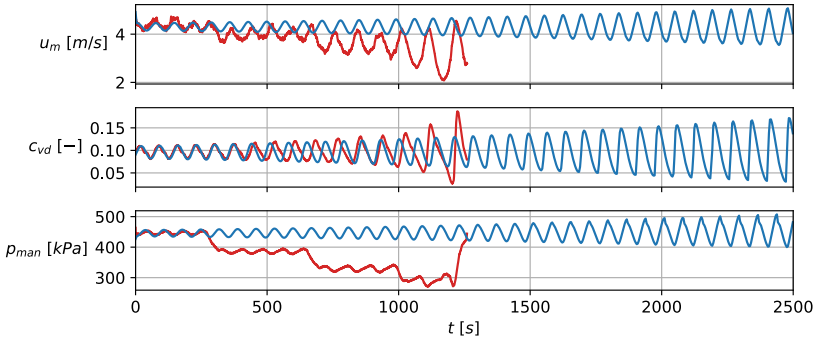

Figure 6.8: Simulation using a constant power drive: Coarse sand, $c = 0.09$. Red: experimental data. Blue: simulation.

All three simulations show significantly smaller variation in mixture velocity, which is caused by the constant power drive characteristics (see Figure 6.2). The rate of amplification of the density wave is less compared to the data, but amplification has not been mitigated completely. This solution seems only marginally effective.

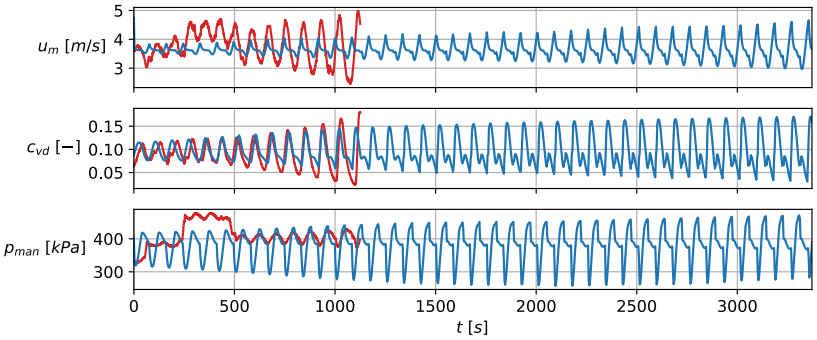

Figure 6.9: Simulation using a constant power drive: Medium gravel, $c = 0.10$. Red: experimental data. Blue: simulation.

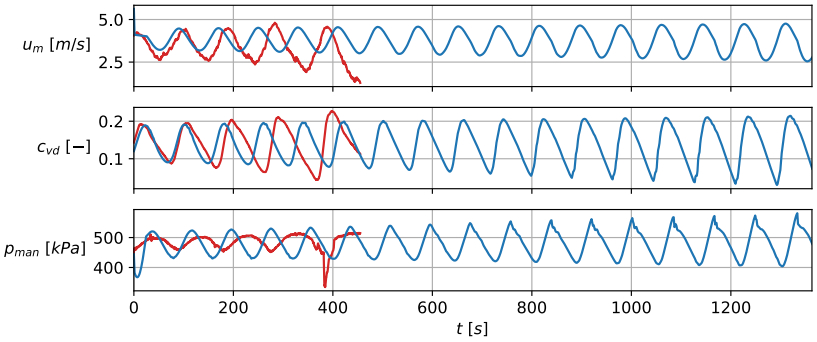

Figure 6.10: Simulation using a constant power drive: Medium gravel, $c = 0.15$. Red: experimental data. Blue: simulation.

6.4.3. Simulations using a PID controller for steady flow

The simulations using the PID controller can be viewed in Figures 6.11, 6.12, 6.13 and 6.14. All pipe diameters are 150 mm. The controller constant were chosen at $K_P = 10000$, $K_I = 2000$, $K_D = 0$. The controller is initially disabled, and enabled near the end of the experiment. From this point on the revolutions of the pump are the result of the controller output, evident by the pump manometric pressure. The controller works well to maintain the velocity fluctuations to a minimum, and the wave amplification ceases. The density waves in Figure 6.11, 6.12 and 6.13 even dampen out. As such the controller is able to reverse amplification, and maintain a stable transport process. This solutions seems very effective according to the simulations.

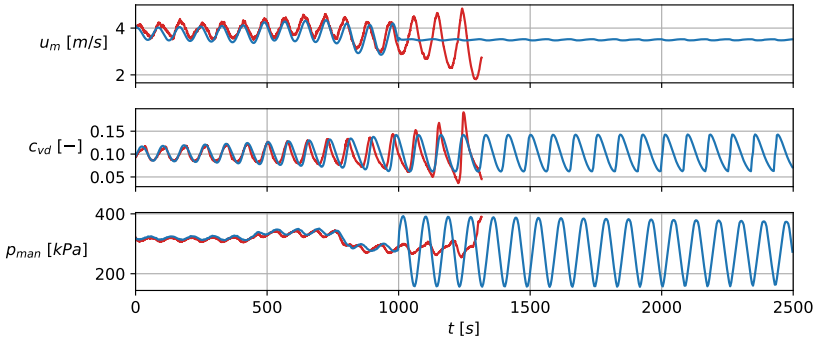

Figure 6.11: Simulation using a PID controller: Coarse sand, $c = 0.10$. Red: experimental data. Blue: simulation.

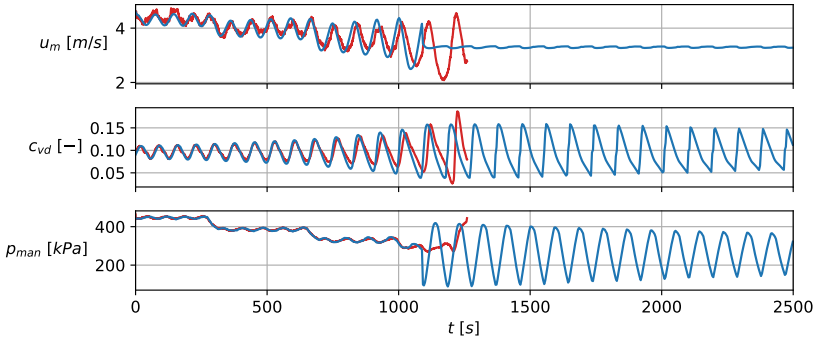

Figure 6.12: Simulation using a PID controller: Coarse sand, $c = 0.09$. Red: experimental data. Blue: simulation.

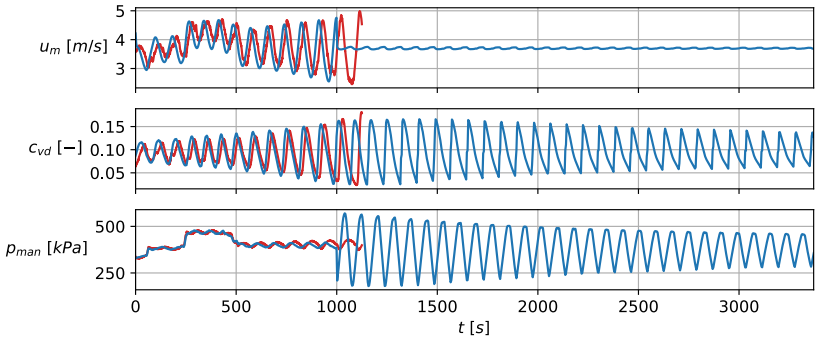

Figure 6.13: Simulation using a PID controller: Medium gravel, $c = 0.10$. Red: experimental data. Blue: simulation.

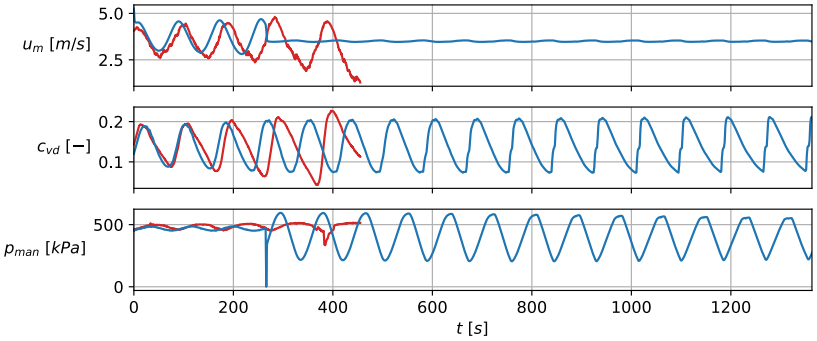

Figure 6.14: Simulation using a PID controller: Medium gravel, $c = 0.15$. Red: experimental data. Blue: simulation.

6.5. Discussion and Conclusions

Transient accumulation can be mitigated using three measures, as shown by 1D CFD simulations in this chapter. The first measure is to reduce the pipe diameter of the horizontal sections. This diminishes the mismatch in particle velocity between the riser and the horizontal pipes. Two out of three simulations show that this passive design measure can lead to damping of the density waves, and the other simulation showed that the waves did not grow further. The second measure is to use a constant power drive, with the idea to reduce the mixture velocity fluctuations caused by the density waves. This measure works as theorized, but is not able to completely reverse amplification like the first measure. The third measure is to use a PID controller to maintain a steady mixture velocity. This is by far the most effective solution, however this is also the most economically expensive, as this requires an overpowered drive (to allow for revolutions control) and a frequency controller. Designing the controller and choosing the correct drive power can be done well using simulations, by simulating large waves and designing the controller to cope with the waves.

Passive density wave mitigation measures are changing the pipe diameter of horizontal sections, and designing the pump drive in a constant power range (however then PID control is not possible). Matching particle flow rate by changing the pipe diameter, is most effective of the passive methods, however not as effective as PID control. If a passive density wave mitigation design is desired combining the two passive measures mentioned above will yield the best result. The advantage is that both passive methods can be designed for using steady state calculations (Figures 6.3 and 6.4), therefore the pipeline designer does not need to carry out 1D simulations. However, to know how effective these two solutions are for a certain pipeline system, still requires doing 1D simulations.

7

Conclusions and Recommendations

In this chapter the main conclusions of this thesis are summarized and recommendations for future research are provided.

7.1. CONCLUSIONS

THIS section aims to answer the main research question. The main research question defined in Chapter 1 is:

How do transients influence slurry flow stability of hydraulic transport pipelines?

Transients in hydraulic transport pipelines come in many forms and sizes, such as tiny ripples and dunes above a stationary particle bed layer, velocity fluctuations at various time scales, or density waves several hundred meters long (see Chapter 2). An important insight from this research is that local phenomena, can globally affect the mixture velocity in the entire pipeline system. This occurs as two main processes. Firstly, by two-way interaction between density fluctuations and the centrifugal pump(s). Secondly, by significantly affecting the local pipeline resistance or local hydro-static load, due to large local density variations. When these transients are large enough in magnitude, both processes cause significant global system-wide mixture velocity variations. These large mixture velocity variations can trigger density wave formation, thus destabilizing the pipeline.

The local-global system interaction explained above can be very complex as demonstrated by the Freiberg case (see Chapter 4), and as such can be difficult to understand and study experimentally. This emphasized the importance and potential of 1D numerical modeling, where local and system-wide processes can both be modelled, including the two-way interaction (see Chapters 4 and 5). Furthermore, the use of 1D-CFD enables analysis of pipelines many kilometers long, due to the computational efficiency of a 1D numerical solver. The 1D-2L-HT model developed in this research shows that it can model detailed local effects, such as particle slip and bed layer erosion, as long as there are suitable closures to represent these processes. More specific details on the conclusions are given in Sections 7.1.1, 7.1.2 and 7.1.3.

7.1.1. THE MOST IMPACTFUL TRANSIENTS THAT AFFECT FLOW STABILITY

This section answers the following research sub-question:

What are the most impactful transients that affect flow stability?

In general terms it can be stated that any mixture velocity transient is the result of the following (see Chapter 2 and 4):

- Changes in frictional losses in the pipeline cause slow changes in mixture velocity, typically with the same order of time as the slurry needs to flow through the pipeline.
- Changes in local hydrostatic pressure can cause changes in mixture velocity in a pipeline with a significantly long vertical section. As such, a local density wave, which can affect the hydrostatic load severely enough to affect the mixture velocity of the entire pipeline, as seen in the Freiberg density wave case.
- Changes of the pump manometric pressure cause fast short term variations in

mixture velocity, caused by a local unsteady mixture concentration flowing through the pump. The time scale is equal to the time required for a fluctuation to flow through the pump. Concentration changes through a centrifugal pump are by definition a local effect, and can affect the mixture velocity in the entire pipeline. The magnitude of the mixture velocity change is a function of the pipeline inertia, and the amplitude of the density variation.

Significant fluctuations of the mixture velocity can trigger density waves, which can lead to an unstable pipeline. A system is considered unstable, if the density waves are significant enough in amplitude and length to negatively influence flow assurance, either by overloading pump drives with an excessively high mixture density, or causing blockages in the pipeline. Three mechanisms that cause density waves have been identified during this research and are considered unstable transients:

- Erosion driven density waves in horizontal pipe sections (see Chapter 3 and 5), occur when the mixture velocity is around the deposit limit velocity. The maximum amplitude of these waves is found to be ~ 1.5 times the mean concentration, according to this research.
- Sliding bed driven density waves in horizontal pipe sections (see Chapter 3), occur when the mixture velocity is around the deposit limit velocity. The maximum amplitude is found to be ~ 2.0 times the mean concentration of the density wave, according to this research.
- Transient accumulation density waves (see Chapters 4 and 6) occur in the transition from vertical to horizontal pipes (or vice versa). This mechanism can trigger at mixture velocities far above the deposit limit velocity. A maximum (steady) peak concentration has never been observed in the Freiberg experiments, as the waves seemed to keep increasing in amplitude and the tests had to be aborted for safety considerations. As such, it is yet unclear if transient accumulation waves can reach a steady-state amplitude or will always amplify.

7.1.2. THE PHYSICAL PHENOMENA RESPONSIBLE FOR UNSTABLE TRANSIENTS

This section answers the following research sub-question:

What are the physical phenomena responsible for unstable transients?

The main transient instabilities are the three density wave mechanisms. Erosion driven density waves are caused by the erosion-sedimentation imbalance (Talmon, 1999): an inverse relationship between erosion and sedimentation of a stationary bed layer in pipe (see Chapter 3). These waves develop slowly as seen in the experiments of Chapter 3. This occurs for finer particles, which are transported in turbulent suspension. In this research a particle size of 308 μm in a 42 mm diameter pipe, but the exact transition is as of yet difficult to point out.

Sliding bed driven density waves are caused by the inverse proportionally between the deposit limit velocity and the local solids concentration in a pipe, at concentrations

above ~ 0.10 (see Chapter 3). This causes low concentrations to form stationary deposits, while high concentrations form sliding bed layers. The transition from a stationary bed to a sliding bed is abrupt. Therefore, sliding bed driven density waves amplify rapidly by absorbing the stationary bed layers. In this research sliding bed driven waves were observed for particles of 617 μm and larger in a 42 mm diameter pipe.

Transient accumulation is caused by a spatial particle velocity difference between two pipe segments. For instance a vertical and a horizontal pipe. This requires mixtures with significant slip and therefore particle sizes, 600 μm or larger based on this research in a 150 mm diameter pipe. For transient accumulation density waves to form, a pipeline wide change in mixture velocity is also required, caused by shift of the pump operating point. This can for instance occur when a density waves exits a vertical pipe, causing the mixture to accelerate (see Chapters 4 and 6).

7.1.3. Simulating unstable transients using a 1D-Driftflux model

This section answers the following research sub-question:

How can unstable transients be simulated with a 1D-Driftflux model?

Part of this research focused on developing the 1-dimensional-2-layer-hydraulic-transport (1D-2L-HT) model, see Chapter 5. The aim of this model is to simulate transient accumulation and erosion driven density waves. To enable the simulation of these density waves, the following physics and elements have been incorporated into the 1D-2L-HT model:

- Particle slip, as a function of the particle diameter, particle density, local concentration and the pipe orientation.
- Pipes of different orientation and diameter in the same simulation domain.
- A two layer structure to simulate a stationary bed layer. This was achieved mathematically and numerically by implementation of spatial and temporal changes of the simulation cell volume.
- Bed layer erosion and sedimentation. In this research, erosion and sedimentation is modelled using empirically based closures.
- Inertia of the mixture is modelled using a momentum equation and a pressure driven solver. A centrifugal pump model is applied as a pressure source, which enables two-way coupling between the local mixture concentration and the centrifugal pump pressure.

7.1.4. Mitigating the risk of density waves

This section answers the following research sub-question:

How can the risk of unstable transients be mitigated in the pipeline design?

In the steady-state design phase mitigation techniques can be applied to reduce the risk of erosion driven- and sliding bed driven waves, based on the results of Chapter 3. The design strategy is to ensure that the operating point of a pipeline remains above the deposit limit velocity under heavy transient conditions. This requires an accurate predictive model for the deposit limit velocity and on top a well estimated margin to take into account the effect of transients. Specifically, the margin has to incorporate the following aspects:

- An estimation of the variation of soil conditions over the operating time of the pipeline. The particle diameter changes over time depending on the excavation site, and the the particle fraction with the highest deposit limit velocity should decisive in the design.

- In case the operator makes a mistake and a sudden large influx of solids enter the pipeline, the operating velocity could decrease below deposit limit in case of a constant power or constant torque driven centrifugal pump. This should be avoided, otherwise density waves may form in the pipeline. How large the maximum peak concentration may be, can be judged by applying an increased concentration to the first pump in the pipeline and thereafter considering the working point with the pipeline at normal operating concentration in the rest of the pipeline (without increased concentration).

- When the pipeline contains a booster station, the effect of a density wave can be studied by applying a higher concentration (1.5 times or 2.0 times the normal operating concentration, see Chapter 3) only at the booster. Then the operating point should not be below the deposit limit velocity, otherwise new density waves may form in the pipeline. With this design philosophy, the designer assumes that density waves will form, but makes sure that booster stations can cope with the waves.

Fully managing the risk of erosion- and sliding bed driven density waves, enables hydraulic transport in long horizontal dredging pipelines at higher mixture concentration, as discussed in Chapter 3. This allows for a higher solids flow rate, which is more cost and energy efficient.

Chapter 6 compares methods to mitigate the effect of transient accumulation using simulation with the calibrated 1D-2L-HT model. Chapter 6 discusses that mitigation of transient accumulation density wave can partially be achieved by using steady-state principles, and partially be means of simulation the pipeline using the 1D-2L-HT model. The best mitigation measures are:

- Reducing the pipe diameter of horizontal pipes to better match the particle velocity between horizontal and vertical pipes. This can be done with a good steady-state slip ratio model. However, quantifying the effectiveness of this mitigation technique still requires simulations to be carried out, using the 1D-2L-HT model.

- Applying flow feedback control to maintain a steady mixture velocity: This was found to be the best mitigation technique. Designing the controller and the power margin required for the pump drives to enable flow feedback control, can be achieved by simulations using the 1D-2L-HT model.

7.2. Recommendations and Outlook

7.2.1. Improve particle slip models

Accurate particle slip prediction is very important to be able to simulate transient accumulation density waves. In the 1D-2L-HT model the particle slip is modelled using an empirical closure. For vertical pipes this closure is well developed (van Wijk, 2016), but for horizontal pipes empirical models are scarce. Especially for pipe diameters larger than typical laboratory sizes ($D > 150mm$). To expand the utility of the 1D-2L-HT model to larger pipes, better horizontal slip ratio models are required. Large diameter laboratory loops do not exist ($> 500mm$), because of their excessive costs, nor do most laboratory flow loops have the capability to measure particle slip accurately. Fortunately, the state of the art in 3D-CFD can play a role in scaling up experimental results from small experimental pipe diameters to larger full scale pipe diameters (Messa et al., 2021, Schouten et al., 2021).

7.2.2. Simulation of sliding bed driven density waves

The 1D-2L-HT model was originally developed to simulate erosion driven density waves. This is because at the start of the development the sliding bed driven density wave mechanism was not yet identified. However, the experiments of Chapter 3 showed that in fact the sliding bed driven density waves have a larger impact on flow assurance, as sliding bed driven density waves have higher wave amplitudes and amplification rates compared to erosion driven density waves. As such, sliding bed driven density waves have the potential to significantly affect booster pump station(s) positioned along a long pipeline. The hypothesis is, that once a density wave flows through the booster pump(s) (driven by constant power or torque), the mixture velocity can decrease below the deposit limit velocity, which triggers the formation of new density waves in the pipeline. The new waves will again flow through booster station(s), and cause new density waves to form. This repeating cycle creates an unstable pipeline, which constantly self-excites density waves. Whether this scenario is possible, can be studied with the 1D-2L-HT model once it is expanded with the sliding bed driven density waves. Therefore, adapting the 1D-2L-HT model to simulate sliding bed driven density waves is a valuable next step.

Simulating sliding bed driven density waves with the 1D-2L-HT model can be achieved by adapting a few closures:

- The resistance model should be suitable for a sliding bed flow regime.
- The mean particle slip should be representative of the sliding flow regime.

- The transition from a stationary bed to sliding bed can be modelled by numerically transitioning to advection of the bed layer, once the hydrodynamic force pulling on the top of the bed layer exceeds the Coulombic friction force of the bed on the pipe wall.

7.2.3. THE ROLE OF THE PARTICLE SIZE DISTRIBUTION

CHAPTER 3 ends with an important question: "What is the influence of the particle size distribution on the type of density wave that develops?" Unfortunately, it is yet uncertain what type of wave mechanism prevailed in the Prins Claus Plein Pipeline. Chapter 3 discusses that the Prins Claus Plein data suggests sliding bed driven density waves, but the d_{50} particle diameter suggests erosion driven density waves, if compared to the experiments of Chapter 3. On the other hand, the particle size distribution of the Prins Claus Plein case is known to have been very broad. As such, the hypothesis is that the coarser part of the distribution forms a sliding bed and causes sliding bed driven density waves. This is important to research, especially because most laboratory tests are typically conducted using narrow graded soil, but broadly graded soils are more common in nature and encountered often during dredging projects. Therefore, to be able to accurately estimate the prevailing wave mechanism in a hydraulic transport pipeline, the influence of the particle size distribution grading on density wave formation needs to be understood better.

REFERENCES

Alajbegović, A., Assad, A., Bonetto, F., and Lahey, R. T. (1994). Phase distribution and turbulence structure for solid/fluid upflow in a pipe. *International Journal of Multiphase Flow*, 20(3):453–479.

Berzi, D. and Jenkins, J. T. (2011). Surface flows of inelastic spheres. *Physics of Fluids*, 23(1):355.

Bisschop, F. (2018). *Erosion of Sand at High flow velocities: An experimental study*. Phd thesis, Delft University of Technology, the Netherlands.

Chao, B. T., Sha, W. T., and Soo, S. L. (1978). On inertial coupling in dynamic equations of components in a mixture. *International Journal of Multiphase Flow*, 4(2):219–223.

Charru, F. and Hinch, E. J. (2006). Ripple formation on a particle bed sheared by a viscous liquid. part 1. steady flow. *Journal of Fluid Mechanics*, 550(1):111.

Chauchat, J., Cheng, Z., Nagel, T., Bonamy, C., and Hsu, T. J. (2017). Sedfoam-2.0: a 3-d two-phase flow numerical model for sediment transport. *Geoscientific Model Development*, 10(12):4367–4392.

Clift, R. and Manning Clift, D. H. (1981). Continuous measurement of the density of flowing slurries. *International Journal of Multiphase Flow*, 7(5):555–561.

de Hoog, E., in 't Veld, J. M., van Wijk, J. M., and Talmon, A. M. (2017). An experimental study into flow assurance of coarse inclined slurries. In *18th Conference on the Transport and Sedimentation of solid particles, Prague, Czech Republic*, pages 113–120. Wroclaw University of Environmental and Life Sciences, Wroclaw, Poland.

de Hoog, E., Talmon, A. M., and van Rhee, C. (2021). Unstable transients affecting flow assurance during hydraulic transportation of granular two-phase slurries. *Journal of Hydraulic Engineering*, 147(9):04021029.

de Hoog, E., van der Ven, O., Helmons, R. L. J., Talmon, A. M., and van Rhee, C. (2024a). Experimental research on self-amplifying density waves in horizontal pipelines of two phase granular slurries: measurements on the effect of particle diameter and concentration. *International Journal of Multiphase Flow*, Under review.

de Hoog, E., van der Voort, T., Talmon, A. M., and van Rhee, C. (2024b). A 1-dimensional-two-layer transient drift-flux model for hydraulic transport pipelines: modelling and experiments of bed layer erosion and density wave amplification. *Journal of Hydrology and Hydromechanics*, 72(1):64–79.

de Hoog, E., van Wijk, J. M., Talmon, A. M., and van Rhee, C. (2022). Predicting density wave amplification of settling slurries using a 1d driftux model. *Powder Technology*, 400(3):117252.

Doron, P., Granica, D., and Barnea, D. (1987). Slurry flow in horizontal pipes—experimental and modeling. *International Journal of Multiphase Flow*, 13(4):535–547.

Doron, P., Simkhis, M., and Barnea, D. (1997). Flow of solid-liquid mixtures in inclined pipes. *International Journal of Multiphase Flow*, 23(2):313–323.

Durand, R. and Condolios, E. (1952). Transport hydraulique et decantation des materiaux solides. *Compte Rendu des Deuxièmes: Journees de l'hydraulique, Grenoble*, 16(2):27–55.

Durand, R. and Condolios, E. (1956). Donnees techniques sur le refoulement hydraulique des materiaux solides en conduite. *Revue de l'industie minerale*, 1F:460:482.

Ferguson, R. I. and Church, M. (2004). A simple universal equation for grain settling velocity. *Journal of Sedimentary Research*, 74(6):933–937.

Franklin, E. M. and Charru, F. (2009). Morphology and displacement of dunes in a closed-conduit flow. *Powder Technology*, 190(1-2):247–251.

Garside, J. and Al-Dibouni, M. R. (1977). Velocity-voidage relationships for fluidization and sedimentation in solid-liquid systems. *Industrial & Engineering Chemistry Process Design and Development*, 16(2):206–214.

Gibert, R. (1960). Transport hydraulique et refoulement des mixtures en conduits. *Annales de Ponts et Chausees*, 130(3):307–374.

Gillies, R. G., Shook, C. A., and Wilson, K. C. (1991). An improved two layer model for horizontal slurry pipeline flow. *The Canadian Journal of Chemical Engineering*, 69(1):173–178.

Gillies, R. G., Shook, C. A., and Xu, J. (2004). Modelling heterogeneous slurry flows at high velocities. *The Canadian Journal of Chemical Engineering*, 82(5):1060–1065.

Goeree, J. (2018). *Drift-flux modeling of hyper-concentrated solid-liquid flows in dredging applications*. Phd, Delft University of Technology, Delft, the Netherlands.

Hirsch, C. (2007). *Numerical computation of internal and external flows: Fundamentals of computational fluid dynamics / Charles Hirsch*. Butterworth-Heinemann, Amsterdam and London, 2nd edition.

Ishii, M. and Hibiki, T. (2011). *Thermo-fluid dynamics of two-phase flow*. Springer US, New York, 2nd edition.

Keetels, G., Chauchat, J., and Breugem, W. P. (2023). Role of turbulent kinetic energy modulation by particle–fluid interaction in sediment pick-up. *Journal of Fluid Mechanics*, 955:A37 1–29.

Keetels, G. H. (2017). Global stability of concentration profiles in uniform sediment-laden channel flow. In *18th Conference on the Transport and Sedimentation of solid particles, Prague, Czech Republic*, pages 153–160. Wroclaw University of Environmental and Life Sciences, Wroclaw, Poland.

Keetels, G. H., Goeree, J. C., and van Rhee, C. (2018). Advection-diffusion sediment models in a two-phase flow perspective. *Journal of Hydraulic Research*, 56(1):136–140.

Kennedy, J. F. (1969). The formation of sediment ripples, dunes, and antidunes. *Annual Review of Fluid Mechanics*, 1(1):147–168.

Matoušek, V. (1995). Non-stationary solids flow in a long slurry pipeline with pumps in series - process of material aggregation. *8th Conference on the Transport and Sedimentation of solid particles*, pages D5–1–10.

Matoušek, V. (1996a). Solids transportation in a long pipeline connected with a dredge. *Terra et Aqua*, 62:3–11.

Matoušek, V. (1996b). Unsteady solids flow in a long slurry pipeline with pumps in series - process of material aggregation. *Journal of Hydrology and Hydromechanics*, 44(6):396–409.

Matoušek, V. (1997). *Flow Mechanism of Sand-Water Mixtures in Pipelines*. Phd thesis, Delft University of Technology, Delft, Netherlands.

Matoušek, V. (2001). On the amplification of density waves in long distance pipelines connected with a dredge. In *Proceedings of the 16th World Dredging Congress, Bonsall, California, USA*, pages 55–73. World Organization of Dredging Associations.

Matoušek, V. (2011). Solids transport formula in predictive model for pipe flow of slurry above deposit. *Particulate Science and Technology*, 29(1):89–106.

Matoušek, V., Kesely, M., and Chára, Z. (2019). Effect of pipe inclination on internal structure of settling slurry flow at and close to deposition limit. *Powder Technology*, 343(1):533–541.

Matoušek, V. and Krupička, J. (2010). Modeling of settling-slurry flow around deposition-limit velocity. In *18th International Conference on Hydrotransport, Rio de Janeiro, Brazil*, pages 1–12. BHR Group, Cranfield.

Matoušek, V. and Krupička, J. (2013). Different types of unsteady flow of solids generated in laboratory slurry pipe loop. In *16th Conference on the Transport and Sedimentation of solid particles, Rostock, Germany*. Wroclaw University of Environmental and Life Sciences, Wroclaw, Poland.

Matoušek, V. and Krupička, J. (2014). One-dimensional modeling of concentration distribution in pipe flow of combined-load slurry. *Powder Technology*, 260(7):42–51.

Matoušek, V., Krupička, J., and Kesely, M. (2018). A layered model for inclined pipe flow of settling slurry. *Powder Technology*, 333:317–326.

Messa, G. V. and Malavasi, S. (2014). Numerical prediction of dispersed turbulent liquid–solid flows in vertical pipes. *Journal of Hydraulic Research*, 52(5):684–692.

Messa, G. V., Yang, Q., Adedeji, O. E., Chára, Z., Duarte, C. A. R., Matoušek, V., Rasteiro, M. G., Sanders, R. S., Silva, R. C., and de de Souza, F. J. (2021). Computational fluid dynamics modelling of liquid–solid slurry flows in pipelines: State-of-the-art and future perspectives. *Processes*, 9(9):1566.

Miedema, S. A., Lu, Z., and Matoušek, V. (2003). Numerical simulation of a development of a density wave in a long slurry pipeline. In *23rd WEDA Technical Conference & 35th TAMU Dredging Seminar, Chicago, USA*, pages 99–109.

Miedema, S. A. and Ramsdell, R. C. (2019). *Slurry Transport: Fundamentals, A Historical Overview & The Delft Head Loss & Limit Deposit Velocity Framework*. TU Delft Open Access, 2nd edition.

Mueller, T., van Wijk, J. M., and Mischo, H. (2018). Eu blue mining project - building a large scale test system and flow tests for vertical transport systems in deep sea mining. *GeoResource Journal*, 3:38–45.

Newitt, D. M., Richardson, J. F., Abbot, M., and Turtle, R. B. (1955). Hydraulic conveying of solids in horizontal pipes. *Transactions of the Institution of Chemical Engineers*, 33:93–113.

Reimann, L., Vafeidis, A. T., and Honsel, L. E. (2023). Population development as a driver of coastal risk: Current trends and future pathways. *Cambridge Prisms: Coastal Futures*, 1(1):5844.

Richardson, J. F. and Zaki, W. N. (1954). Sedimentation and fluidisation: Part i. *Trans. Institution of Chemical Engineers*, 32(dec):S82–S100.

Rowe, P. N. (1987). A convenient empirical equation for estimation of the richardson-zaki exponent. *Chemical Engineering Science*, 42(11):2795–2796.

Schouten, T., van Rhee, C., and Keetels, G. (2021). Two-phase modelling for sediment water mixtures above the limit deposit velocity in horizontal pipelines. *Journal of Hydrology and Hydromechanics*, 69(3):263–274.

Sobota, J. and Kril, S. I. (1992). Liquid and solid velocity during mixture flow. In *Proc. 19th Int. Kolloquium Massenguttransport durch Rohrleitungen, Merschede, Germany*, pages 1–11. Univ. Paderborn.

Soo, S. L. (1976). On one-dimensional motion of a single component in two phases. *International Journal of Multiphase Flow*, 3(1):79–82.

Southard, J. B. (1991). Experimental determination of bed-form stability. *Annual Review of Earth and Planetary Sciences*, 19(1):423–455.

Spelay, R. B., Gillies, R. G., Hashemi, S. A., and Sanders, R. S. (2016). Effect of pipe inclination on the deposition velocity of settling slurries. *The Canadian Journal of Chemical Engineering*, 94(6):1032–1039.

Stepanoff, A. J. (1965). *Pumps and Blowers. Selected Advanced Topics. Two-phase Flow; Flow and Pumping of Solids in Suspension and Fluid Mixtures.* John Wiley, New York, USA, 1st edition.

Talmon, A. M. (1999). Mathematical analysis of the amplification of density variations in long-distance sand transport pipelines. In *Proceedings 14th Int. Conf. on Slurry Handling and Pipeline Transport*, pages 3–20. BHR Group, Cranfield UK.

Talmon, A. M. (2002). Solid transport instability in the sliding bed regime. In *11th Conference on the Transport and Sedimentation of solid particles, Gent, Belgium*, pages 373–381. Wroclaw University of Environmental and Life Sciences, Wroclaw, Poland.

Talmon, A. M., Aanen, L., and Bakker-Vos, R. (2007). Laboratory tests on self-excitation of concentration fluctuations in slurry pipelines. *Journal of Hydraulic Research*, 45(5):653–660.

Taylor, G. I. (1954). The dispersion of matter in turbulent flow through a pipe. *Proceedings of Roy. Soc. London, ser A., Mathematical and Physical Sciences*, ser A., Mathematical and Physical Sciences(446-468).

van den Berg, C. (2013). *IHC Handbook for Centrifugal pumps and Slurry transportation.* Royal IHC, Kinderdijk, the Netherlands, 1st edition.

van Rhee, C. (2002). *On the sedimentation process in a trailing suction hopper dredger.* Phd, Delft University of Technology, Delft, the Netherlands.

van Rhee, C. (2010). Sediment entrainment at high flow velocity. *Journal of Hydraulic Engineering*, 136(9):572–582.

van Rhee, C. and Talmon, A. M. (2010). Sedimentation and erosion of sediment at high solids concentration. In *18th International Conference on Hydrotransport, Rio de Janeiro, Brazil.* BHR Group, Cranfield, UK.

van Rijn, L. C. (1984). Sediment pick–up functions. *Journal of Hydraulic Engineering*, 110 (10):1494–1502.

van Rijn, L. C., Bisschop, F., and van Rhee, C. (2019). Modified sediment pick-up function. *Journal of Hydraulic Engineering*, 145(1):06018017.

van Wijk, J. M. (2016). *Vertical Hydraulic Transport for deep sea mining: a study into flow assurance.* Phd thesis, Delft University of Technology, Delft, the Netherlands.

van Wijk, J. M. (2018). Blue mining public report: Breakthrough solutions for mineral extraction and processing in extreme environments. IHC MTI B.V. (Royal IHC), the Netherlands.

van Wijk, J. M., van Grunsven, F., Talmon, A. M., and van Rhee, C. (2015). Simulation and experimental proof of plug formation and riser blockage during vertical hydraulic transport. *Ocean Engineering*, 101:58–66.

van Wijk, J. M., van Rhee, C., and Talmon, A. M. (2014). Axial dispersion of suspended sediments in vertical upward pipe flow. *Ocean Engineering*, 92(1):20–30.

Verloop, W. C. (1995). The inertial coupling force. *International Journal of Multiphase Flow*, 21(5):929–933.

Visintainer, R., Matoušek, V., Pullum, L., and Sellgren, A., editors (2023). *Slurry Transport Using Centrifugal Pumps*. Springer International Publishing, Cham.

Vlasák, P., Matoušek, V., Chára, Z., Krupička, J., Konfršt, J., and Kesely, M. (2020). Concentration distribution and deposition limit of medium-coarse sand-water slurry in inclined pipe. *Journal of Hydrology and Hydromechanics*, 68(1):83–91.

Wilson, K. C. (1976). A unified physically-based analysis of solid-liquid pipeline flow. In *4th International Conference on the Hydraulic Transport of Solids in Pipes*. BHR Group, Cranfield, UK.

Wilson, K. C. (1997). Development of the layered model for pipeline transport of solids. In *9th Conference on the Transport and Sedimentation of solid particles, Cracow, Poland*, pages 13–23.

Wilson, K. C., Addie, G. R., Sellgren, A., and Clift, R. (2006). *Slurry Transport using Centrifugal Pumps*. Springer US, 3rd edition.

Wilson, K. C. and Tse, J. (1984). Deposition limit for coarse-particle transport in inclined pipes. In *9th International Conference on the Hydraulic Transport of Solids in Pipes, Rome, Italy*, pages 149–161.

Winterwerp, J. C., Bakker, W. T., Mastbergen, D. R., and van Rossum, H. (1992). Hyperconcentrated sand–water mixture flows over erodible bed. *Journal of Hydraulic Engineering*, 118(11):1508–1525.

Winterwerp, J. C., Groot, M. B. d., Mastbergen, D. R., and Verwoert, H. (1990). Hyperconcentrated sand–water mixture flows over a flat bed. *Journal of Hydraulic Engineering*, 116(1):36–54.

Worster, R. C. and Denny, D. F. (1955). Hydraulic transport of solid material in pipes. *Proceedings of the Institution of Mechanical Engineers*, 169(1):563–586.

A

ALL EXPERIMENTS ON DENSITY WAVE AMPLIFICATION IN HORIZONTAL PIPES

These are the supplemental figures of all experiments of Chapter 3. The naming convention of the experiments is linked to Table 3.1 and 3.2.

Parts of this chapter have been published in the International Journal of Multiphase flow **Under review** (2024).

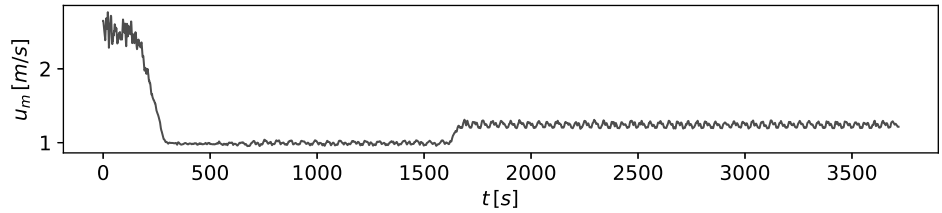

(a) Mixture velocity

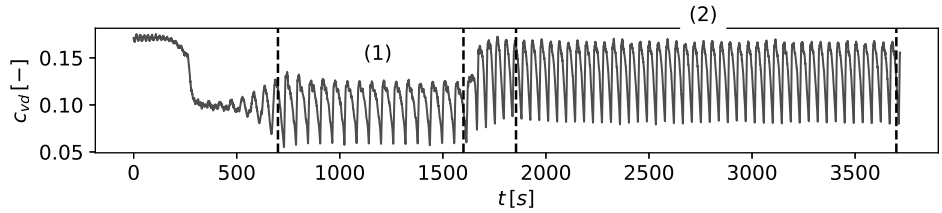

(b) Delivered concentration

Figure A.1: Tests Zilverzand (Zz), nrs. 2.1 and 2.2, $d_{50} = 242\mu m$.

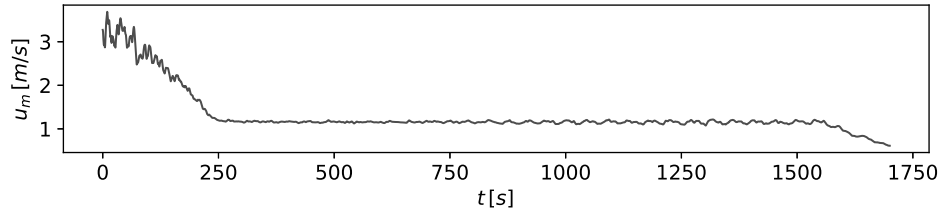

(a) Mixture velocity

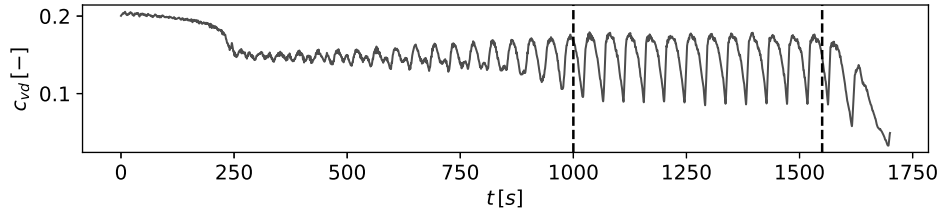

(b) Delivered concentration

Figure A.2: Tests Zilverzand (Zz), nrs. 3.1 and 3.2, $d_{50} = 242\mu m$.

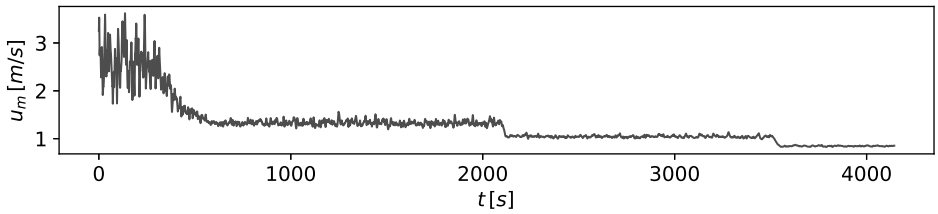

(a) Mixture velocity

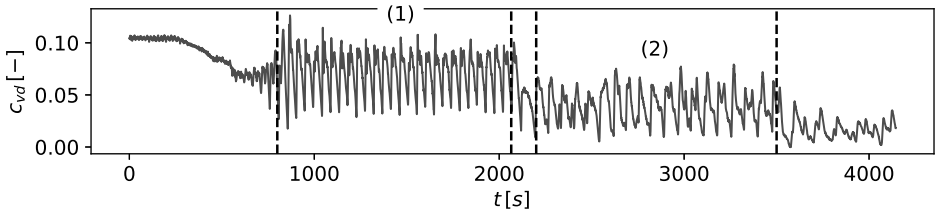

(b) Delivered concentration

Figure A.3: Tests Dorsilit 9 (D9), nrs. 1.1 and 1.2, $d_{50} = 308\mu m$.

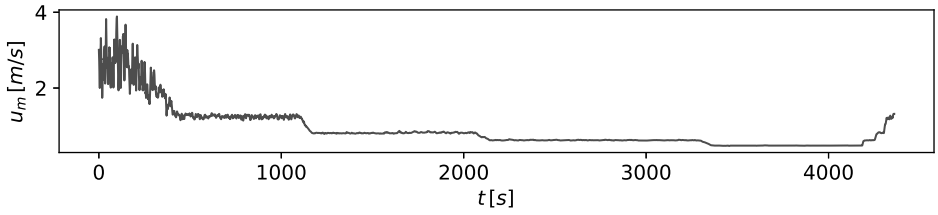

(a) Mixture velocity

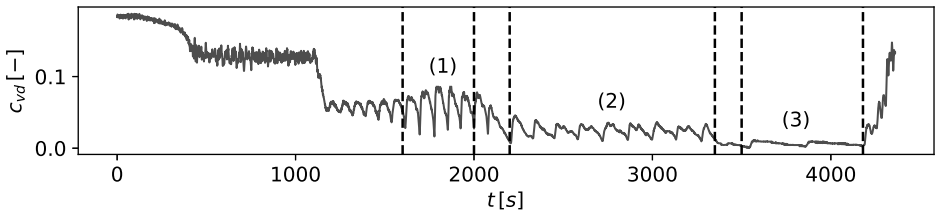

(b) Delivered concentration

Figure A.4: Tests Dorsilit 9 (D9), nrs. 2.1, 2.2 and 2.3, $d_{50} = 308\mu m$.

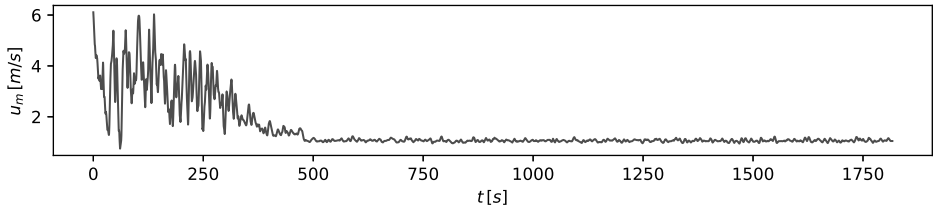

(a) Mixture velocity

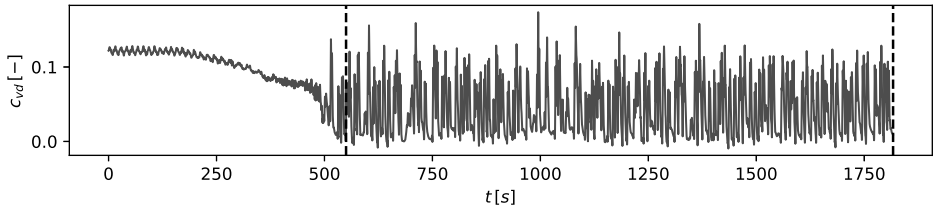

(b) Delivered concentration

Figure A.5: Tests Dorsilit 8 (D8), nr. 1, $d_{50} = 617\mu m$.

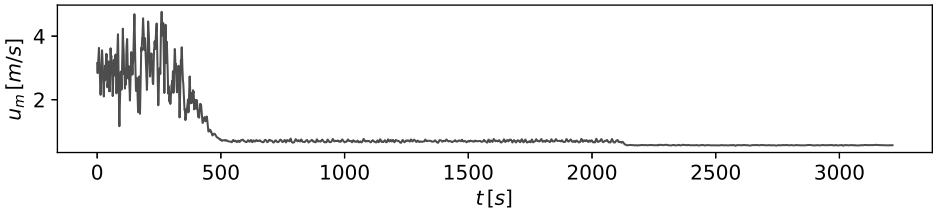

(a) Mixture velocity

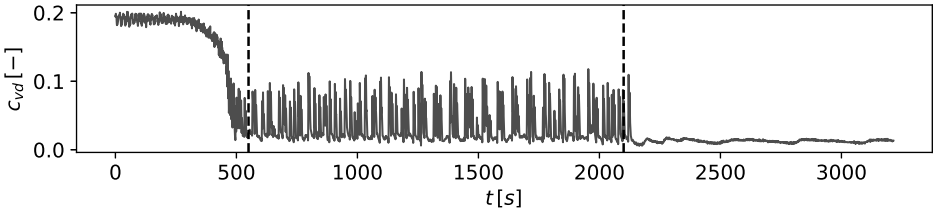

(b) Delivered concentration

Figure A.6: Tests Dorsilit 8 (D8), nr. 2, $d_{50} = 617\mu m$.

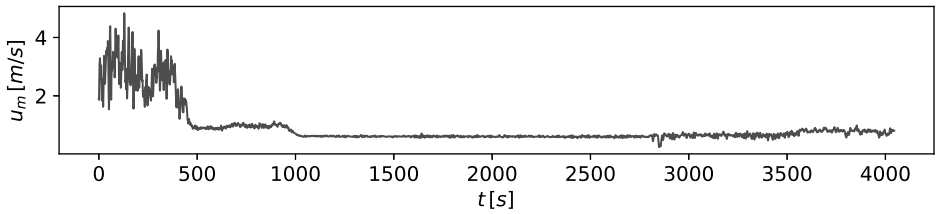

(a) Mixture velocity

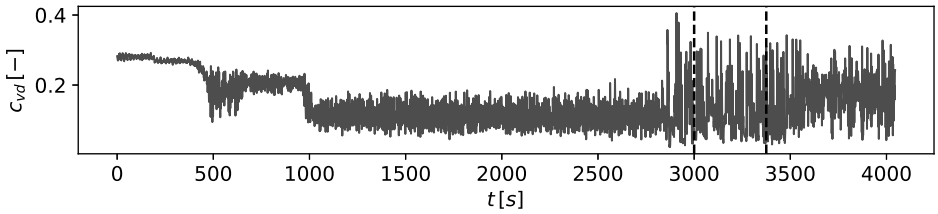

(b) Delivered concentration

Figure A.7: Tests Dorsilit 8 (D8), nr. 3, $d_{50} = 617\mu m$.

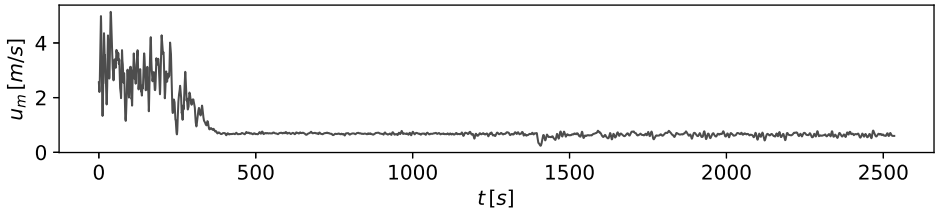

(a) Mixture velocity

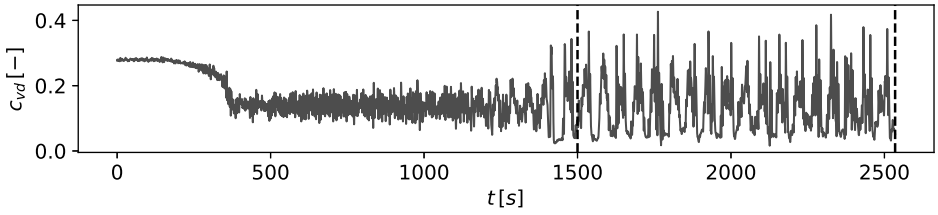

(b) Delivered concentration

Figure A.8: Tests Dorsilit 8 (D8), nr. 4, $d_{50} = 617\mu m$.

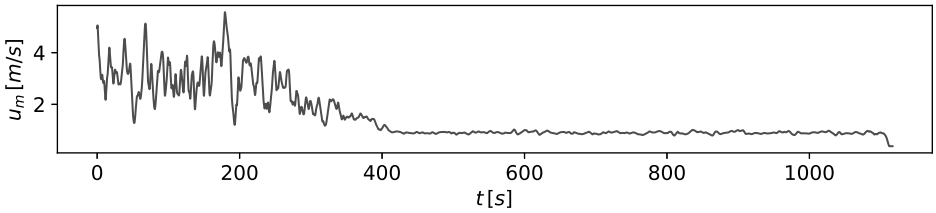

(a) Mixture velocity

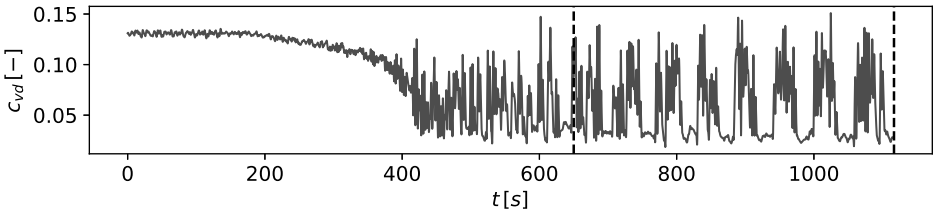

(b) Delivered concentration

Figure A.9: Tests Dorsilit 7 (D7), nr. 1, $d_{50} = 1.08mm$.

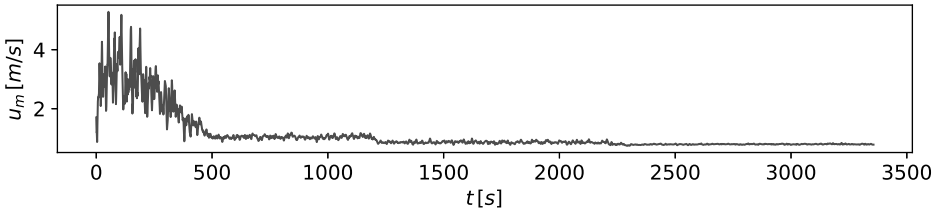

(a) Mixture velocity

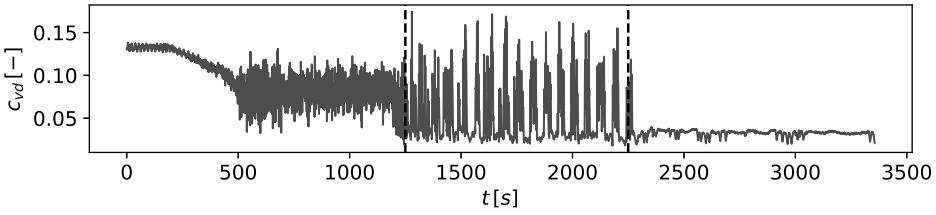

(b) Delivered concentration

Figure A.10: Tests Dorsilit 7 (D7), nr. 2, $d_{50} = 1.08mm$.

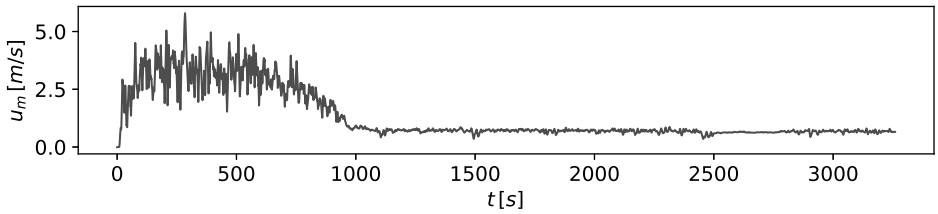

(a) Mixture velocity

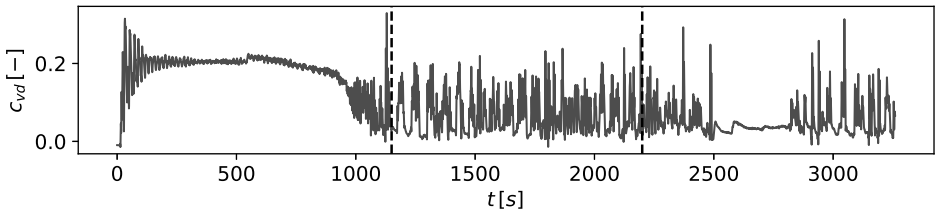

(b) Delivered concentration

Figure A.11: Tests Dorsilit 7 (D7), nr. 3, $d_{50} = 1.08mm$.

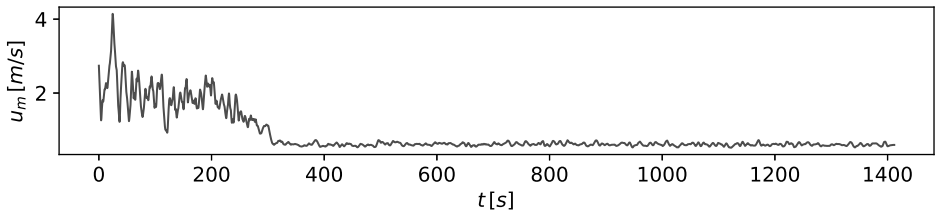

(a) Mixture velocity

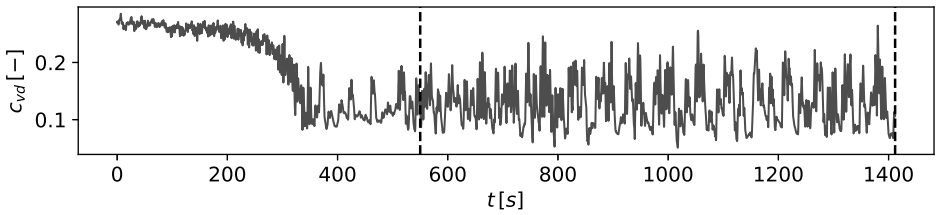

(b) Delivered concentration

Figure A.12: Tests Dorsilit 7 (D7), nr. 4, $d_{50} = 1.08mm$.

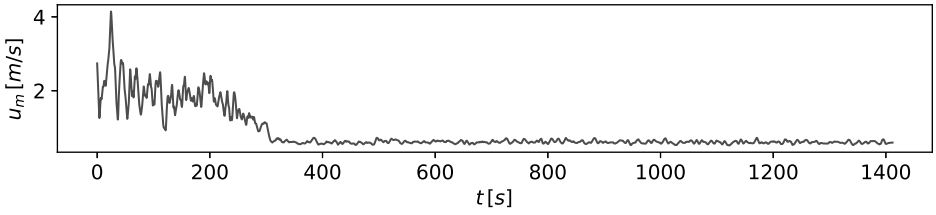

(a) Mixture velocity

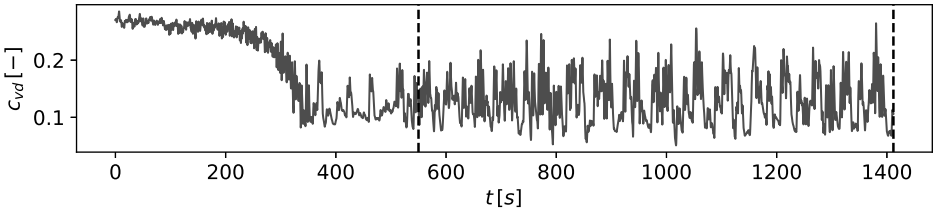

(b) Delivered concentration

Figure A.13: Tests Dorsilit 7 (D7), nr. 5, $d_{50} = 1.08mm$.

B

1D-2L-HT MODEL

This appendix contains the mathematical derivation of the transport- and momentum equation of the 1D-2L-HT model of Chapter 5.

Parts of this chapter have been published in the Journal of Hydrology and Hydromechanics **72(1)** (2024).

B.1. General Finite Volume Method formulation

According to Hirsch (2007) the general formulation of the Finite Volume Method in integral form, for a scalar quantity U, is:

$$\frac{\partial}{\partial t}\int_V U dV + \oint_S \vec{F}\cdot d\vec{S} = \int_V q dV \tag{B.1}$$

Where V is the volume of a numerical cell, S the surface of a cell, $\vec{F}$ the numerical flux and q a source term. This equation can be rewritten in a discrete form by expressing volume integrals as volume averaged values, and surface integrals as a sum of numerical fluxes of cell boundaries:

$$\frac{\partial}{\partial t}(U V) + \sum_{faces} \vec{F}\cdot\Delta\vec{S} = qV \tag{B.2}$$

The numerical flux $\vec{F}$ equals the product of the scalar value U and velocity $\vec{u}$:

$$\vec{F} = U\vec{u} \tag{B.3}$$

For the numerical grid defined by Figure 5.2, S equals the area of the cell boundary above the bed, A. The source term is rewritten to a volumetric source term per unit time:

$$\Gamma_v = qV \tag{B.4}$$

Therefore the final general formulation of the FVM for 1D grid in Figure 5.2 becomes:

$$\frac{\partial}{\partial t}(U V) + \sum_{faces} (F A) = \Gamma_v \tag{B.5}$$

B.2. Particle transport equation

To derive the transport equation of the solids phase, and using the 1D grid defined in Figure 5.2 and $U = c$, $F = u_s c$.

$$\frac{\partial}{\partial t}(cV) + \sum_{faces} (u_s c A) = \Gamma_v \tag{B.6}$$

This can be rewritten in differential form by applying $V = \Delta x A$:

$$\frac{\partial}{\partial t}(cA) + \frac{\partial}{\partial x}(u_s c A) = \Gamma_v \tag{B.7}$$

B.3. Momentum equation

To derive the momentum equation of the mixture the sum over the momentum equations of the phases is applied. Therefore, first the momentum equation of a phase is derived. Equation B.1 is applied in vector form, with $\vec{U} = c_k \rho_k \vec{u}_k$, in which c_k, ρ_k and u_k are phase volumetric concentration, density and velocity respectively:

$$\frac{\partial}{\partial t}\int_V c_k\rho_k\vec{u}_k dV + \oint_S c_k\rho_k\vec{u}_k(\vec{u}_k\cdot d\vec{S}) = \int_V c_k\vec{f}_k dV \tag{B.8}$$

With $\vec{f}_k$ being a force term, which is the sum of internal forces $\vec{f}_{k,i}$ and external forces $\vec{f}_{k,e}$. According to Hirsch (2007), internal forces and external forces can be applied as momentum source terms. Internal forces are:

$$\vec{f}_{k,i} = \boldsymbol{\sigma}\cdot\vec{n} \tag{B.9}$$

With $\vec{n}$ the unit vector and $\boldsymbol{\sigma}$ the total internal stress tensor:

$$\boldsymbol{\sigma} = -p_k\boldsymbol{I} + \boldsymbol{\tau} \tag{B.10}$$

In the above $\boldsymbol{I}$ is the unit tensor, p_k the pressure of a phase and $\boldsymbol{\tau}$ internal viscous stresses, which represent internal friction forces between fluid layers. Since the model is 1D, internal viscous stresses cannot be modelled in this way, rather momentum source terms are applied in a later stage of the derivation (see Equation B.21). Additionally, pressure is only resolved in axial direction, in 1D. Therefore, the source term for internal forces simply reduces to:

$$f_i = -p_k \tag{B.11}$$

Hirsch (2007) states that internal forces act as surface sources, therefore are integrated over the cell surfaces. The momentum equation of a phase now becomes:

$$\frac{\partial}{\partial t}\int_V c_k\rho_k\vec{u}_k dV + \oint_S c_k\rho_k\vec{u}_k(\vec{u}_k\cdot d\vec{S}) = -\oint_S c_k p_k\cdot d\vec{S} + \int_V c_k\vec{f}_{k,e}dV \tag{B.12}$$

For the 1D numerical grid defined by Figure 5.2, S equals the area of the cell boundary above the bed, A. The 1D momentum equation of a phase becomes:

$$\frac{\partial}{\partial t}(c_k\rho_k u_k V) + \sum_{faces}(c_k\rho_k u_k u_k A) = -\sum_{faces}(c_k p_k A) + c_k F_{e,k} \tag{B.13}$$

With $F_{e,k}$ being the total integrated phase external force acting on a volume V, and the "faces" being the numerical cell faces. The mixture density ρ_m, by summation of all phases k, is defined as:

$$\rho_m = \sum_{k=0}^{N} c_k\rho_k \tag{B.14}$$

The Favre averaged mixture velocity is $\hat{u}_m$ defined as (Ishii and Hibiki, 2011):

$$\hat{u}_m = \frac{1}{\rho_m}\sum_{k=0}^{N} c_k\rho_k u_k \tag{B.15}$$

The drift velocity $u_{k/m}$ is defined as the velocity difference between the phase and the mixture velocity:

$$u_{k/m} = u_k - \hat{u}_m \tag{B.16}$$

Summation of the drift velocity over all fraction must equal zero (Ishii and Hibiki, 2011):

$$\sum_{k=0}^{N} c_k \rho_k u_{k/m} = 0 \tag{B.17}$$

Finally, the mixture momentum equation is attained by summing Equation B.13 over all k phases:

$$\frac{\partial}{\partial t} \sum_{k=0}^{N} (c_k \rho_k u_k V) + \sum_{faces} \left[\sum_{k=0}^{N} (c_k \rho_k u_k u_k A) \right] = - \sum_{faces} \left[\sum_{k=0}^{N} (c_k p_k A) \right] + \sum_{k=0}^{N} c_k F_{e,k} \tag{B.18}$$

Substitution of Equations B.14, B.15, B.16 by applying B.17, into B.18, leads to the mixture momentum equation:

$$\frac{\partial}{\partial t}(\rho_m \hat{u}_m V) + \sum_{faces} (\rho_m \hat{u}_m \hat{u}_m A) = - \sum_{faces} (p A) - \sum_{faces} \left[\sum_{k=0}^{N} A c_k \rho_k u_{k/m} u_{k/m} \right] + F_e \tag{B.19}$$

In which p is the pressure of the mixture and F_e the external forces on the entire mixture. The equation is slightly rewritten. Specifically, the water phase ($k = 0$) is replaced by subscript f, the solids phase ($k = 1$) with subscript s:

$$\begin{aligned} \frac{\partial}{\partial t}(\rho_m \hat{u}_m V) + \sum_{faces} (\rho_m \hat{u}_m \hat{u}_m A) = &- \sum_{faces} (p A) + \dots \\ &- \sum_{faces} \left[A c \rho_s (u_s - \hat{u}_m)^2 + A(1-c) \rho_f (u_f - \hat{u}_m)^2 \right] + F_e \end{aligned} \tag{B.20}$$

In which F_e are external frictional forces over the entire mixture and p the pressure over the mixture. The external forces are:

$$F_e = -F_m - F_b - F_s + F_p \tag{B.21}$$

In which F_m are frictional forces of the mixture against the pipe wall, F_b frictional forces of the mixture flow over a bed layer, F_s hydrostatic forces and F_p are driving forces caused by the pressure of the pump.

$$F_m = \tau_m O \tag{B.22}$$

$$F_b = \tau_b W \tag{B.23}$$

$$F_s = \rho_m g A \sin(\omega) \tag{B.24}$$

$$F_p = A\,S_p \tag{B.25}$$

The final momentum equation becomes:

$$\begin{aligned}\frac{\partial}{\partial t}(\rho_m \hat{u}_m V) + \sum_{faces}(\rho_m \hat{u}_m \hat{u}_m A) = &-\sum_{faces}(p\,A) - \tau_m O - \tau_b W + ... \\ &- \rho_m g A \sin(\omega) - \sum_{faces}\left[Ac\rho_s(u_s - \hat{u}_m)^2 + A(1-c)\rho_f(u_f - \hat{u}_m)^2\right] + A\,S_p\end{aligned} \tag{B.26}$$

C

BISSCHOP (2018) EROSION MODEL EXPLICIT SOLUTION

This appendix contains an explicit solution to the Bisschop (2018) erosion model, used in Chapter 5.

Parts of this chapter have been published in the Journal of Hydrology and Hydromechanics **72(1)** (2024).

The erosion model by Bisschop (2018) is a physical-analytical model, based on turbulent sweeps eroding parts of the bed layer. The pick function of Bisschop (2018) is as follows:

$$E = \frac{h_s \lambda_b (1 - n_0) \rho_s}{4 T_B} \tag{C.1}$$

With h_s the shear layer thickness, ρ_s the particle density, n_0 the bed porosity, λ_b a coefficient for the amount to turbulent bursts eroding the bed layer and T_B the mean bursting period of a turbulent sweep. The shear layer thickness is estimated with:

$$h_s = (p^{'} - \sigma_a) \frac{\tan(\frac{\pi}{4} + \frac{\phi}{2})}{N_\gamma g (\rho_s - \rho_f + i\,\rho_f)}) \tag{C.2}$$

With $p^{'}$ the normal pressure on the sand bed caused by turbulent bursts, σ_a the resisting pressure of a sand wedge in the bed to be removed by turbulent bursts, ϕ the sand internal friction angle, N_γ a soil strength related constant, ρ_b the in-situ density of the sand bed and i the hydraulic gradient caused by inward flow of water normal to the bed layer, due to soil dilatation. The normal pressure $p^{'}$ is calculated as:

$$p^{'} = \frac{1}{2} \rho_f \hat{w}^2 \tag{C.3}$$

With $\hat{w}$ the mean vertical velocity of the turbulent bursts, which is a function of the mixture velocity above the bed u_b.

$$\hat{w} = 1.0 u_b \tag{C.4}$$

The sand bed resistance vertical pressure σ_a equals:

$$\sigma_a = \frac{h_s u_b}{2 T_B} \rho_s (1 - n_0) \tag{C.5}$$

The hydraulic gradient of the bed water inflow i is calculated as:

$$i = \frac{h_s}{T_B\, k_{max}} \frac{n_{max} - n_0}{1 - n_{max}} \tag{C.6}$$

In the Equation above n_{max} is the maximum porosity the soil can have, and k_{max} the permeability at n_{max}. N_γ is computed as:

$$N_\gamma = \frac{1}{2} \left[\left(\frac{1 + \sin(\phi)}{1 - \sin(\phi)} \right)^{5/2} - \left(\frac{1 + \sin(\phi)}{1 - \sin(\phi)} \right)^{1/2} \right] \tag{C.7}$$

Bisschop (2018) states this model needs to be solved iteratively as both σ_a and i are a function of h_s. Fortunately, by substitution of Equations C.5 and C.6 into Equation C.2, a second order polynomial equation can be derived with the following analytical solution:

$$h_s = \frac{-C_1 + (C_1^2 + C_2)^{0.5}}{C_3} \tag{C.8}$$

$$C_1 = \frac{\rho_s}{2}(1-n_0)\frac{u_b}{T_B}\tan\left(\frac{\pi}{4}+\frac{\phi}{2}\right) \tag{C.9}$$

$$C_2 = \frac{4}{T_B k_{max}}\left(\frac{n_{max}-n_0}{1-n_{max}}\right)N_\gamma g \rho_f p' \tan\left(\frac{\pi}{4}+\frac{\phi}{2}\right) \tag{C.10}$$

$$C_3 = \frac{2}{T_B k_{max}}\left(\frac{n_{max}-n_0}{1-n_{max}}\right)N_\gamma g \rho_f \tag{C.11}$$

List of Publications

Journal Publications

8. **E. de Hoog, O. van der Ven, R.L.J. Helmons, A.M. Talmon, C. van Rhee**, *Experimental research on self-amplifying density waves in horizontal pipelines of two phase granular slurries: measurements on the effect of particle diameter and concentration*, International Journal of Multiphase Flow **Under review** (2024).

7. **E. de Hoog, T. van der Voort, A.M. Talmon, C. van Rhee**, *A 1-dimensional-two-layer transient drift-flux model for hydraulic transport pipelines: modelling and experiments of bed layer erosion and density wave amplification*, Journal of Hydrology and Hydromechanics **72**(1): 64-79 (2024).

6. **E. de Hoog, J.M. van Wijk, A.M. Talmon, C. van Rhee**, *Predicting density wave amplification of settling slurries using a 1D Driftflux model*, Powder Technology **400**(3): 117252 (2022).

5. **J.M. van Wijk, E. de Hoog, A.M. Talmon, C. van Rhee**, *Concentration and pressure measurements of dense sand and gravel multiphase flows under transient flow conditions in a vertically oriented closed conduit — Assessment of system and sensor performance*, Flow Measurement and Instrumentation **84**(4): 102126 (2021).

4. **E. de Hoog, A.M. Talmon, C. van Rhee**, *Unstable Transients Affecting Flow Assurance during Hydraulic Transportation of Granular Two-Phase Slurries*, Journal of Hydraulic Engineering **147**(9): 04021029 (2021).

3. **E. de Hoog, J.M. van Wijk, J.T.M. Wijnands, A.M. Talmon**, *Degradation of polymetallic nodules during hydraulic transport under influence of particle-wall and particle-particle interaction*, Minerals Engineering **155**(8): 106415 (2020).

2. **J.M. van Wijk & E. de Hoog**, *Size reduction of CCZ polymetallic nodules under repeated impact fragmentation*, Results in Engineering **7**(7): 100154 (2020).

1. **J.M. van Wijk, S. Haalboom, E. de Hoog, H. de Stigter, M.G. Smit**, *Impact fragmentation of polymetallic nodules under deep ocean pressure conditions*, Minerals Engineering **134**(4): 250-260 (2019).

Conferences

5. **E. de Hoog, J.M. in 't Veld, C.F. Hofstra, A.M. Talmon**, *NPSHr scaling for centrifugal pumps*, CEDA Dredging Days, 27-29 May 2024, Rotterdam, the Netherlands.

4. **E. de Hoog, J.M. van Wijk, A.M. Talmon, C. van Rhee**, *Deep Sea Mining Vertical Hydraulic Transport Pipelines: Design Guidelines and Operational Considerations*, 51st Under Water Minerals Conference, 1-6 Oct. 2023, Rotterdam, the Netherlands.

3. **E. de Hoog, A.M. Talmon, C. van Rhee**, *Density Wave Amplification During Hydraulic Transport: The Effect of Pipeline Design Parameters*, 20th Int. Conf. on Transport and Sedimentation of Solid particles, 26-29 Sept. 2023, Wroclaw, Poland.

2. **E. de Hoog, A.M. Talmon, C. van Rhee**, *The relevance of time domain effects for the design and stability of hydraulic transport pipelines*, CEDA Dredging Days, 28-29 Sept. 2021, Virtual Conference.

1. **E. de Hoog, J.M. in 't Veld, J.M. van Wijk, A.M. Talmon**, *An Experimental Study into Flow Assurance of Coarse Inclined Slurries*, 18th Int. Conf. on Transport and Sedimentation of Solid particles, 11-18 Sept. 2017, Prague, Czech Republic.

MAGAZINES

1. **E. de Hoog, A.M. Talmon, C. van Rhee**, *Pipeline design - Density wave amplification and slurry dynamics*, Terra et Aqua, IADC, **166**(2): 15-25 (2022).

CURRICULUM VITÆ

Edwin DE HOOG

08-03-1990 Born in Zoetermeer, the Netherlands.

EDUCATION

2002–2008 Elementary School
Atheneum Oranje Nassau College, Zoetermeer

2008–2013 Bachelor of Science - Mechanical Engineering
Delft University of Technology

2013-2016 Master of Science - Offshore and Dredging Engineering
Delft University of Technology

2019-2024 Doctor of Philosophy - Offshore and Dredging Engineering
Delft University of Technology
Thesis: Transient Hydraulic Transport in Pipelines – on flow assurance influenced by slurry dynamics
Promotors: Prof. dr. ir. C. van Rhee
Dr. ir. R.L.J. Helmons
Copromotor: Dr. ir. A.M. Talmon

WORK EXPERIENCE

2016–2022 Research & Development Engineer, MTI Holland B.V. (Royal IHC)
2019–2024 PhD researcher (part-time), Delft University of Technology
2022–present Senior Research & Development Engineer, Royal IHC

AWARDS

2021 IADC Young Author Award, awarded at the CEDA Dredging Days 2021 conference

ACKNOWLEDGEMENTS

11-9-2017, Prague, the Czech Republic: the week of the 18th Conference on Transportation & Sedimentation of Solid particles. I forgot to register for the conference excursion, Joep decided to skip the excursion, and Jort missed his flight home that morning. So we had spare time. The three of use were walking in the Letná Park, on a beautiful sunny morning, contemplating and discussing the future of hydraulic transport research. That same summer of 2017 we were conducting the "Freiberg experiments", and we just learnt about these nasty density waves, having no clue what caused them. Joep mentioned "het treintjes model", a 1-dimensional-CFD model used in the oil and gas industry to simulate transient pipeline flows for gas-oil mixtures. That morning we understood that that is the way forward, to include the time domain in our pipeline design methods, and we understood that this was the way to get a grasp on the density waves. A year later I approached Cees and Arno with the problem and a plan to do a part-time PhD, they were onboard right away. On May the first 2019, the research started and now the results are in this dissertation.

First and foremost I want to thank Cees van Rhee, my original promotor, who unfortunately is not with us today to see the end results of the project. I will always remember Cees as a very knowledgeable and approachable person, and always up for a conversation. It turned out that Cees and I had some shared hobbies and interests, especially 3D-printing, which we discussed vividly during lunch and coffee breaks. I also appreciate the advice Cees gave unrelated to dredging, such as project management and getting things done within large commercial companies. Cees had plenty of experience on this and many interesting stories to tell from his time at the HAM and Van Oord. Thanks for everything.

I want to thank Arno Talmon. Arno was also my supervisor during my Master thesis, and as such our shared interest for particles mixed with water goes back almost 10 years. I always enjoyed our moments philosophizing about slurries and thinking of new theories, talking about the tiny details, and realizing that there are only a handful of people in the world with such in-depth knowledge. I also enjoyed the week together at the T&S conference in 2023, and our struggle to find something to eat other than potatos in Wroclaw.

I also want to thank Rudy Helmons for stepping in as promotor in the last months of the project, and investing considerable time in a short period to make sure that work could finish without delay. This was very appreciated, thanks a lot! Also thanks for the collaboration on other projects, such as writing the chapter for the deep sea mining book, and the guest lectures. I'm sure that future collaborations will be plenty.

Royal IHC is quite unique to allow some of its employees to work part-time at the university on a PhD project. Of course this is only possible with vision and trust from people that understand what research is, and who are confident in the direction that

they set out to improve knowledge, to enable the long term future of IHC. For this I want to thank Jort van Wijk, Léon Seijbel, Bernardete Goncalves Castro, Erik van der Blom and Henk van Muijen, for their continued support and faith in the work.

Special thanks need to go to Tjalie van der Voort and Oscar van der Ven for their help with the experiments. Tjalie, without your measurements calibration of the 2L model would not be possible, and seeing the sand flow through your fully transparent experimental flow loop made me understand the transient accumulation mechanism. Oscar, you can be proud of your contribution to the discovery of the third density wave mechanism, unravelled during your experiments. Thank you both, your contributions are very significant, and you are now both ambassadors to spread this new knowledge among the sector!

I would also like to thank the staff of the dredging engineering department. Sape, Geert, Antonio, Said and Pauline. Thanks for all the advice, aid and coffee break conversations. Special thanks to Andre van den Bosch and Ed Stok, for helping with the design and construction of the experiments at the university, and the many coffees we shared early morning before the rest arrived.

A special bond forms between fellow PhD students, spending considerable time together, bonded by mutual struggles, lapses in motivation and discussions to help each other out. Bas, you were a great help in my first year to get me going in CFD, and you are still the one I approach with questions today. Xiuhan, neither was I aware of the "free-drinks" on the fourth floor not being free, they were nice though! Thijs, as a fellow Dutchman its was our job to spread the Dutch culture to our foreign colleagues, and we were always sharing notes on how to keep Opels in a running state. Mohamed, we started our PhD at the same time, working together to understand the Driftflux model and doing some GS school courses together. Stefano, fond memories of the machine learning course we followed in Eindhoven together with Mohamed, infiltrating the TU/e Italian mafia, and I agree with you, no cappuccino after dinner. Justus, good luck sailing around the world! Jian, good luck with your academic career at Civil Engineering. Frans, always discussing deep sea mining with you, who knows for how many years to come. Mark, I definitely agree, age is just a number, good luck in finishing your PhD. Shaheen, Sterre and Mosaab, the three of you were the second group of office mates I had, suddenly making me the "old one". Thanks for the good times, and good luck finishing your PhDs.

Doing a part-time PhD means you have two jobs with two groups of colleagues. During busy and stressful weeks at the university, I could recover on Thursday and Friday at IHC, by distracting my colleagues, thus spreading Fridayitis. Yarno, Jazzie and Maarten thanks for the help and the many years of collaboration in the lab. Amy and Rick, thanks for reviewing some of my papers. And to all other IHC colleagues with whom I worked closely the past years, thank you all.

Last but not least, thanks to my closest friends and my family. Chris and Phebe, the two of you have started a nice life in the east of the country, with a nice spacious house, with plenty of room for future "projects", where I hope to visit for many years to come to recharge my batteries.

Thanks to my dearest family: my parents, Jos & Sandra, Christa & Phillippe and my dear two little nieces, Anna and Sofia.

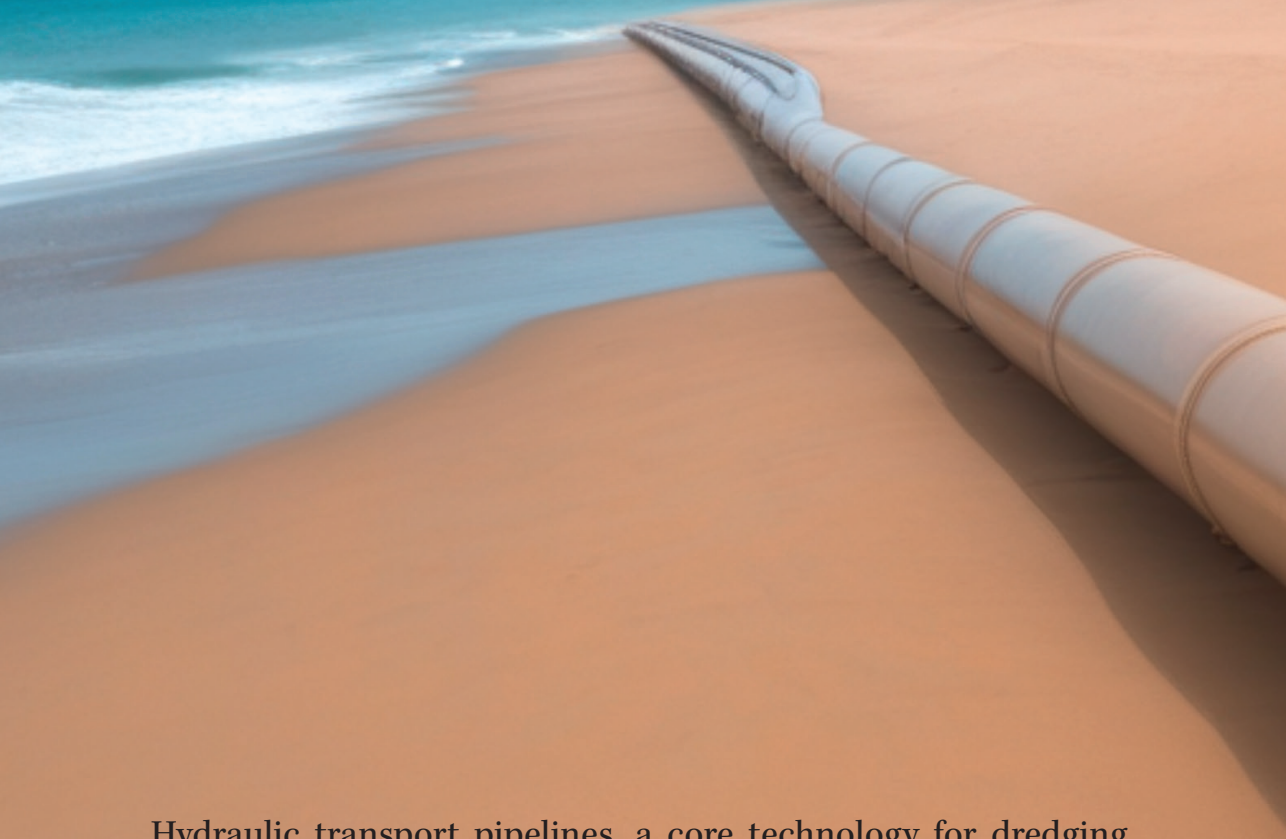

Hydraulic transport pipelines, a core technology for dredging, (wet) mining and deep sea mining. These pipelines transport the building materials of our modern society.

Steady-state principles have formed the foundation of pipeline design methods, while associated slurry dynamics are scarcely researched. More knowledge on the effect of transients on flow assurance can still be gained.

How can transients destabilize pipeline flows? Can we model these instabilities using 1-dimensional Computational Fluid Dynamics? How can we further optimize pipelines and improve our design methods, while maintaining transient stability?

ISBN 978-94-6506-147-4